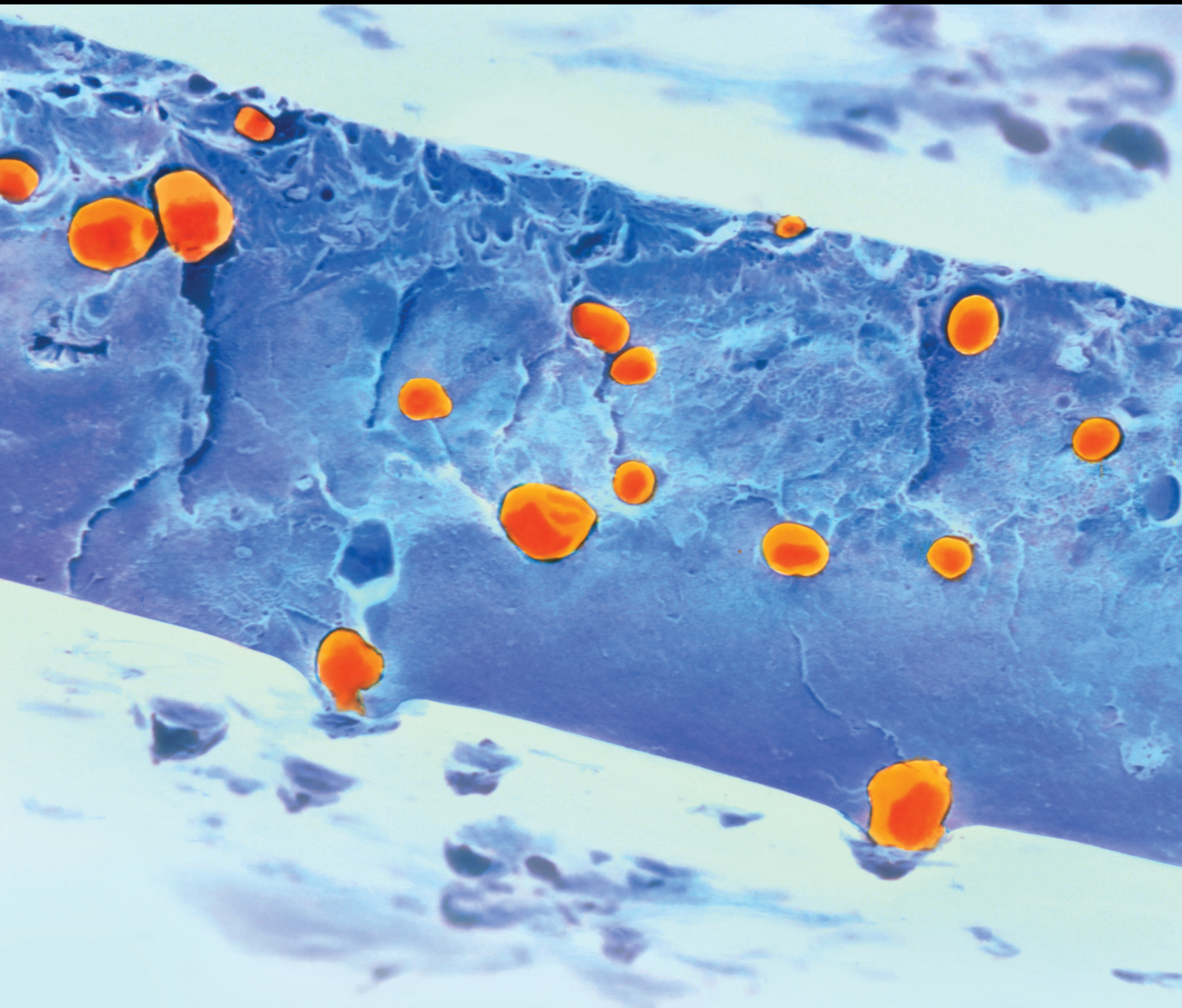


Natural Fiber-Reinforced Biopolymer Composites

Lead Guest Editor: S.M. Sapuan

Guest Editors: R.A. Ilyas and Hairul Abral





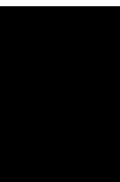
Natural Fiber-Reinforced Biopolymer Composites

International Journal of Polymer Science

**Natural Fiber-Reinforced Biopolymer
Composites**

Lead Guest Editor: S.M. Sapuan


Guest Editors: R.A. Ilyas and Hairul Abral



Copyright © 2021 Hindawi Limited. All rights reserved.

This is a special issue published in "International Journal of Polymer Science." All articles are open access articles distributed under the Creative Commons Attribution License, which permits unrestricted use, distribution, and reproduction in any medium, provided the original work is properly cited.

Chief Editor

Qinglin Wu , USA

Academic Editors

Ragab Abouzeid, Egypt
Sheraz Ahmad , Pakistan
M. R. M. Asyraf, Malaysia
Luc Averous , France
Marc Behl , Germany
Laurent Billon, France
Antonio Caggiano , Germany
Wen Shyang Chow , Malaysia
Angel Concheiro , Spain
Cedric Delattre , France
Maria Laura Di Lorenzo , Italy
Marta Fernández-García , Spain
Peter Foot , United Kingdom
Cristiano Fragassa , Italy
Peng He , USA
Jojo P. Joseph , USA
Nobuhiro Kawatsuki, Japan
Saad Khan, USA
Jui-Yang Lai , Taiwan
Chenggao Li , China
Zhi Li , China
Ulrich Maschke , France
Subrata Mondal , India
Hamouda Mousa, Egypt
Karthik Reddy Peddireddy , USA
Alessandro Pegoretti , Italy
Önder Pekcan , Turkey
Zhonghua Peng , USA
Victor H. Perez , Brazil
Debora Puglia , Italy
Miriam H. Rafailovich , USA
Subramaniam Ramesh , Malaysia
Umer Rashid, Malaysia
Bernabé L. Rivas, Chile
Hossein Roghani-Mamaqani , Iran
Mehdi Salami-Kalajahi , Iran
Markus Schmid , Germany
Matthias Schnabelrauch , Germany
Robert A. Shanks , Australia
Vito Speranza , Italy
Atsushi Sudo, Japan
Ahmed Tayel, Egypt
Stefano Turri, Italy

Hiroshi Uyama , Japan
Cornelia Vasile , Romania
Alenka Vesel , Slovenia
Voon-Loong Wong , Malaysia
Huining Xiao, Canada
Pengwu Xu , China
Yiqi Yang , USA









Contents

Stability, Viscosity, and Tribology Properties of Polyol Ester Oil-Based Biolubricant Filled with TEMPO-Oxidized Bacterial Cellulose Nanofiber

Dieter Rahmadiawan , Hairul Abral , N. Nasruddin , and Zahrul Fuadi 






Research Article (9 pages), Article ID 5536047, Volume 2021 (2021)

Antimicrobial Edible Film Prepared from Bacterial Cellulose Nanofibers/Starch/Chitosan for a Food Packaging Alternative

Hairul Abral , Angga Bahri Pratama , Dian Handayani , Melbi Mahardika , Ibtisamatul Aminah , Neny Sandrawati , Eni Sugiarti, Ahmad Novi Muslimin , S. M. Sapuan , and R. A. Ilyas 

Research Article (11 pages), Article ID 6641284, Volume 2021 (2021)

Experimental Investigation on the Mechanical Properties of a Sandwich Structure Made of Flax/Glass Hybrid Composite Facsheet and Honeycomb Core

W. Ashraf , M. R. Ishak , M. Y. M. Zuhri , N. Yidris , and A. M. Ya'acob 

Research Article (10 pages), Article ID 8855952, Volume 2021 (2021)

Jatropha Oil as a Substituent for Palm Oil in Biobased Polyurethane

Mohamad Ridzuan Amri, Syeed Saifulazry Osman Al-Edrus , Chuah Teong Guan , Faizah Md Yasin, and Lee Seng Hua

Review Article (12 pages), Article ID 6655936, Volume 2021 (2021)

Potential Application of Green Composites for Cross Arm Component in Transmission Tower: A Brief Review

M. R. M. Asyraf , M. R. Ishak , S. M. Sapuan , N. Yidris , R. A. Ilyas , M. Rafidah, and M. R. Razman 

Review Article (15 pages), Article ID 8878300, Volume 2020 (2020)

Research Article

Stability, Viscosity, and Tribology Properties of Polyol Ester Oil-Based Biolubricant Filled with TEMPO-Oxidized Bacterial Cellulose Nanofiber

Dieter Rahmadiawan ¹, Hairul Abral ², N. Nasruddin ¹, and Zahrul Fuadi ³

¹Department of Mechanical Engineering, Universitas Indonesia, Depok 16424, Indonesia

²Department of Mechanical Engineering, Andalas University, 25163 Padang, Sumatera Barat, Indonesia

³Department of Mechanical and Industrial Engineering, Universitas Syiah Kuala, Banda Aceh 23111, Indonesia

Correspondence should be addressed to Hairul Abral; habral@yahoo.com and N. Nasruddin; nasruddin@eng.ui.ac.id

Received 14 January 2021; Revised 18 March 2021; Accepted 2 April 2021; Published 15 April 2021

Academic Editor: Subrata Mondal

Copyright © 2021 Dieter Rahmadiawan et al. This is an open access article distributed under the Creative Commons Attribution License, which permits unrestricted use, distribution, and reproduction in any medium, provided the original work is properly cited.

This research is aimed at studying the stability and tribology properties of the polyol ester oil- (POE-) based biolubricant mixed with various filler loadings from microparticle of TEMPO-oxidized bacterial cellulose (NDCt) as an additive and sorbitan monostearate (Span 60) as a surfactant. Morphology, rheology, and tribology tests were conducted. The addition of NDCt and Span 60 to pure POE as a base fluid showed elevated viscosity, lower value of coefficient friction (COF), and a remarkable decrease in the wear rate (WR). The presence of 0.6 wt% NDCt and 1.8 wt% Span 60 in POE (N2S4) decreased the COF value by 79% in comparison to POE. At room temperature, this N2S4 biolubricant sample showed a higher thermal conductivity by 4% and lower WR value by 49% compared to POE. This study introduced the preparation of the ecofriendly biolubricant filled with NDCt improving the tribology properties remarkably.

1. Introduction

Development of green lubrication technology with high efficiency, energy saving, and environmentally friendly has attracted great attention recently for many researchers [1]. The demand for using renewable energy in all aspects has led to increased research on natural-based lubricants. [2]. One way to improve lubricant performance is by providing additives. Additives with various functions had been applied and proven to be viscosity improvers, antiwear agents, thermal conductivity enhancer, detergents, etc. [3, 4]. Despite the required technical characteristics, lubricants' pollution and environmental health problems have led to more attention in recent years [5]. A million tons of loss are released into the environment every year [6]. The role of lubricant additives in the world is also vital in environmentally friendly applications [7, 8]. Calcium sulphonates, tricresyl phosphates, and zinc dialkyl dithiophosphates are conventional additives with heavy metals and unhealthy elements [9].

Therefore, the demand for ecofriendly lubricant additives is developing rapidly at present.

Ecofriendly additives from sustainable sources are considered more by researchers rather than conventional additives [8, 10, 11]. A recent study has explored cellulose from the plant as an additive of biolubricant for improvement of its tribology performance [12]. Generally, isolation of the nanocellulose used a chemical treatment. Pure nanocellulose can be obtained from bacterial cellulose (BC) without the need for acid hydrolysis which provides environmental benefits [13]. Source of BC is *Komagataeibacter xylinus*, a bacterium commonly used for the production of *nata de coco* [14]. BC has high thermal and mechanical resistance, a high degree of crystallinity, low cost, and density [15].

BC is hydrophilic in nature and has a large number of hydroxyl groups [16]. The disintegrated hydrophilic BC alone is agglomerated in hydrophobic synthetic lubricant reducing its tribology performance. Individual cellulose nanofiber dispersed in a lubricant is essential. Using 2,2,6,6-

tetramethylpiperidine-1-oxyl (TEMPO) is a usual method to reduce the agglomeration of the cellulose [17]. TEMPO also has the antiwear ability and the free radical group which could enhance the oxidative stability of POE oil [17–19]. Better stability of the individual fibers in lubricant plays an important role in the improvement of the tribology properties of the lubricant [20]. Treatment of cellulose using a surfactant is a common strategy to look for the better stability of the cellulose in a lubricant. Recently, Span 60 has been used as a surfactant improving the stability of the nanofluid [21, 22]. A surfactant also has the antiwear ability, which, once again, in this case, is very suitable as lubricant additives [23].

Numerous works have reported a biolubricant filled with cellulose [24–26]. Recent research which is relatively similar to our present investigation has quantified the characterization of biolubricant mixed with cellulose from plant [12, 27, 28]. However, the study on tribology performance and viscosity of POE-based biolubricant mixed with NDCt as an additive and Span 60 as a surfactant is yet to be explored. Therefore, the present work is aimed at preparing this biolubricant which was filled with various filler loadings of NDCt and Span 60. Stability and tribology performance of the biolubricant were explored and discussed.

2. Materials and Methods

2.1. Materials. 2,2,6,6-Tetramethylpiperidine-1-oxyl (TEMPO) with the purity of 98%, Span 60, sodium hypochlorite (NaClO), and sodium bromide (NaBr) were purchased from Sigma-Aldrich Company. POE (Emkarate) was obtained from The Lubrizol Corporation. Wet BC pellicle (300 mm × 300 mm × 10 mm) as a raw material for TEMPO-oxidized bacterial cellulose (NDCt) was purchased from a small local market in Padang, West Sumatera, Indonesia. The dried BC nanofiber has a crystallinity index of 80% [15].

2.2. Preparation of Disintegrated NDCt. Figure 1 illustrates the working flow of this research. The wet BC was soaked with NaOH (10 wt%) for 24 h to remove the impurity and then washed several times with distilled water until pH 7. This wet pellicle was disintegrated using an electrical blender for 30 minutes. The wet disintegrated BC was dried using a drying oven (Memmert UN-55) at 75°C for three days. The dried BC film (about 5 g) was reblended and manually ground using porcelain mortar to form a small particle powder and then filtered using a handmade sieve (100 mesh) to obtain a homogeneous particle size.

The dried BC particle was treated using a solution mixed with TEMPO at room temperature. The treatment process was similar as reported by a previous study with a little modification [29]. The dried BC powder (5 g) was suspended into a solution from distilled water (300 ml), TEMPO (0.1 g), NaBr (0.3 gr), and NaClO (30 ml). The mixture was stirred using a plate stirrer (Daihan Scientific MSH-200) at 350 rpm for 2 h. The suspension was filtered using a custom sieve (500 mesh) and neutralized with ethanol (250 ml) for several times until pH 7, then fibrillated by a high-speed

homogenizer (IKA T-25) at 12000 rpm for 30 min. This NDCt/ethanol suspension was used as an additive in POE.

2.3. Preparation of Biolubricant. Biolubricant from the mixture of NDCt/Span 60/POE was prepared by the following method as shown in Table 1. POE oil as the base fluid was compounded with various NDCt and Span 60 loadings. NDCt and Span 60 with a ratio of 1 : 2 and 1 : 3 were dispersed into the POE oil. Firstly, Span 60 was dissolved in POE oil and stirred using a hot plate stirrer (Daihan Scientific MSH-200) at 75°C for 30 min [26]. Further, the NDCt/ethanol suspension was slowly added and then stirred at 110°C for 2 h to evaporate the remaining ethanol until constant weight and reach the exact amount as the composition of the designed sample in Table 1. The obtained biolubricants were homogenized using high-speed homogenizer (IKA T-25) at 12000 rpm for 15 min to disperse fillers in the suspension.

2.4. Stability via Photo Capturing. The stability of the biolubricant (NDCt/Span 60 in POE) as a function of time was observed using the same method that is used in the literature, photo capturing [28, 30]. A conventional camera was used to capture each sample (20 ml) in a glass bottle at various time intervals for 0, 24, 48, 120, 240, and 720 h.

2.5. Morphology Investigation of BC and Wear Scar of the Disk. Surface morphology of the dried NDCt sample was observed using FE-SEM (JFIB4610, JEOL) with 15 kV and 8 mA. Before the FE-SEM observation, each NDCt sample was coated using a gold evaporator system for 10 s and 10 mA to reduce electron charge. Furthermore, the NDCt size in suspension was measured using a particle size analyzer (PSA) from Shimadzu SALD-2300 instrument equipped with a cyclone injection-type dry measurement unit, “SALD-DS5,” a batch cell-sample dispersion unit, “SALD-BC23” (approximately 12 ml). The measurement unit used to investigate the NDCt particle was a semiconductor laser operating at 680 nm. The morphology of the wear scar of the disk was investigated using SEM (FEI QUANTA 650).

2.6. FTIR. The FTIR was determined with Spectrum Two-UATR (Perkin Elmer, United States) which is integrated with a detector of MIR TGS to detect the spectra. The scanning range of the measurements was 500–4000 cm⁻¹ with a scanning speed of 0.2 cm/s.

2.7. Thermal Conductivity. Thermal conductivity of PO and biolubricants are measured using a KD2 thermal property analyzer (Decagon, USA, version 5). This equipment works with the principle of a transient hot-wire technique. The KS-1 sensor (60 mm length, 1.27 mm diameter) was used for the thermal conductivity measurement. A circulating thermostatic bath was used for controlling the samples' temperature within ±1°C. Thermal conductivity of PO and biolubricants are investigated within a temperature range of 20 to 60°C. Each sample was measured with five repetitions. Identification of the significance of any differences in thermal conductivity between PO and biolubricants was carried out using one-way analysis of variance (ANOVA) and a *p*-test.

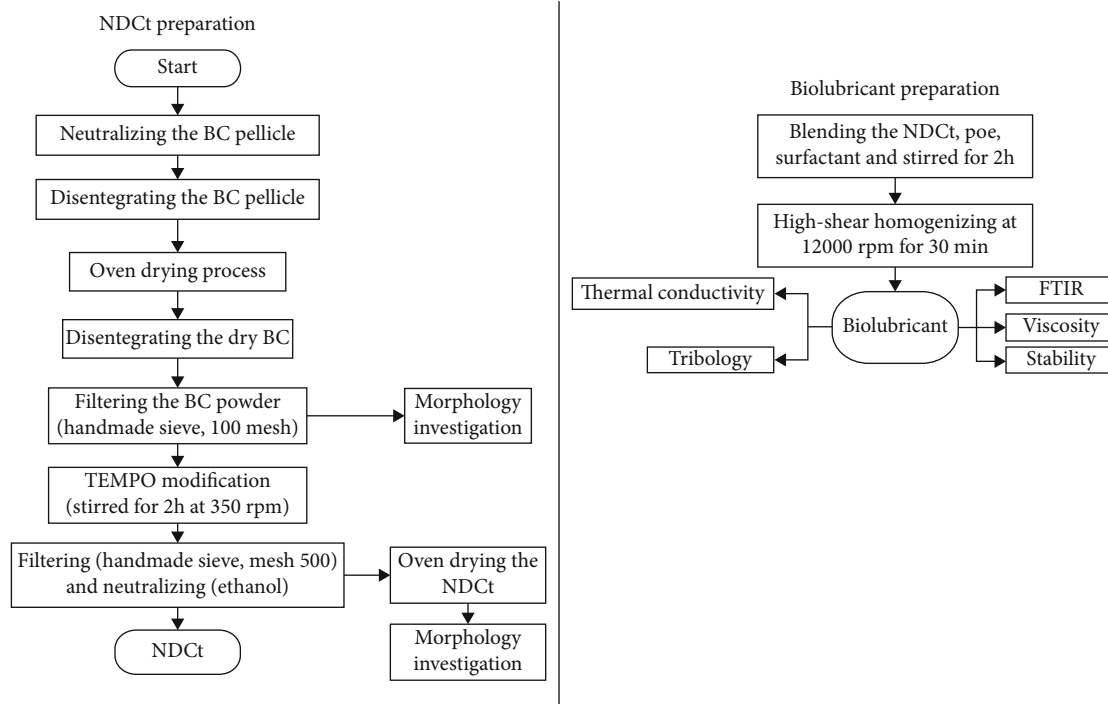


FIGURE 1: Flowchart of NDCt and biolubricant preparation.

TABLE 1: The composition of NDCt (N) and Span 60 (S) in the POE biolubricant.

Sample	Ratio of NDCt to Span 60	Mass fraction (wt%)		
		POE	NDCt	Span 60
PO	0	100	0	0
N1S2	1 : 2	99.1	0.3	0.6
N1S3	1 : 3	98.8	0.3	0.9
N2S4	2 : 4	98.2	0.6	1.2

Duncan multiple range tests were subsequently used using a 95% ($p \leq 0.05$) confidence level. Experimental data were analyzed using IBM SPSS Statistics 25.0 (IBM Corporation, Chicago, USA).

2.8. Viscosity. DHR-1 rheometer (TA Instruments, USA) accompanied by a 40 mm diameter parallel geometry was used to measure the viscosity of the samples. The samples were placed between parallel plates with a diameter of 40 mm and a gap of 1000 μm and equilibrated at 20°C for 4 min. The analysis conducted with a defined shear rate at room temperature.

2.9. Tribology. The tribological tests were conducted using a tribometer designed by Fuadi et al. [31]. Briefly, the equipment has an AISI52100 ball (diameter of 8 mm) and a grey cast iron disk (30 mm diameter) with a thickness of 5 mm. The surface roughness of both the ball and the disk was about 0.04 μm . The friction test was carried out with a sliding speed of 200 rpm at room temperature and a normal load of 5.5 N. The initial contact pressure between the ball and disk surfaces was 989 MPa (Hertzian) as simulating friction in

boundary lubrication regimes. Wear rate (WR) of the disk and ball with the unit of ($\text{mm}^3/\text{N m}$) is calculated using Equation (1) [32]:

$$\text{WR} = \frac{\Delta V}{F \times S}, \quad (1)$$

where ΔV is the volume loss (mm^3), S is the sliding distance of the ball (m), and F is the load applied to the disk (N). Volume loss for the disk is calculated using Equation (2).

$$\Delta V = 2\pi R \left[r^2 \sin^{-1} \left(\frac{d}{2r} \right) - \left(\frac{d}{4} \right) (4r^2 - d^2)^{1/2} \right], \quad (2)$$

where R is the radius of the wear scar, r is the diameter of the ball, and d is the diameter of the wear scar.

3. Results and Discussion

3.1. The Physical Appearance of BC Nanofiber. Figure 2 shows the FE-SEM morphology of (a) the BC film (before TEMPO treatment) and (b) the NDCt film (after the mash and high-shear homogenization process). Both films had many inter-linked BC nanofibers from intermolecular hydrogen bonding [14]. The diameter of a BC nanofiber was less than 100 nm (see Figures 2(a) and 2(b)). Figure 2(c) displays the distribution of the NDCt size in suspension. The average value of the NDCt was about 230 μm , smaller than that of the BC powder (250 μm) without TEMPO treatment. The reduction of this size was attributable to the process of mash and homogenizing which may disintegrate some BC fibers as shown in Figure 2(b) (brown arrow).

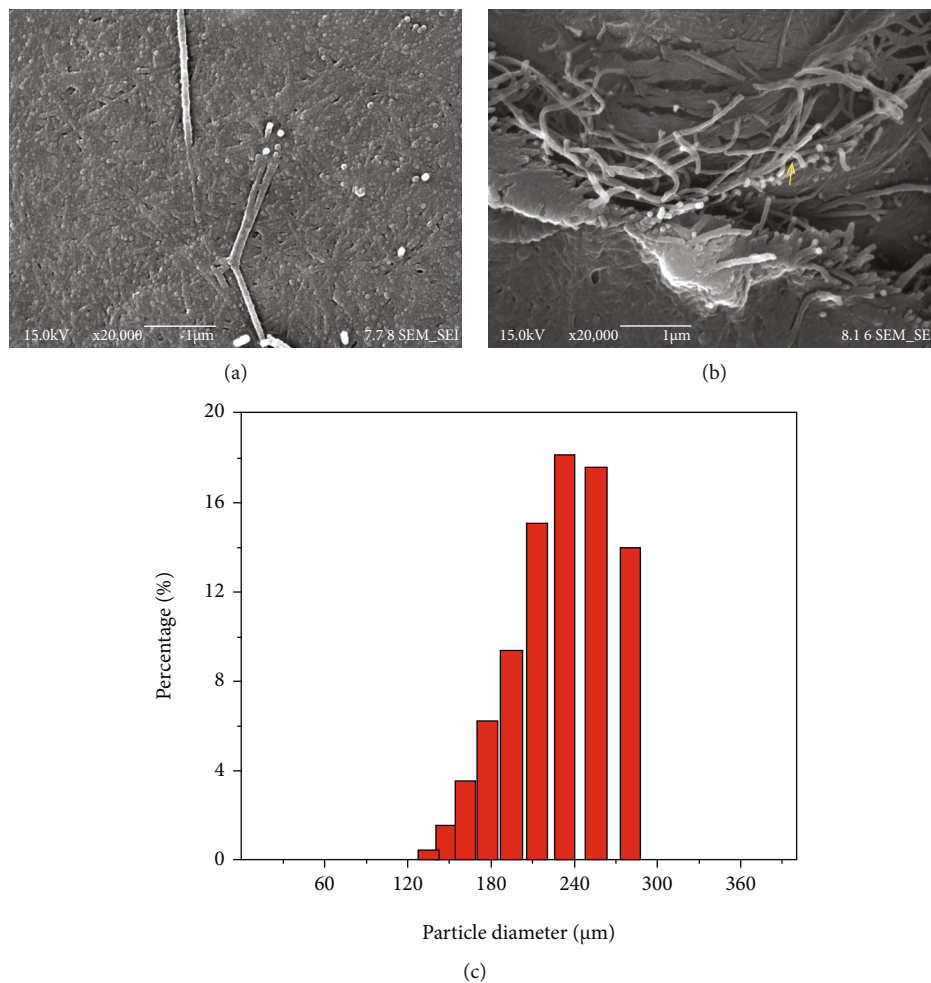


FIGURE 2: FE-SEM of (a) BC film, (b) the NDcT film, and (c) NDcT size in suspension after measuring using a PSA.

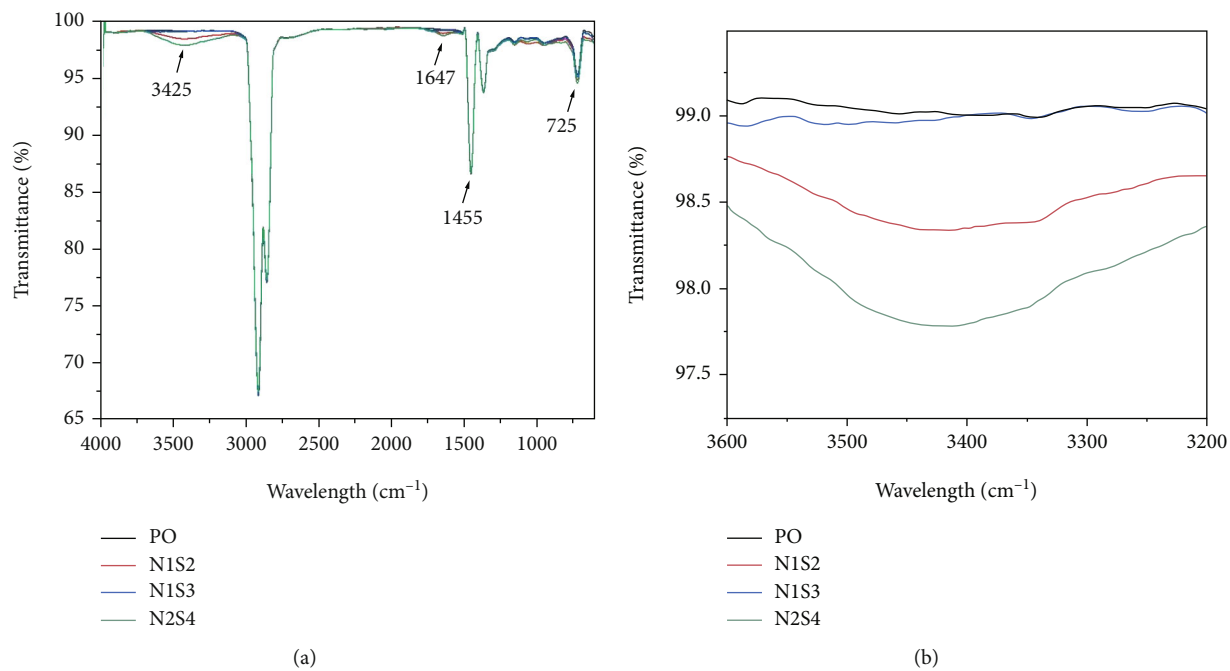


FIGURE 3: FTIR spectra of PO and biolubricant with (a) complete spectrum and (b) sections of the hydroxyl groups.

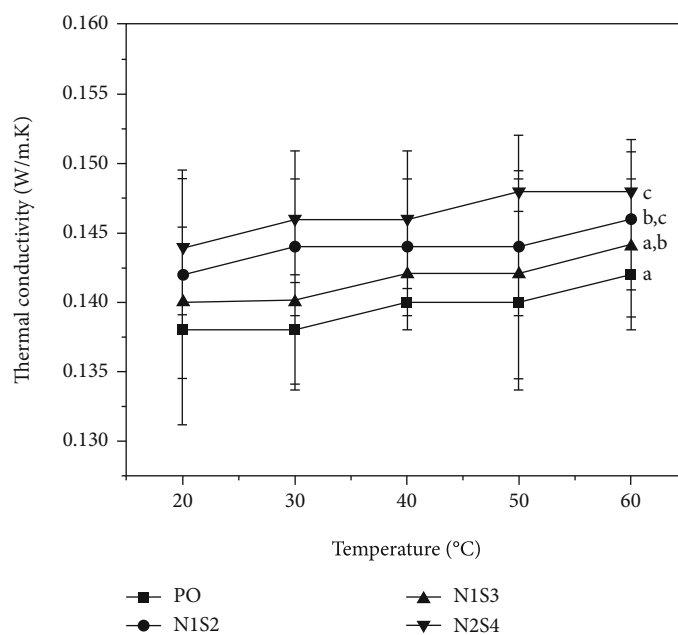


FIGURE 4: Thermal conductivity of PO and biolubricants. Different subscripts (a, b, c) indicate significant differences at $p \leq 0.05$.

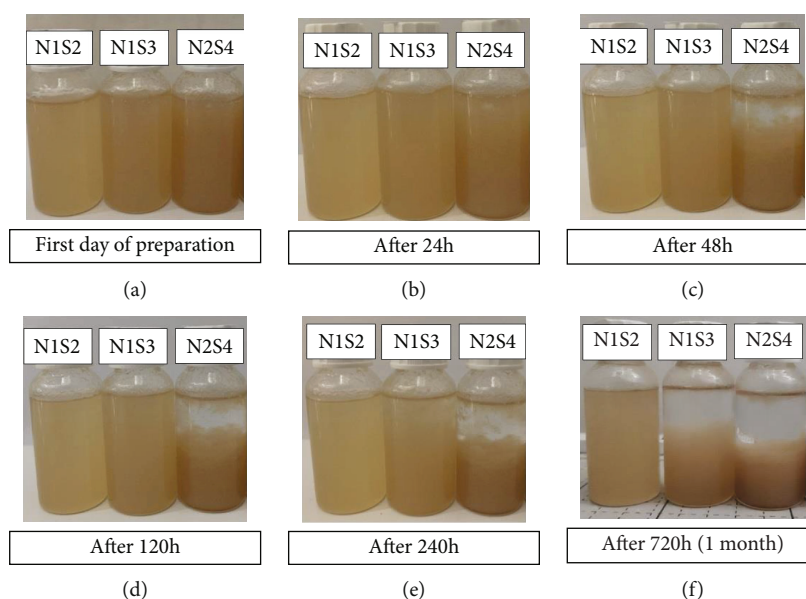


FIGURE 5: Stability observation of biolubricants at particular time.

3.2. FTIR. The FTIR spectra of biolubricants were shown in Figure 3. All samples display a similar form of the spectrum, but the difference in the bands and intensity. Figure 3(b) presents O-H stretching vibration in the range of $3100\text{--}3500\text{ cm}^{-1}$ which is a characteristic of the bacterial cellulose nanofiber [15]. A band of --C=O groups at the peak of 1647 cm^{-1} confirms ester corresponds to the POE's methyl group [33]. The peak at 1455 cm^{-1} belongs to --CH_2 groups of alkyl chains [34, 35]. A band at the peak of 725 cm^{-1} is due to the presence of C-H vibrations [33]. PO sample did not have a peak of the O-H functional group (Figure 3(b)). As expected, the addition of NDCt in the PO sample led to the broader band and

stronger intensity shown by the N1S2 and N2S4 samples. The strongest intensity was observed on the N2S4 sample corresponding to the highest amount of NDCt in the fluid [36]. However, the N1S3 biolubricant displays weaker intensity of the peak of the O-H group than the N1S2 sample. This is probably a result of an excessive amount of surfactant which is more hydrophobic than NDCt [37].

3.3. Thermal Conductivity. Figure 4 showed the thermal conductivity of the PO and biolubricant samples as a function of temperature. Increasing temperature improved the thermal conductivity resulting from an increase of the Brownian

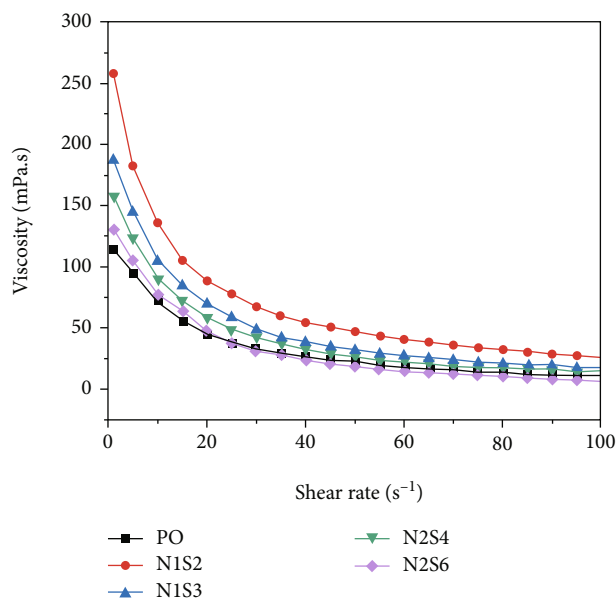


FIGURE 6: Viscosity of PO and biolubricants.

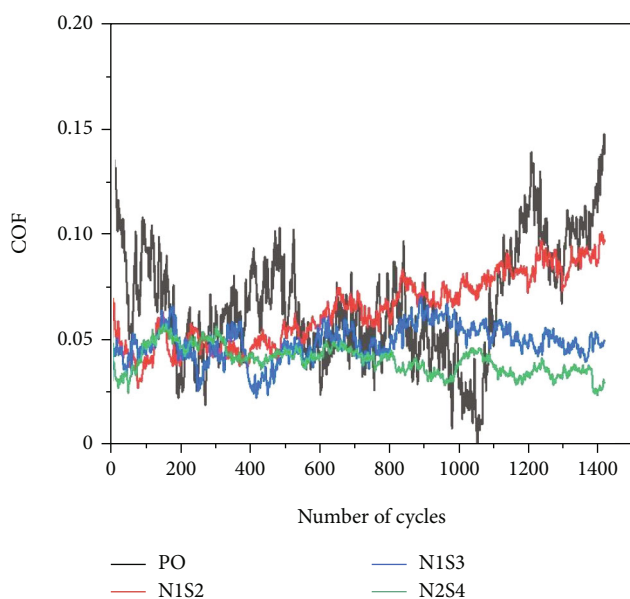


FIGURE 7: The friction coefficient of PO and biolubricants.

motion of nanoparticles [38]. Biolubricants had higher thermal conductivity compared to the PO sample. This corresponds to the thermal conductivity of bacterial cellulose (0.9 W/m.K) which is higher than POE (0.14 W/m.K) at room temperature [16]. Adding NDCt and Span 60 with ratio 1:2 to the PO sample led to a significant increase ($p < 0.05$) in thermal conductivity of the biolubricant. The most conductive sample was measured on the N2S4 biolubricant with the average value of 0.146 W/mK (at 60°C) which is increased significantly by 4% compared to PO sample. This increment is because the mobility of the NDCt particle in the fluid-created microscopic motion which caused micro-convection [39]. Further adding the NDCt particle into the fluid will create faster motion due to more intense van der

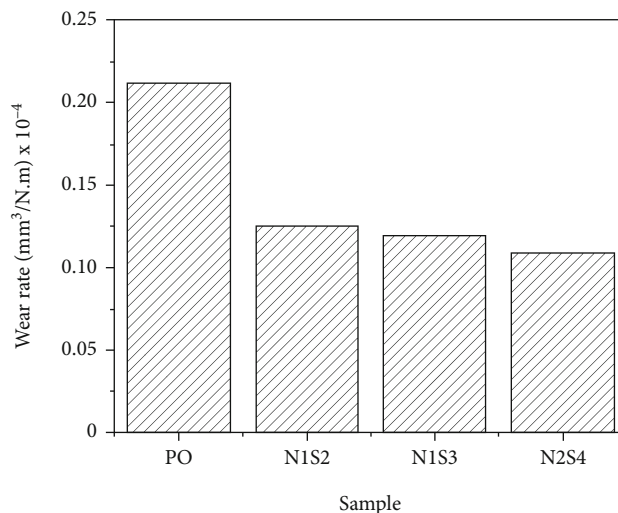


FIGURE 8: The wear rate for the lubricants under speed of 200 rpm and 5.5 N load.

Wall forces between the NDCt particles, which increases the heat transfer process [39]. Thermal conductivity of the N1S3 sample was lower than the case of N1S2 probably as a result of excessive surfactant which is consistent with Figure 3.

3.4. Stability and Viscosity. To stabilize the fibers in the oil, a low hydrophilic-lipophilic balance (HLB) of surfactant is required [20]. Span 60 has an HLB value of 4.7, which is ideal in this condition [24]. The qualitative sedimentation method via photo capturing was used to observe the biolubricant's stability, as presented in Figure 5. A good stability nanofluid is indicated with no more than 30% sedimentation after a month [40]. It shows that N1S2 is the most stable sample with no NDCt accumulation at the bottom of the test tube after a month of sedimentation observation (Figure 5(f)).

On the other hand, the N2S4 sample was sedimented after two days of investigation (Figure 5(c)). The N1S2 and N2S4 samples have the same NDCt and Span 60 ratios (1:2). The N1S2 sample obtained better stability than the N2S4. This result is probably due to the higher concentration of the surfactant (span 60) decreasing the viscosity of biolubricants, thus increasing the particle's sedimentation velocity due to the effect of the faster Brownian motion and higher activity of van der Waals forces [41].

Figure 6 shows the viscosity of all samples measured with increasing shear rate ranges from 5 to 100/s at 25°C. It can be seen that the viscosity of the biolubricant is increased with the addition of NDCt. The N1S2 sample has the highest viscosity compared to POE. A decrease in viscosity occurs when the amount of the surfactant is increased. The N2S4 sample had the lowest viscosity value compared to other biolubricant samples. This tendency corresponds to a high concentration of Span 60 reducing the viscosity value [42]. The long chain of saturated hydrocarbon molecules in POE can crystallize with the alkane groups from Span 60; thus, the POE bonds become weaker [42].

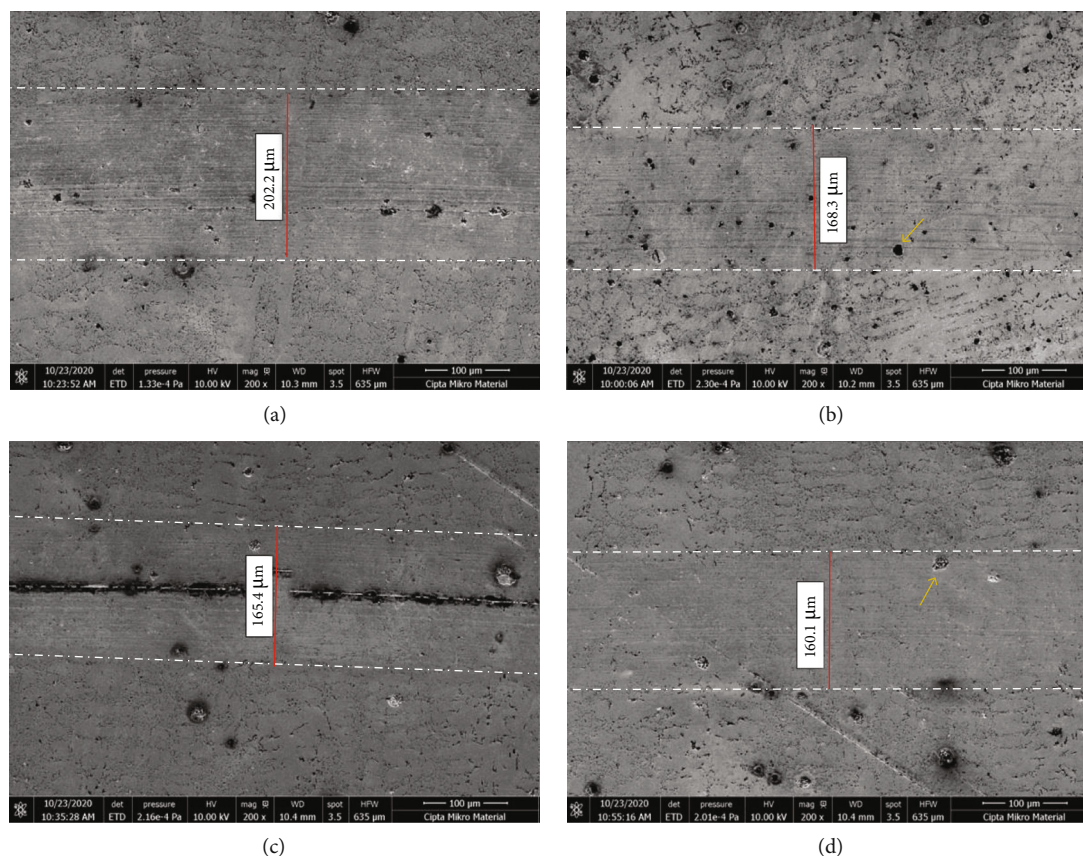


FIGURE 9: The SEM micrographs of wear scar width (distance between two white dash-dot lines) on the surface of grey cast iron disk after the friction test using (a) PO, (b) N1S2, (c) N1S3, and (d) N2S4. Brown arrows indicate black pits.

3.5. Tribological Studies (Friction and Worn Analysis). The coefficient of friction (COF) along the cycle number for each sample is displayed in Figure 7. The PO without filler shows the rougher curve during the running-in period probably because of higher friction between the ball and disk surface [12]. After the addition of fillers (NDCt and Span 60) in POE, the curve became smoother due to lower friction. At the cycle number of 1395, the N2S4 sample displayed the lowest COF value (0.024), a decrease of 79% compared with POE (0.1). This is consistent with Figure 8 showing the addition of NDCt and Span 60 into POE decreased the WR of sliding surfaces. The lowest WR value was observed on the N2S4 sample, reduced to 49% compared to the PO sample. This tendency is also supported by Figure 9 showing the SEM surface morphology of worn block on the disk surface after using each sample. As shown in the figure, the wear scar width (the distance between two white dash-dot lines) after using the biolubricant was reduced. The width value of the PO, N1S2, N1S3, and N2S4 samples directly measured from SEM observation was 202.2, 168.3, 165.4, and 160.1 μm , respectively. The lowest value for the N2S4 sample corresponds to the smallest contact between the sliding surface resulting from the formation of a triboboundary film from the biolubricant between these sliding surfaces [43]. The use of this N2S4 sample also resulted in the smoothest surfaces and the fewest number of black pits (brown arrow in Figure 9(d)) on the wear track area. This phenomenon may

be the nanosized NDCt fibers which fill the scars and grooves of the rubbing surface (the mending and polishing effect) minimize surface roughness [44]. These results are similar to a previous research on lubrication performance of polyalphaolefin oil with cellulose nanocrystals [27]. This work observed a COF improvement of 30% compared to the base oil.

4. Conclusion

This research work has explored tribology properties of the biolubricant prepared from POE mixed with the NDCt microparticle and Span 60. The results have demonstrated that the NDCt effectively improved the tribological properties of the base oil. The addition of NDCt as an additive in POE has decreased the wear rate and the wear scar as a result of the decreased contact between the sliding surfaces. The best tribology performance was found on the N2S4 sample from mixing of 0.6 wt.% of NDCt and 1.2 wt% surfactant. The use of this sample reduced the average COF value of about 40% and resulted in the smallest contact between the sliding surface, the smoothest surfaces of the wear tracks, and the maximum wear rate reduction of about 49% compared with POE. These results offer deeper insights into the effect of fillers on the improvement of tribology properties of ecofriendly biolubricant prepared from bacterial cellulose nanofibers.

Data Availability

The participants of this study agree for their data to be shared publicly.

Conflicts of Interest

We affirm that there is no conflict of interest.

Acknowledgments

This study was supported by the Hibah Publikasi di Jurnal Internasional terindeks Scopus, tahun 2021; the Jurusan Teknik Mesin, Fakultas Teknik, Universitas Andalas, tahun 2021; and the Research and Development Directorates Universitas Indonesia for supporting research funding with project name "PUTI KI 2Q2," number NKB-787UN2.RST/HKP.05.00/2020.











References

- [1] M. Z. Sharif, W. H. Azmi, A. A. M. Redhwan, R. Mamat, and G. Najafi, "Energy saving in automotive air conditioning system performance using SiO₂/PAG nanolubricants," *Journal of Thermal Analysis and Calorimetry*, vol. 135, no. 2, pp. 1285–1297, 2019.
- [2] W. K. Shafi, A. Raina, and M. I. Ul Haq, "Performance evaluation of hazelnut oil with copper nanoparticles - a new entrant for sustainable lubrication," *Industrial Lubrication and Tribology*, vol. 71, no. 6, pp. 749–757, 2019.
- [3] I. Minami, "Molecular science of lubricant additives," *Applied Sciences*, vol. 7, no. 5, p. 445, 2017.
- [4] R. Anand, A. Raina, M. I. Ul Haq, M. J. Mir, O. Gulzar, and M. Wani, "Synergism of TiO₂ and graphene as nano-additives in bio-based cutting fluid-an experimental investigation," *Tribology Transactions*, pp. 1–18, 2021.
- [5] H. Wu, F. Jia, J. Zhao et al., "Effect of water-based nanolubricant containing nano-TiO₂ on friction and wear behaviour of chrome steel at ambient and elevated temperatures," *Wear*, vol. 426–427, pp. 792–804, 2019.
- [6] S. Gryglewicz and B. Kolwzan, "Synthesis and biodegradation of synthetic oils based on adipic and sebacic esters," *Journal of Synthetic Lubrication*, vol. 20, no. 4, pp. 281–288, 2004.
- [7] A. Z. Syahir, N. W. M. Zulkifli, H. H. Masjuki et al., "A review on bio-based lubricants and their applications," *Journal of Cleaner Production*, vol. 168, pp. 997–1016, 2017.
- [8] S. Shankar, M. Manikandan, D. K. Karupannasamy, C. Jagadeesh, A. Pramanik, and A. K. Basak, "Investigations on the tribological behaviour, toxicity, and biodegradability of kapok oil bio-lubricant blended with (SAE20W40) mineral oil," *Biomass Conversion and Biorefinery*, pp. 1–13, 2021.
- [9] R. K. Hewstone, "Environmental health aspects of lubricant additives," *Science of the total environment*, vol. 156, no. 3, pp. 243–254, 1994.
- [10] R. Kumar, M. I. Ul Haq, A. Raina, and A. Anand, "Industrial applications of natural fibre-reinforced polymer composites – challenges and opportunities," *International Journal of Sustainable Engineering*, vol. 12, no. 3, pp. 212–220, 2019.
- [11] I. Bhushan, V. K. Singh, and D. K. Tripathi, *Nanomaterial and Environmental Biotechnology*, Springer, Cham, 2020.
- [12] N. W. Awang, D. Ramasamy, K. Kadirgama, G. Najafi, and N. A. Che Sidik, "Study on friction and wear of cellulose nanocrystal (CNC) nanoparticle as lubricating additive in engine oil," *International Journal of Heat and Mass Transfer*, vol. 131, pp. 1196–1204, 2019.
- [13] N. Din, N. R. Gilkes, B. Tekant, R. C. Miller, R. A. J. Warren, and D. G. Kilburn, "Non-hydrolytic disruption of cellulose fibres by the binding domain of a bacterial cellulase," *Bio/Technology*, vol. 9, no. 11, pp. 1096–1099, 1991.
- [14] D. Klemm, E. D. Cranston, D. Fischer et al., "Nanocellulose as a natural source for groundbreaking applications in materials science: today's state," *Materials Today*, vol. 21, no. 7, pp. 720–748, 2018.
- [15] H. Abral, V. Lawrensius, D. Handayani, and E. Sugiarti, "Preparation of nano-sized particles from bacterial cellulose using ultrasonication and their characterization," *Carbohydrate Polymers*, vol. 191, pp. 161–167, 2018.
- [16] K. Uetani, T. Okada, and H. T. Oyama, "In-plane anisotropic thermally conductive nanopapers by drawing bacterial cellulose hydrogels," *ACS Macro Letters*, vol. 6, no. 4, pp. 345–349, 2017.
- [17] Z. Tang, W. Li, X. Lin et al., "TEMPO-oxidized cellulose with high degree of oxidation," *Polymers*, vol. 9, no. 12, p. 421, 2017.
- [18] D. Li, P. Gao, X. Sun, S. Zhang, F. Zhou, and W. Liu, "The study of TEMPOs as additives in different lubrication oils for steel/steel contacts," *Tribology International*, vol. 73, pp. 83–87, 2014.
- [19] T. Saito, S. Kimura, Y. Nishiyama, and A. Isogai, "Cellulose nanofibers prepared by TEMPO-mediated oxidation of native cellulose," *Biomacromolecules*, vol. 8, no. 8, pp. 2485–2491, 2007.
- [20] W. Yu and H. Xie, "A review on nanofluids: preparation, stability mechanisms, and applications," *Journal of Nanomaterials*, vol. 2012, 17 pages, 2012.
- [21] M. A. Khairul, K. Shah, E. Doroodchi, R. Azizian, and B. Moghtaderi, "Effects of surfactant on stability and thermophysical properties of metal oxide nanofluids," *International Journal of Heat and Mass Transfer*, vol. 98, pp. 778–787, 2016.
- [22] H. W. Xian, N. A. C. Sidik, and R. Saidur, "Impact of different surfactants and ultrasonication time on the stability and thermophysical properties of hybrid nanofluids," *International Communications in Heat and Mass Transfer*, vol. 110, p. 104389, 2020.
- [23] S. A. Savrik, D. Balköse, and S. Lku, "Synthesis of zinc borate by inverse emulsion technique for lubrication," *Journal of Thermal Analysis and Calorimetry*, vol. 104, no. 2, pp. 605–612, 2011.
- [24] K. Gao, Q. Chang, and B. Wang, "The dispersion and tribological performances of magnesium silicate hydroxide nanoparticles enhanced by Span 60 oleogel," *Journal of Sol-Gel Science and Technology*, vol. 94, no. 1, pp. 165–173, 2020.
- [25] L. Yu, M. Dong, B. Ding, and Y. Yuan, "Emulsification of heavy crude oil in brine and its plugging performance in porous media," *Chemical Engineering Science*, vol. 178, pp. 335–347, 2018.
- [26] K. Uvanesh, S. S. Sagiri, K. Senthilguru et al., "Effect of span 60 on the microstructure, crystallization kinetics, and mechanical properties of stearic acid oleogels : an in-depth analysis," *Journal of Food Science*, vol. 81, no. 2, pp. E380–E387, 2016.
- [27] K. Li, X. Zhang, C. Du et al., "Friction reduction and viscosity modification of cellulose nanocrystals as biolubricant additives

- in polyalphaolefin oil,” *Carbohydrate Polymers*, vol. 220, pp. 228–235, 2019.
- [28] N. W. Awang, D. Ramasamy, K. Kadirgama, M. Samykano, G. Najafi, and N. A. Che Sidik, “An experimental study on characterization and properties of nano lubricant containing cellulose nanocrystal (CNC),” *International Journal of Heat and Mass Transfer*, vol. 130, pp. 1163–1169, 2019.
- [29] C. Huang, H. Ji, Y. Yang et al., “TEMPO-oxidized bacterial cellulose nanofiber membranes as high-performance separators for lithium-ion batteries,” *Carbohydrate polymers*, vol. 230, p. 115570, 2020.
- [30] I. M. Shahrul, I. M. Mahbubul, R. Saidur, and M. F. M. Sabri, “Experimental investigation on Al_2O_3 -W, SiO_2 -W and ZnO-W nanofluids and their application in a shell and tube heat exchanger,” *International Journal of Heat and Mass Transfer*, vol. 97, pp. 547–558, 2016.
- [31] Z. Fuadi, K. Adachi, and T. Muhammad, “Formation of carbon-based tribofilm under palm methyl ester,” *Tribology Letters*, vol. 66, no. 3, p. 88, 2018.
- [32] M. Fella, M. Abdul Samad, M. Labaiz, O. Assala, and A. Iost, “Sliding friction and wear performance of the nanobioceramic α - Al_2O_3 prepared by high energy milling,” *Tribology International*, vol. 91, pp. 151–159, 2015.
- [33] V. Bonu, N. Kumar, A. Das, S. Dash, and A. K. Tyagi, “Enhanced lubricity of SnO₂ nanoparticles dispersed polyolester nanofluid,” *Industrial and Engineering Chemistry Research*, vol. 55, no. 10, pp. 2696–2703, 2016.
- [34] T. Aging and A. Munajad, “Fourier transform infrared (FTIR) spectroscopy analysis of transformer paper in mineral oil-paper composite insulation under accelerated thermal aging,” *Energies*, vol. 11, no. 2, p. 364, 2018.
- [35] F. Niu, M. Li, Q. Huang et al., “The characteristic and dispersion stability of nanocellulose produced by mixed acid hydrolysis and ultrasonic assistance,” *Carbohydrate Polymers*, vol. 165, pp. 197–204, 2017.
- [36] Y. Chen, F. Wang, L. Dong et al., “Design and optimization of flexible polypyrrole/bacterial cellulose conductive nanocomposites using response surface methodology,” *Polymers*, vol. 11, no. 6, p. 960, 2019.
- [37] D. H. Khan, S. Bashir, P. Figueiredo, H. A. Santos, M. I. Khan, and L. Peltonen, “Process optimization of ecological probe sonication technique for production of rifampicin loaded niosomes,” *Journal of Drug Delivery Science and Technology*, vol. 50, pp. 27–33, 2019.
- [38] M. R. Esfahani, E. M. Languri, and M. R. Nunna, “Effect of particle size and viscosity on thermal conductivity enhancement of graphene oxide nanofluid,” *International Communications in Heat and Mass Transfer*, vol. 76, pp. 308–315, 2016.
- [39] K. H. Solangi, S. N. Kazi, M. R. Luhur et al., “A comprehensive review of thermo-physical properties and convective heat transfer to nanofluids,” *Energy*, vol. 89, pp. 1065–1086, 2015.
- [40] L. Samylingam, K. Anamalai, K. Kadirgama et al., “Thermal analysis of cellulose nanocrystal-ethylene glycol nanofluid coolant,” *International Journal of Heat and Mass Transfer*, vol. 127, pp. 173–181, 2018.
- [41] A. Ghadimi, R. Saidur, and H. S. C. Metselaar, “A review of nanofluid stability properties and characterization in stationary conditions,” *International Journal of Heat and Mass Transfer*, vol. 54, no. 17–18, pp. 4051–4068, 2011.
- [42] X. Gu, L. Gao, Y. Li et al., “Performance and mechanism of span surfactants as clean flow improvers for crude oil,” *Petroleum Chemistry*, vol. 60, no. 1, pp. 140–145, 2020.
- [43] L. Kerni, A. Raina, and M. I. U. Haq, “Friction and wear performance of olive oil containing nanoparticles in boundary and mixed lubrication regimes,” *Wear*, vol. 426–427, pp. 819–827, 2019.
- [44] G. Liu, X. Li, B. Qin, D. Xing, Y. Guo, and R. Fan, “Investigation of the mending effect and mechanism of copper nanoparticles on a tribologically stressed surface,” *Tribology Letters*, vol. 17, no. 4, pp. 961–966, 2004.

Research Article

Antimicrobial Edible Film Prepared from Bacterial Cellulose Nanofibers/Starch/Chitosan for a Food Packaging Alternative

Hairul Abral ¹, Angga Bahri Pratama ², Dian Handayani ³, Melbi Mahardika ⁴,
Ibtisamatul Aminah ³, Neny Sandrawati ³, Eni Sugiarti ⁵, Ahmad Novi Muslimin ⁵,
S. M. Sapuan ⁶, and R. A. Ilyas ⁷

¹Department of Mechanical Engineering, Andalas University, 25163 Padang Sumatera Barat, Indonesia

²Program Studi Teknik Mesin, Universitas Dharma Andalas, 25000 Padang Sumatera Barat, Indonesia

³Laboratory of Sumatran Biotal/Faculty of Pharmacy, Andalas University, 25163 Padang, Sumatera Barat, Indonesia

⁴Department of Biosystems Engineering, Institut Teknologi Sumatera, 35365 South Lampung, Indonesia

⁵Laboratory of High-Temperature Coating, Research Center for Physics Indonesian Institute of Sciences (LIPI), Serpong, Indonesia

⁶Department of Mechanical and Manufacturing Engineering, Faculty of Engineering, Universiti Putra Malaysia, 43400 UPM Serdang, Selangor, Malaysia

⁷School of Chemical and Energy Engineering, Faculty of Engineering, Universiti Teknologi Malaysia, 81310 Skudai, Johor Bahru, Johor, Malaysia

Correspondence should be addressed to Hairul Abral; habral@yahoo.com

Received 2 January 2021; Revised 9 March 2021; Accepted 15 March 2021; Published 1 April 2021

Academic Editor: Victor H. Perez

Copyright © 2021 Hairul Abral et al. This is an open access article distributed under the Creative Commons Attribution License, which permits unrestricted use, distribution, and reproduction in any medium, provided the original work is properly cited.

As a contribution to the growing demand for environmentally friendly food packaging films, this work produced and characterized a biocomposite of disintegrated bacterial cellulose (BC) nanofibers and tapioca starch/chitosan-based films. Ultrasonication dispersed all fillers throughout the film homogeneously. The highest fraction of dried BC nanofibers (0.136 g) in the film resulted in the maximum tensile strength of 4.7 MPa. 0.136 g BC nanofiber addition to the tapioca starch/chitosan matrix increased the thermal resistance (the temperature of maximum decomposition rate from 307 to 317°C), moisture resistance (after 8 h) by 8.9%, and water vapor barrier (24 h) by 27%. All chitosan-based films displayed antibacterial activity. This characterization suggests that this environmentally friendly edible biocomposite film is a potential candidate for applications in food packaging.

1. Introduction

The demand for affordable environmentally friendly plastic substitutes made from renewable sources continues to increase resulting in a growing interest in the research community in plant-based replacements for nondegradable plastics [1–3]. For the food packaging industry, promising cheap and abundant eco-friendly edible film-forming materials include starches, pure bacterial cellulose nanofibers, and chitosan [4]. However, films made of starch alone have low mechanical and thermal properties, high moisture absorption, and poor antimicrobial resistance [5, 6]. Many attempts have been conducted previously to reduce these

weaknesses by adding environmentally friendly fillers to the starch film [7–10]. Of these edible fillers, cellulose fiber and chitosan have significant potential, with one being one of the most abundant in nature [10, 11]. Cellulose fiber has good mechanical properties and flexibility but no antimicrobial activity [12]. The tensile and thermal properties of the starch film were improved after reinforcement with randomly oriented cellulose fibers from kenaf [13], water hyacinth [14], and softwood [15]. However, these short cellulose nanofiber preparation methods tend to use potentially harmful chemicals and result in a high residue of hemicellulose, lignin, or other impurities. Nanofiber from bacterial cellulose pellicle has none of these disadvantages because it consists of large

amounts of pure cellulose fibers with nanosized diameters [16]. Short BC nanofibers can be prepared from this pellicle using a high-shear homogenizer with a rotating blade to disintegrate the long fibers into nanosized lengths [17]. Recently, previous work has reported the interesting results that the microbial activity of the disintegrated BC/chitosan film was less than that of the BC sheet/chitosan one [1].

Chitosan has several advantages including antimicrobial activity, controlled release of food ingredients and drugs, relatively low cost, and widespread availability from a stable renewable source [5, 18]. Numerous studies have been performed on the development of edible biocomposite films made from chitosan, cellulose, and starch [19, 20]. Of course, as a food packaging material, this polysaccharide-based edible film should protect foods against deterioration due to microorganisms, moisture, dust, odors, and mechanical forces [21, 22]. There have been many previous studies reporting on the improved properties of the biocomposite film. However, characterizations of chitosan and disintegrated BC nanofiber content on tapioca starch-based biocomposites' properties have yet to be reported. This study understands the effect of the addition of both chitosan and disintegrated nanofiber from BC pellicle on the properties of this edible biocomposite film more completely. All samples were characterized by field emission scanning electron microscopy (FESEM), X-ray diffraction (XRD), Fourier transform infrared (FTIR), and thermogravimetric analysis (TGA). Opacity, moisture absorption (MA), water vapor permeability (WVP), and tensile properties were also measured.

2. Materials and Experiment

2.1. Materials. Local (Padang, Indonesia) commercially available tapioca starch (Cap Pak Tani brand) was washed once with distilled water to obtain pure tapioca starch. The pure wet starch was dried using a drying oven (Universal Oven Memmert UN-55) for 20 h at 50°C. The dried starch was filtered through a 63 μm mesh cloth. The chemical composition of dry starch granules was analyzed according to a previous amylopectin method [23]. The pure dried granular starch for this present work contained 14.5% of amylose and 85.5% of glycogen (Brataco brand) purchased from Brataco (Padang, Indonesia) and chitosan (degree of deacetylation: 94%) from CV. Chi Multiguna (Indramayu, Indonesia). Acetic acid (CH_3COOH , 5%) was used as the solvent for chitosan.

2.2. Preparation of Single BC Nanofiber and Films. Single BC nanofiber was isolated and characterized as in our previous work [24]. Briefly, a wet pellicle with a dimension ($248 \times 151 \times 22$ mm) was purchased from a local small-scale industry in Padang, Indonesia. This pellicle, which is a common addition to drinks or desserts in the form of nata de coco, is the result of a week-long fermentation of coconut water, glucose, and acetic acid with *Acetobacter xylinum* in a static closed container. Integration of the pellicle was carried out with a homogenizer and ultrasonication probe. The crystallinity index of the disintegrated BC nanofiber was about 71%. Figure 1 displays the steps of sample preparation from

raw BC until biocomposite. The film sample was prepared as follows:

Starch film. About 10 g purified tapioca granules, 100 mL distilled water, and 2 mL glycerol were mixed in a glass beaker (250 mL) using a hot plate stirrer (Daihan Scientific MSH-200) at 500 rpm and 65°C until completely gelatinized. The gel suspension was sonicated using an ultrasonic cell crusher (SJIA-1200W) at 600 W for 1 min, then poured onto a petri dish ($d = 145$ mm) and dried in a drying oven (Memmert Germany, Model 55 UN) at 50°C for 20 h.

Chitosan film. Simultaneously, a mixture of 2.5 g chitosan and 100 mL acetic acid was prepared in a glass beaker (250 mL) and heated using a hot plate stirrer at 80°C for 2 hours until gelatinization. The chitosan gel was filtered using 74 μm cheesecloth. The gel was poured onto a petri dish which was dried using the drying oven at 50°C for 20 h.

Starch/chitosan film. The two gels, starch and chitosan, were blended in the ratio of 80:20 (70 g total weight) using an ultrasonic cell crusher at 600 W for 1 min keeping the temperature below 65°C. The gel was poured onto a petri dish for drying as described in the starch sample preparation.

Biocomposite film. The blended starch/chitosan gels were mixed with the appropriate BC suspension (10, 15, or 20 mL). Each gel suspension was sonicated at 600 W for 1 min, then cast onto a petri dish and dried in the drying oven at 50°C for 20 h.

Abbreviations used for the studied samples with their compositions are shown in Table 1.

2.3. Characterization

2.3.1. FESEM Morphology of the Fracture Surface. The tensile sample's fracture surface morphology after the tensile test was observed using JIB-4610F FESEM from JEOL (Tokyo, Japan). At about 25 mm from its fracture surface, the tensile specimen was cut using a steel scissor (in perpendicular tensile direction) and placed on a specimen holder. All samples were coated with gold (Au). An accelerating voltage of 10 kV with 8 mA was set up for testing.

2.3.2. X-Ray Diffraction. The XRD pattern was recorded using an X'Pert PRO PANalytical instrument (Philips Analytical, Netherlands) with $\text{CuK}\alpha$ radiation ($\lambda = 0.154$) at 40 kV and 30 mA. The scanning range was 5° to 50°. The crystallinity index (CI) of the biocomposites was calculated using

$$\text{CI} = \left[\frac{(I_{002} - I_{\text{am}})}{I_{002}} \right] \times 100, \quad (1)$$

where I_{002} and I_{am} are the peak intensities of crystalline and amorphous regions, respectively [25].

2.3.3. Opacity Measurement. The opacity of the film was measured using a UV-Vis spectrophotometer (Shimadzu UV 1800, Japan) in the range 400-800 nm according to ASTM D 1003-00 (Standard Test Method for Haze and Luminous Transmittance of Transparent Plastics). Films of 0.38 mm thickness were cut into 10 mm \times 25 mm rectangles. The opacity measurement was repeated 3 times.



FIGURE 1: Steps of sample preparations for biocomposite.

TABLE 1: Composition of the starch film, chitosan film, and biocomposite films used in the study.

Sample code	Tapioca starch (g)	Nanofiber suspension (mL)	Dried nanofibers (g)	Aquades (mL)	Glycerol (mL)	Chitosan (g)	Acetic acid (mL)
GU	10	—	—	100	2	—	—
CH	—	—	—	—	—	2.5	100
GU/CH	10	—	—	100	2	2.5	100
GU/CH/10BC	10	10	0.068	100	2	2.5	100
GU/CH/15BC	10	15	0.102	100	2	2.5	100
GU/CH/20BC	10	20	0.136	100	2	2.5	100

2.3.4. Fourier Transform Infrared. FTIR spectra of films were recorded using a PerkinElmer FTIR spectrometer (Frontier Instrument, USA), equipped with deuterated triglycine sulfate, DTGS, detector, and extended range KBr beam splitter. This spectrometer was used in the frequency range in the wavenumber range of $4000\text{--}600\text{ cm}^{-1}$, at resolution 4 cm^{-1} with 32 scans per sample. Samples ($10\text{ mm} \times 10\text{ mm}$) were dried in the oven at 50°C until constant weight before characterization. The samples were made in powder and mixed with KBr as well as followed by the pressure within the pellet ultrathin layer [26].

2.3.5. Moisture Absorption and Water Vapor Permeability. *Moisture absorption (MA).* MA was determined using the method described in a previous study [27]. All biocomposite samples were dried in a drying oven (Memmert Germany, Model 55 UN) at 50°C until a constant weight was achieved. The dried sample was stored in a closed chamber with 75% RH at 25°C . The samples were weighed every 30 min for 7 h

with a precision balance (Kenko) with a 0.1 mg accuracy. MA was calculated using

$$MA = \frac{(w_h - w_o)}{w_o}, \quad (2)$$

where w_h is the final weight and w_o is the initial weight of the sample. MA determination was repeated 5 times for each film.

Water vapor permeability (WVP). WVP was measured according to the method described by previous work [28]. WVP determination was repeated 3 times for each film.

2.3.6. Thermogravimetric Analysis (TGA) and Derivative Thermogravimetry (DTG). TGA and DTG of all samples were characterized using a differential scanning calorimeter (Linseis TA type PT 1600, Germany). About 25 mg of the film was positioned on the microbalance located inside the

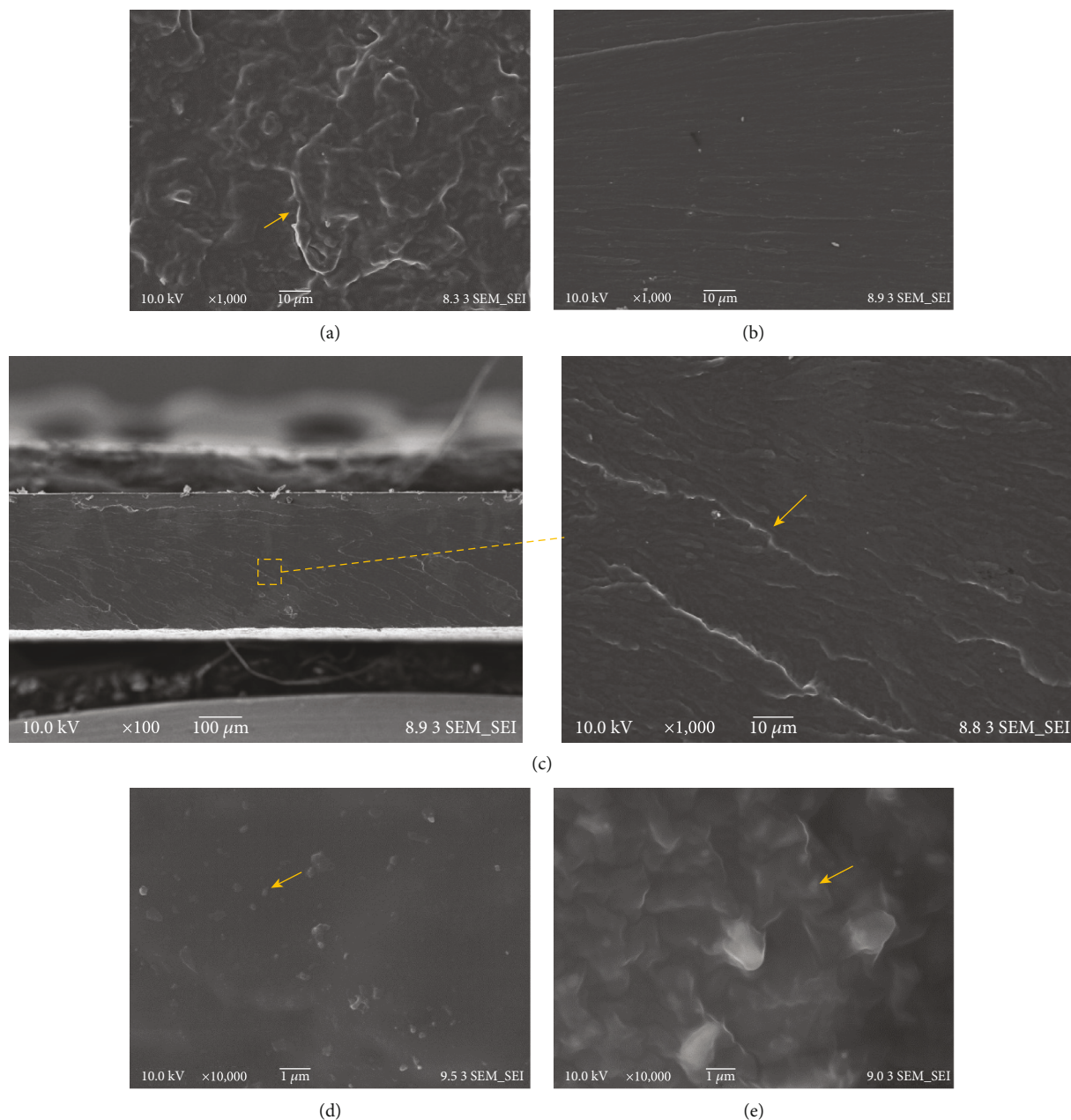


FIGURE 2: FESEM images of the fracture surface for the pure starch film (a), pure chitosan film (b), starch/chitosan film (c), GU/CH/15BC film (d), and GU/CH/20BC film (e).

furnace. The test was carried out from 35°C up to 550°C with a heating rate of 10°C/min in a nitrogen atmosphere.

2.3.7. Tensile Properties. Tensile properties of the biocomposites, including tensile strength and elongation at break, were measured using COM-TEN 95T Series 5K (Pinellas Park, USA) and were performed according to the ASTM D 638 type V standard. Before the test, all samples were stored in a desiccator with $50 \pm 5\%$ relative humidity at 25°C for 48 h. Samples were then tested at room temperature and RH 75% using a tensile test speed of 5 mm/min. The testing of the film was repeated at least three times for each fiber content.

2.3.8. Antimicrobial Activity. The antibacterial activity of the starch/chitosan-based biocomposite films was assayed using the agar diffusion method (Bauer, Kirby, Sherris, and Turck, 1966). Four microbe strains were used: Gram-positive *Staphylococcus aureus* and *Bacillus subtilis* bacteria and Gram-negative *Escherichia coli* and *Pseudomonas aeruginosa*. The microbial suspensions in saline solution (NaCl 0.85% sterile) were standardized using the McFarland scale to inoculate petri dishes containing nutrient agar for bacteria. 6 mm film diameter disks were placed on the inoculated agar then incubated at 30°C for 24 h. The diameter of the growth inhibition zones around the film disks was gauged visually. All tests

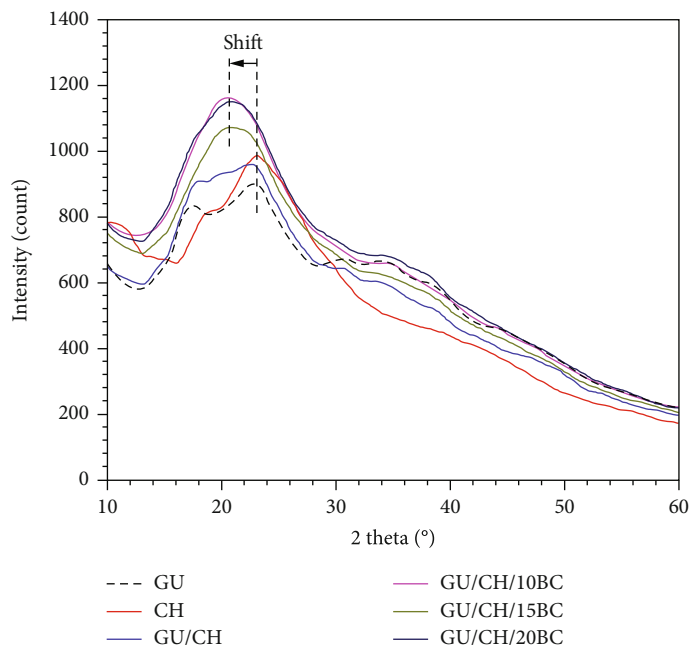


FIGURE 3: The XRD patterns of all samples.

TABLE 2: Crystallinity index, opacity value, and thermal properties of all samples.

Films	Crystallinity index (%)	Opacity (AUnm)*	Maximum decomposition temperature (°C)
GU	11	280.5 ± 0.16 ^d	268
CH	17	450.8 ± 0.04 ^f	311
GU/CH	14	202.3 ± 0.98 ^a	307
GU/CH/10BC	35	208.1 ± 1.09 ^b	313
GU/CH/15BC	36	237.9 ± 0.63 ^c	314
GU/CH/20BC	37	328.3 ± 0.76 ^e	317

*Different letters a, b, c, d, e, and f in the same column indicate significant differences in means ($p \leq 0.05$).

were carried out in triplicate, and the antibacterial activity was expressed as the mean of the inhibition diameters (mm).

2.3.9. Statistical Analysis. Experimental data were analyzed using IBM SPSS Statistics 25.0 (IBM Corporation, Chicago, USA). One-way analysis of variance (ANOVA) and a p test were used to identify the significance of any effects of varying nanofiber content on properties of the biocomposites. Duncan's multiple range tests were used on the MA and WVP results using a 95% ($p \leq 0.05$) confidence level.

3. Results and Discussion

3.1. Morphological Biocomposites. Figure 2 displays FESEM fracture surface micrographs for the pure starch film (a), pure chitosan film (b), starch/chitosan film (c), GU/CH/15BC film (d), and GU/CH/20BC film (e). The surface of the starch film was rough (Figure 2(a)) probably as a result of a long tortuous way of the polymer chains looking for the weak section of the chain structure. Meanwhile, the CH film had a smooth fracture surface (Figure 2(b)) attributed to unimpeded crack propagation and corresponding to its brittle properties.

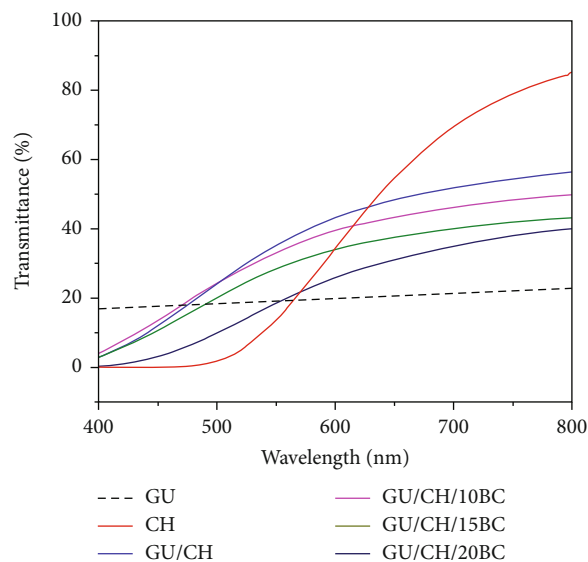


FIGURE 4: The transmittance of all samples.

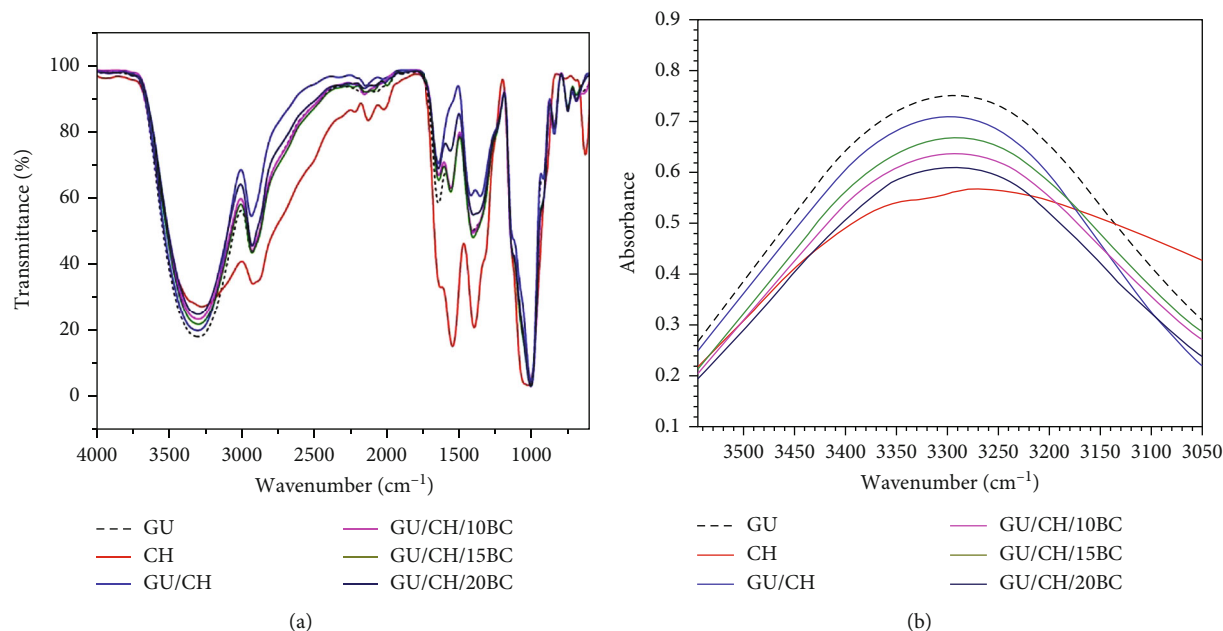


FIGURE 5: FTIR spectrum resulting from triplicate measurements of each film. The full spectrum from 4000 to 250 cm⁻¹ (a). Sections of the spectrum for O-H stretching vibration (b).

Figure 2(c) displays the GU/CH fracture surface, which was rougher than the CH sample. The different chemical structures of both these substances produce a weaker structural section in which the crack propagates with a longer tortuous way resulting in microscopic features known as a beach mark as shown by the yellow arrow in the inset of Figure 2(c) which marks an interruption of the cracking progress. Adding BC into the blends continuously increases the surface roughness of the biocomposite (yellow arrow in Figures 2(d) and 2(e)). In these figures, disintegrated BC nanofibers were dispersed homogeneously after ultrasonication. A similar result also is supported by previous studies [14, 17, 24, 29, 30].

3.2. X-Ray Diffraction. The X-ray diffraction curves for all studied films are shown in Figure 3. All films show a similar semicrystalline pattern with prominent peaks at about $2\theta = 20^\circ$ and 23° . The crystallinity index (CI) of each sample is shown in Table 2. The GU/CH blend film has a CI value of 14% between the CI of chitosan (17%) and the CI of the starch film (11%). The addition of any fraction of nanofibers to the starch-based matrix improves the CI value of the biocomposite films (around 164% increase compared to GU/CH). This increased value indicates better filler dispersion in the starch matrix thanks to ultrasonication [2]. Samples before mixing with nanofibers display the main peak position at $2\theta = 23^\circ$. The addition of the nanofibers shifted the position toward the left side ($2\theta = 20^\circ$). According to previous work, shifting the peak position to the left side can be associated with an increase in tensile residual stress resulting from increases in the polymer chains' interlayer spacing [31].

3.3. Transparency. In food packaging applications, high transparency can be an essential property [32]. The transparency values for all samples are displayed in Figure 4. The GU film displays low transmittance at all wavelengths. The high-

est transparency at 800 nm belongs to the CH film. Therefore, after mixing starch with chitosan, the GU/CH film became more transparent. However, the BC nanofiber addition to this GU/CH film significantly decreased ($p \leq 0.05$) the transparency of the biocomposite film. This phenomenon is because increasing amounts of the nanofiber increase the amount of reflected light in the film. The lowest transparency was consequently measured on the film with the highest fiber loading, the GU/CH/20BC film (28.9% less than the GU/CH film). This value still agrees with previous work [33]. Despite the decreasing transparency, this film was still clear enough to see through easily. The consistency of transparency readings in each of the repeats for each fiber loading, as shown by the small standard deviation values, confirms that the cellulose fibers are homogeneously dispersed in the starch-based matrix. This result is consistent with Figure 2(e) which shows beach marks spread evenly on all fracture surfaces of the biocomposite film.

3.4. FTIR Spectra. Structural changes in the starch-based film after mixing with chitosan or/and nanofibers can be observed using an FTIR curve. Figure 5 displays an FTIR curve of the mean transmittance values for three samples of each biocomposite. Shifts of peak intensity, broadening of absorption peaks, and appearance of new bands in the FTIR spectra correspond to structural changes [34]. There are absorption peaks in the GU film at about 3247 cm⁻¹ (-OH stretching) and 2917 cm⁻¹ due to CH stretching. The band at 1650 cm⁻¹ is present due to the deformation vibration of the absorbed water molecules. The characteristic absorption peak of chitosan is the band at 1559 cm⁻¹, which is assigned to the stretching vibration of the amino group of chitosan. Another band at 3367 cm⁻¹ is due to amine NH symmetric vibration. The wavenumber and T value of O-H stretching shift from

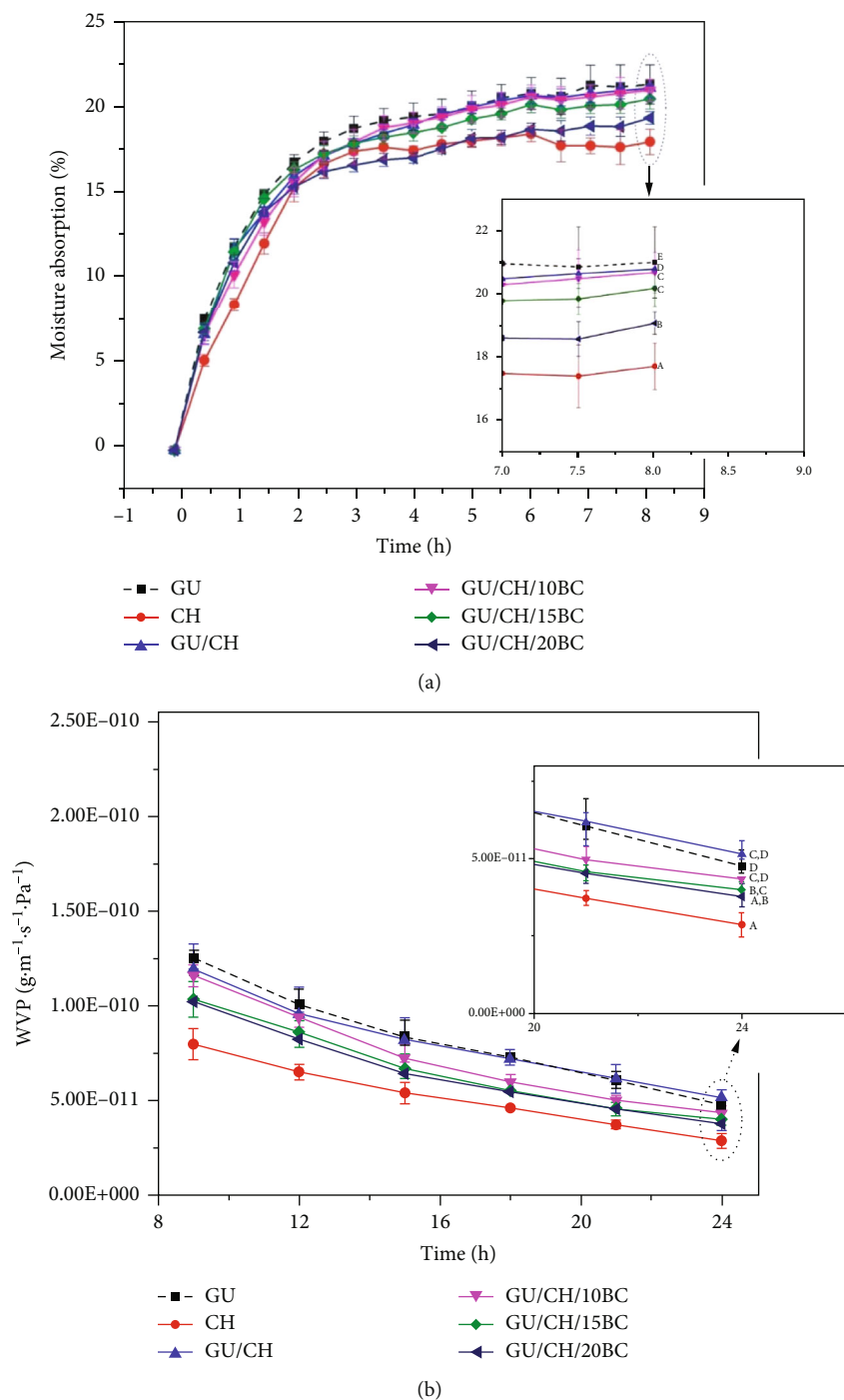


FIGURE 6: Average value of moisture absorption (a) and WVP (b) of each studied film. Different letters a, b, c, d, and e in the inset indicate significant differences ($p \leq 0.05$).

3290 cm^{-1} and 17.9% for the GU film to 3288 cm^{-1} and 19.6% for the GU/CH blend film. Similar shifting was also observed on the GU/CH-based biocomposite film due to the presence of nanofibers. For example, T of the GU/CH film at about 3290 cm^{-1} is 19.6% but 24.5% for the GU/CH/20BC film. As expected, increasing concentrations of BC increased the peak T and shifted the wavenumber of O-H functional groups. This case is probably a result of

increasing hydrogen bonds between starch and/or nanofiber polymer chains and amino functional groups [35].

3.5. Moisture Absorption and Water Vapor Permeability. Figure 6(a) shows the moisture absorption (MA) of the pure starch film, chitosan film, and starch/chitosan-based biocomposite film. The pure chitosan film has the lowest MA (17.7% after 8 h in the humid chamber). The presence of nanofibers

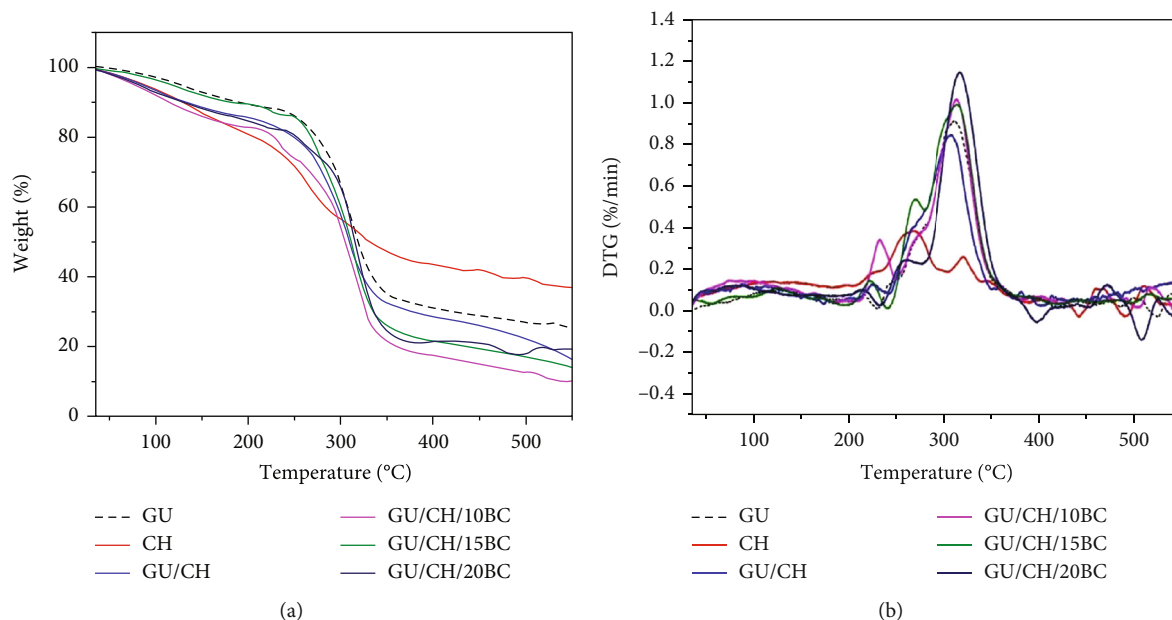


FIGURE 7: TGA (a) and DTG (b) charts of all samples.

in the starch/chitosan-based film results in a decrease in MA of the biocomposites. Higher nanofiber loading leads to lower average MA values. This result is because nanofiber and chitosan are more hydrophobic than the neat starch film. Dispersion of fillers in the starch film homogeneously results in decreasing MA of the biocomposite film. Better intermolecular hydrogen bonding between the starch matrix and the chitosan and fiber improves the moisture resistance of the biocomposite film due to reducing the number of free hydroxyl groups. This result is consistent with the FTIR pattern (Figure 5) showing the weakest intensity of O-H stretching and O-H of absorbed water peaks in the films with the highest nanofiber content due to the reduction in free hydroxyl groups. Similar findings of reducing moisture absorption with increased fiber loadings have also been reported previously [30]. Figure 5(b) shows water vapor permeability (WVP) of both starch and chitosan films and biocomposite films. As expected, the pattern of WVP with the addition of nanofibers is similar to that of MA. There is a decrease in the WVP value in films that contain more nanofibers. WVP of the GU/CH/20BC sample is 27% lower than that of the GU/CH film after 24 h. The decrease in WVP is because moisture is absorbed less readily into the biocomposite for the reasons described above.

Also, well-dispersed nanofiber hinders the path for water molecule diffusion through the film due to the more compact, homogeneous polymer structures [29]. As shown in Figure 6, the WVP value of the GU/CH/20BC film is $3.7 \times 10^{-11} \text{ g m}^{-1} \text{ s}^{-1} \text{ Pa}^{-1}$ (24 h), similar to that found in a previous study on the improvement of the shelf life of yam starch/chitosan-coated apples [36]. Therefore, this film has a good potential for the shelf life of various food types.

3.6. Thermal Properties. Figures 7(a) and 7(b) show TGA and DTG curves of each tested film as a function of temperature. There are three stages of weight loss of the film shown in a

TGA graph. The first stage at 100–150°C is related to weight loss in the film due to the evaporation of the absorbed moisture. This small amount of dehydration is evident in the DTG curve (Figure 7(b)). The weight loss for the second stage at 250–350°C is attributed to the decomposition of starch, chitosan, and nanofibers. In the temperature range of 360–570°C, a third weight loss was observed due to a final decomposition to ash. The temperature of the maximum decomposition rate (T_m) at the second stage was higher (311°C) for starch than for chitosan (268°C). As expected, the addition of chitosan to starch decreased the T_m value slightly (307°C). However, the thermal resistance of the starch/chitosan-based film became higher with the addition of nanofibers (Figures 7(a) and 7(b)). For example, the T_m of the GU/CH film increased from 10°C to 317°C after adding dried nanofibers of 0.136 g. This increased value is probably because of the higher crystallinity in the sample [30]. Also, the higher thermal resistance resulted from better interfacial hydrogen bonding between starch and nanofiber dispersed homogeneously [17, 30]. This result is consistent with the high CI value of films with high nanofiber content, as shown in the XRD curve (Table 2).

3.7. Tensile Properties. Figure 8 shows the tensile properties of all tested samples. TS for the GU/CH film was 2.6 MPa, a value between pure GU (1.4 MPa) and CH (3.2 MPa). As expected, the nanofiber addition to the GU/CH film led to an increase in its TS value. The maximum TS was 4.7 MPa, measured on the GU/CH/20BC film, reinforced with the highest fiber loading (0.136 g). This increased TS value probably results from the increased crystallinity index (Table 2), better nanofiber dispersion (Figure 2), and better interfacial hydrogen bonding between the nanofibers with the GU/CH matrix [20]. The pure chitosan film is the least brittle of all the films with an EB of only 0.98%. After mixing the chitosan with starch, the EB of the GU/CH film became higher (11%).

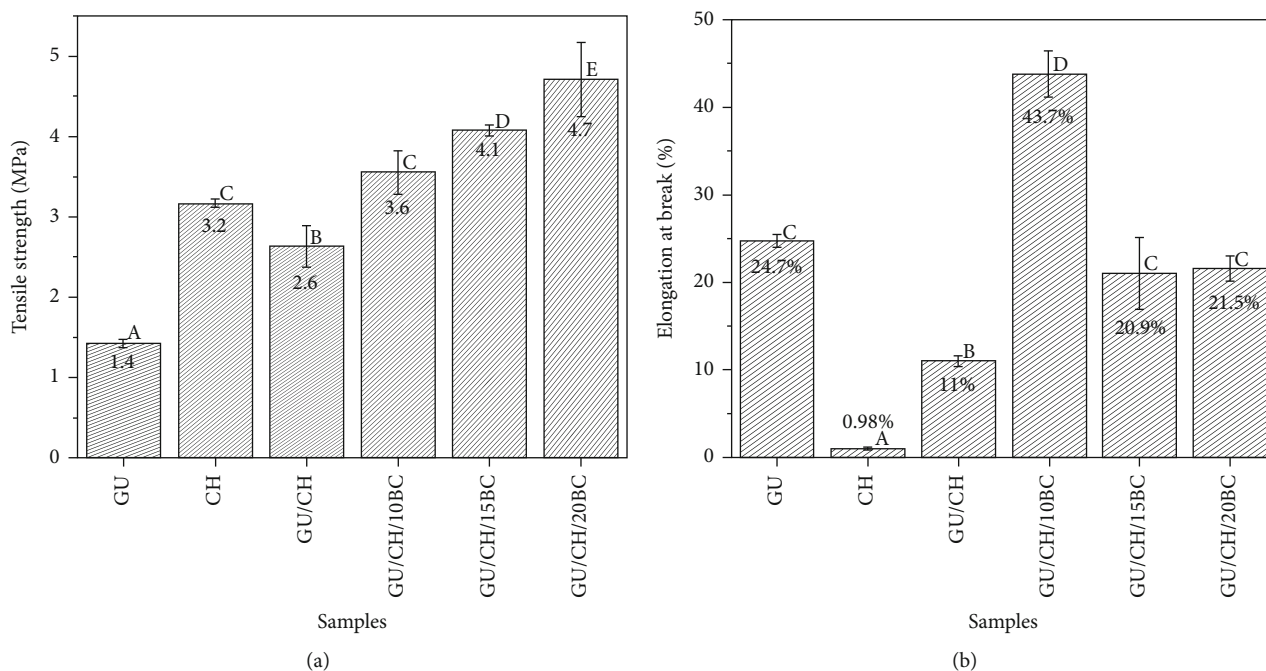


FIGURE 8: Tensile strength (a) and elongation at break (b) of each sample. Different letters a, b, c, d, and e in the vertical bar chart indicate significant differences ($p \leq 0.05$).

TABLE 3: Antibacterial activity of the films.

Films	Diameter of inhibition zones (mm) against microorganisms*			
	SA	BC	EC	PA
CH	20.9 ± 1.9	13.9 ± 7.2	12.8 ± 0.2	15.1 ± 0.1
GU	0	0	0	0
GU/CH	18 ± 1.6	12.3 ± 6.4	12.3 ± 6.9	12.0 ± 3.5
GU/CH/10BC	14.7 ± 6	11.9 ± 6.1	11.4 ± 5.5	11.3 ± 6.5
GU/CH/15BC	12.1 ± 7.2	10.5 ± 4.2	12.5 ± 2.5	10.3 ± 3.9
GU/CH/20BC	14.5 ± 5.8	10.6 ± 4.9	10.3 ± 1.5	13.4 ± 3.3
BC nanofibers	0	0	0	0

*SA = *Staphylococcus aureus*; BC = *Bacillus subtilis*; EC = *Escherichia coli*; PA = *Pseudomonas aeruginosa*.

Even the addition of the BC nanofibers to the GU/CH film improved its EB. This tendency is attributable to longer tortuous pathways of the crack propagation through the matrix due to the BC nanofibers. Further nanofiber loading did not result in statistically significant changes in EB of the biocomposite film.

3.8. Antibacterial Activity. Table 3 displays the diameters of antibacterial activity inhibition zones against all microorganisms tested in studied samples. BC nanofibers did not inhibit any microorganisms. This phenomenon is in good agreement with previous work [37]. A similar appearance was also displayed by the GU film without antibacterial activity. However, all chitosan-contained films were effective against Gram-positive bacteria and Gram-negative bacteria. This result could be due to the numerous active ingredients present in chitosan. Chitosan could adsorb the electronegative

substance in the cell, and it disturbs the physiological activities of the bacteria and kills them [38].

4. Conclusion

This work characterized a tapioca starch/chitosan-based film reinforced by bacterial cellulose nanofiber. All chitosan-based films had antibacterial activity. 0.136 g nanofiber addition to this film led to the highest tensile strength and the highest thermal resistance. The presence of nanofibers increased moisture resistance and water barrier properties. The addition of the nanofibers led to a decrease in transparency. However, the resulting translucent biocomposite film could still be seen through clearly. Overall, this biocomposite film could become a food packaging alternative for replacing hydrocarbon-based plastics.

Data Availability

We have data supporting the results of this work. The Microsoft Word document data used to support the findings of this study are available from the corresponding author upon request. Please email habral@yahoo.com.

Conflicts of Interest

We affirm that there is no conflict of interest.

Acknowledgments

Acknowledgment is addressed to Universitas Andalas for supporting research funding with project name PDU KRP1GB UNAND (number T/5/UN.16.17/PT.01.03/IS-PDU-KRP1GB/2020).

References

- [1] I. Dinika, D. K. Verma, R. Balia, G. L. Utama, and A. R. Patel, "Potential of cheese whey bioactive proteins and peptides in the development of antimicrobial edible film composite: a review of recent trends," *Trends in Food Science and Technology*, vol. 103, pp. 57–67, 2020.
- [2] M. Asrofi, H. Abrial, A. Kasim, A. Pratoto, M. Mahardika, and F. Hafizulhaq, "Characterization of the sonicated yam bean starch bionanocomposites reinforced by nanocellulose water hyacinth fiber (Whf): the effect of various fiber loading," *Journal of Engineering Science and Technology*, vol. 13, pp. 2700–2715, 2018.
- [3] H. Abrial, G. J. Putra, M. Asrofi, J. Park, and H. Kim, "Effect of vibration duration of high ultrasound applied to biocomposite while gelatinized on its properties," *Ultrasonics Sonochemistry*, vol. 40, no. Part A, pp. 697–702, 2018.
- [4] I. Gan and W. S. Chow, "Antimicrobial poly(lactic acid)/cellulose bionanocomposite for food packaging application: a review," *Food Packaging and Shelf Life*, vol. 17, pp. 150–161, 2018.
- [5] L. V. Cabañas-Romero, C. Valls, S. V. Valenzuela et al., "Bacterial cellulose-chitosan paper with antimicrobial and antioxidant activities," *Biomacromolecules*, vol. 21, no. 4, pp. 1568–1577, 2020.
- [6] M. Babaee, M. Jonoobi, Y. Hamzeh, and A. Ashori, "Biodegradability and mechanical properties of reinforced starch nanocomposites using cellulose nanofibers," *Carbohydrate Polymers*, vol. 132, pp. 1–8, 2015.
- [7] S. M. Noorbakhsh-Soltani, M. M. Zerfat, and S. Sabbaghi, "A comparative study of gelatin and starch-based nano-composite films modified by nano-cellulose and chitosan for food packaging applications," *Carbohydrate Polymers*, vol. 189, pp. 48–55, 2018.
- [8] Z. Shariatinia and M. Fazli, "Mechanical properties and antibacterial activities of novel nanobiocomposite films of chitosan and starch," *Food Hydrocolloids*, vol. 46, pp. 112–124, 2015.
- [9] S. Chillo, S. Flores, M. Mastromatteo, A. Conte, L. Gerschenson, and M. A. Del Nobile, "Influence of glycerol and chitosan on tapioca starch-based edible film properties," *Journal of Food Engineering*, vol. 88, no. 2, pp. 159–168, 2008.
- [10] U. Qasim, A. I. Osman, A. H. al-Muhtaseb et al., "Renewable cellulosic nanocomposites for food packaging to avoid fossil fuel plastic pollution: a review," *Environmental Chemistry Letters*, vol. 19, no. 1, pp. 613–641, 2021.
- [11] P. Cazón and M. Vázquez, "Mechanical and barrier properties of chitosan combined with other components as food packaging film," *Environmental Chemistry Letters*, vol. 18, no. 2, pp. 257–267, 2020.
- [12] I. M. S. Araújo, R. R. Silva, G. Pacheco et al., "Hydrothermal synthesis of bacterial cellulose-copper oxide nanocomposites and evaluation of their antimicrobial activity," *Carbohydrate Polymers*, vol. 179, pp. 341–349, 2018.
- [13] S. Y. Z. Zainuddin, I. Ahmad, H. Kargarzadeh, I. Abdullah, and A. Dufresne, "Potential of using multiscale kenaf fibers as reinforcing filler in cassava starch-kenaf biocomposites," *Carbohydrate Polymers*, vol. 92, no. 2, pp. 2299–2305, 2013.
- [14] M. Asrofi, H. Abrial, A. Kasim, A. Pratoto, M. Mahardika, and F. Hafizulhaq, "Mechanical properties of a water hyacinth nanofiber cellulose reinforced thermoplastic starch bionanocomposite: effect of ultrasonic vibration during processing," *Fibers*, vol. 6, no. 2, p. 40, 2018.
- [15] C. M. O. Müller, J. B. Laurindo, and F. Yamashita, "Effect of cellulose fibers addition on the mechanical properties and water vapor barrier of starch-based films," *Food Hydrocolloids*, vol. 23, no. 5, pp. 1328–1333, 2009.
- [16] H. Abrial, V. Lawrensus, D. Handayani, and E. Sugiarti, "Preparation of nano-sized particles from bacterial cellulose using ultrasonication and their characterization," *Carbohydrate Polymers*, vol. 191, pp. 161–167, 2018.
- [17] H. Abrial, A. Hartono, F. Hafizulhaq, D. Handayani, E. Sugiarti, and O. Pradipta, "Characterization of PVA/cassava starch biocomposites fabricated with and without sonication using bacterial cellulose fiber loadings," *Carbohydrate Polymers*, vol. 206, pp. 593–601, 2018.
- [18] T. Bourtoom and M. S. Chinnan, "Preparation and properties of rice starch-chitosan blend biodegradable film," *LWT- Food Science and Technology*, vol. 41, no. 9, pp. 1633–1641, 2008.
- [19] M. M. Marvzadeh, N. Oladzadabbasabadi, A. Mohammadi Nafchi, and M. Jokar, "Preparation and characterization of bionanocomposite film based on tapioca starch/bovine gelatin/nanorod zinc oxide," *International Journal of Biological Macromolecules*, vol. 99, pp. 1–7, 2017.
- [20] M. Mahardika, H. Abrial, A. Kasim, S. Arief, F. Hafizulhaq, and M. Asrofi, "Properties of cellulose nanofiber/bengkoang starch bionanocomposites: effect of fiber loading," *LWT- Food Science and Technology*, vol. 116, article 108554, 2019.
- [21] N. A. Al-Tayyar, A. M. Youssef, and R. Al-hindi, "Antimicrobial food packaging based on sustainable bio-based materials for reducing foodborne pathogens: a review," *Food Chemistry*, vol. 310, article 125915, 2020.
- [22] S. Y. Sung, L. T. Sin, T. T. Tee et al., "Antimicrobial agents for food packaging applications," *Trends in Food Science and Technology*, vol. 33, no. 2, pp. 110–123, 2013.
- [23] S. J. Mcgrance, H. J. Cornell, and C. J. Rix, "A simple and rapid colorimetric method for the determination of amylose in starch products," *Starch/Stärke*, vol. 50, no. 4, pp. 158–163, 1998.
- [24] H. Abrial, M. M. Kadriadi, D. Handayani, E. Sugiarti, and A. N. Muslimin, "Characterization of disintegrated bacterial cellulose nanofibers/PVA bionanocomposites prepared via ultrasonication," *International Journal of Biological Macromolecules*, vol. 135, pp. 591–599, 2019.
- [25] R. A. Ilyas, S. M. Sapuan, and M. R. Ishak, "Isolation and characterization of nanocrystalline cellulose from sugar palm fibres

- (_Arenga pinnata_),” *Carbohydrate Polymers*, vol. 181, pp. 1038–1051, 2018.
- [26] M. Asrofi, H. Abral, A. Kasim, and A. Pratoto, “XRD and FTIR studies of nanocrystalline cellulose from water hyacinth (*Eichornia crassipes*) fiber,” *Journal of Metastable and Nanocrystalline Materials*, vol. 29, pp. 9–16, 2017.
- [27] H. Abral, R. Soni Satria, M. Mahardika et al., “Comparative study of the physical and tensile properties of jicama (*Pachyrhizus erosus*) starch film prepared using three different methods,” *Starch/Staerke*, vol. 71, pp. 1–9, 2019.
- [28] H. Abral, A. Basri, F. Muhammad et al., “A simple method for improving the properties of the sago starch films prepared by using ultrasonication treatment,” *Food Hydrocolloids*, vol. 93, pp. 276–283, 2019.
- [29] A. Khan, R. A. Khan, S. Salmieri et al., “Mechanical and barrier properties of nanocrystalline cellulose reinforced chitosan based nanocomposite films,” *Carbohydrate Polymers*, vol. 90, no. 4, pp. 1601–1608, 2012.
- [30] H. Abral, A. S. Anugrah, F. Hafizulhaq, D. Handayani, E. Sugiarti, and A. N. Muslimin, “Effect of nanofibers fraction on properties of the starch based biocomposite prepared in various ultrasonic powers,” *International Journal of Biological Macromolecules*, vol. 116, pp. 1214–1221, 2018.
- [31] J. Epp, “X-ray diffraction (XRD) techniques for materials characterization,” Elsevier Ltd, 2016.
- [32] W. Cheng, J. Chen, D. Liu, X. Ye, and F. Ke, “Impact of ultrasonic treatment on properties of starch film-forming dispersion and the resulting films,” *Carbohydrate Polymers*, vol. 81, no. 3, pp. 707–711, 2010.
- [33] D. Merino, A. Y. Mansilla, T. J. Gutiérrez, C. A. Casalongué, and V. A. Alvarez, “Chitosan coated-phosphorylated starch films: water interaction, transparency and antibacterial properties,” *Reactive and Functional Polymers*, vol. 131, pp. 445–453, 2018.
- [34] M. S. Goyat, S. Ray, and P. K. Ghosh, “Innovative application of ultrasonic mixing to produce homogeneously mixed nanoparticulate-epoxy composite of improved physical properties,” *Composites. Part A, Applied Science and Manufacturing*, vol. 42, no. 10, pp. 1421–1431, 2011.
- [35] H. Abral, M. H. Dalimunthe, J. Hartono et al., “Characterization of tapioca starch biopolymer composites reinforced with micro scale water hyacinth fibers,” *Starch/Staerke*, vol. 70, no. 7-8, pp. 1–8, 2018.
- [36] J. C. Martins da Costa, K. S. Lima Miki, A. da Silva Ramos, and B. E. Teixeira-Costa, “Development of biodegradable films based on purple yam starch/chitosan for food application,” *Heliyon*, vol. 6, no. 4, p. e03718, 2020.
- [37] J. Kim, Z. Cai, H. S. Lee, G. S. Choi, D. H. Lee, and C. Jo, “Preparation and characterization of a bacterial cellulose/chitosan composite for potential biomedical application,” *Journal of Polymer Research*, vol. 18, no. 4, pp. 739–744, 2011.
- [38] L. Y. Zheng and J. F. Zhu, “Study on antimicrobial activity of chitosan with different molecular weights,” *Carbohydrate Polymers*, vol. 54, no. 4, pp. 527–530, 2003.

Research Article

Experimental Investigation on the Mechanical Properties of a Sandwich Structure Made of Flax/Glass Hybrid Composite Facesheet and Honeycomb Core

W. Ashraf ¹, M. R. Ishak ^{1,2,3}, M. Y. M. Zuhri ⁴, N. Yidris ^{1,2} and A. M. Ya'acob ⁵

¹Department of Aerospace Engineering, Universiti Putra Malaysia, UPM, 43400 Serdang, Selangor, Malaysia

²Aerospace Malaysia Research Centre (AMRC), Faculty of Engineering, Universiti Putra Malaysia, UPM, 43400 Serdang, Selangor, Malaysia

³Laboratory of Biocomposite Technology, Institute of Tropical Forestry and Forest Products (INTROP), Universiti Putra Malaysia, UPM, 43400 Serdang, Selangor, Malaysia

⁴Department of Mechanical and Manufacturing Engineering, Universiti Putra Malaysia, UPM, 43400 Serdang, Selangor, Malaysia

⁵Malaysian Institute of Aviation Technology, Aerospace Section, Universiti Kuala Lumpur, 43800 Dengkil, Sepang, Selangor, Malaysia

Correspondence should be addressed to W. Ashraf; shwaqas88@gmail.com and M. R. Ishak; mohdridzwan@upm.edu.my

Received 30 September 2020; Revised 25 January 2021; Accepted 10 February 2021; Published 11 March 2021

Academic Editor: Hairul Abral

Copyright © 2021 W. Ashraf et al. This is an open access article distributed under the Creative Commons Attribution License, which permits unrestricted use, distribution, and reproduction in any medium, provided the original work is properly cited.

This research is aimed at developing the sandwich structure with a hybrid composite facesheet and investigate its mechanical properties (tensile, edgewise compression, and flexural). The combination of renewable and synthetic materials appears to reduce the weight, cost, and environmental impact compared to pure synthetic materials. The hybrid composite facesheets were fabricated with different ratios and stacking sequence of flax and glass fibers. The nonhybrid flax and glass composite facesheet sandwich structures were fabricated for comparison. The overall mechanical performance of the sandwich structures was improved by increasing the glass fiber ratio in the hybrid composites. The experimental tensile properties of the hybrid facesheet and the edgewise compression strength and ultimate flexural facing stress of the hybrid composites sandwich structures were achieved higher when the results were normalized to the same fiber volume fraction of glass composite. The hybrid composite sandwich structure showed improved compression and flexural facing stress up to 68% and 75%, respectively, compared to nonhybrid flax composites. The hybrid composite using glass in the outer layer achieved the similar flexural stiffness of the nonhybrid glass composite with only a 6% higher thickness than the glass composite sandwich structure.

1. Introduction

The sandwich structures are known for their high bending strength and stiffness at low weight. They are composed of two thin facesheets (FS) and a thick core. The FS is dense, strong, and stiff and carries the inplane load, while the core material, which supports the shear and transverse loads, is relatively low in density [1]. The honeycomb core sandwich structures are being utilized as a primary load-carrying carrying structure in aerospace, railways, automobile, and marine applications [2]. The typical usage of the sandwich composite was reported in aircraft interiors such as floor panels, interior

walls, food-handling galleys, and passenger storage racks [3]. The fiber-reinforced composite has become increasingly of interest as an FS material because of durability, damage tolerance, and offers better strength to weight ratio than conventional metal counterparts [4]. The synthetic fibers such as glass, carbon, and aramid are preferred as a reinforcement in composite materials [5]. However, they have few limitations due to environmental impacts such as nonbiodegradability, complicated recycling process, disposal requirements, and emission of greenhouse gasses [6]. These drawbacks provide an increasing interest in using natural fiber composites. They are used in automobile, building, construction, packaging,

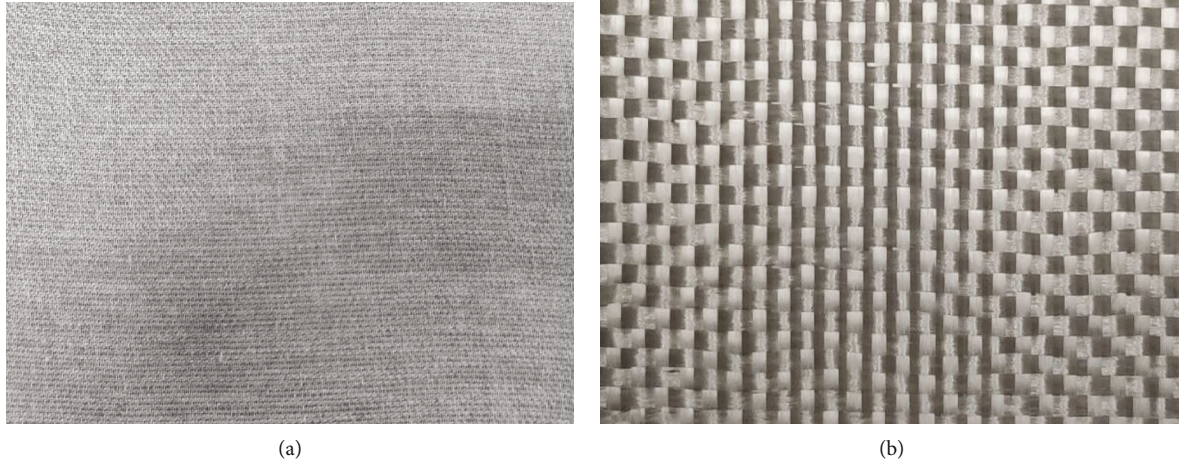


FIGURE 1: Reinforcement for composite FS: (a) flax fabric and (b) glass fabric.

and storage industries, due to low density, high specific strength and stiffness, environmentally friendly, renewable, low production cost, and better damping properties [7]. Still, these composites are limited to nonstructural applications due to poor mechanical properties [8]. There are different techniques reported to improve the mechanical properties of natural fiber composites. Besides all methods, hybridization is the most effective technique by using a combination of natural (flax, kenaf, jute, and sisal) and synthetic (carbon and glass) reinforcement [9]. Zhang et al. [10] investigated the mechanical properties of flax/glass hybrid composites. They indicated that the addition of glass fiber improved the tensile properties of the flax hybrid composite. Saidane et al. [11] proved that the hybridization of flax and glass fibers improved the moisture resistance and Young's modulus compared to the natural fiber composite. The stacking sequence of natural and synthetic fabric plies in laminated composites has a significant effect in terms of load transfer. The alternate stacking of natural and synthetic fiber layers in laminated composites proved to have better interlaminar shear strength [12, 13]. Selver et al. [13] found that using glass fiber in the outer layer in flax/glass and jute/glass hybrid composites provided better flexural strength than glass in the middle layer.

There are few studies reported on the mechanical properties of a sandwich structure using flax fiber composites as an FS material with different core materials like cork core, foam core, and balsa wood [14–16]. Sadeghian et al. [17] investigated the flexural behavior of a sandwich composite made of the flax fiber composite with a cork core and glass fiber with a polypropylene core. They found that the shear rigidity and flexural stiffness of the 12 mm thick polypropylene core with one glass layer exhibited comparable results with a 22 mm thick cork core with two flax fibres layers. However, they did not compare the specific flexural stiffness of the sandwich structure.

The research published relating to the flax fiber composite as an FS material of sandwich structure has focused on the fundamental understanding of the flexural performance and core properties (density, cell size) of the sandwich structures. However, no study reported improving the mechanical per-

TABLE 1: Specifications of reinforcement fibers [8, 18].

Properties	Biotex™ flax	E-glass
Density (g/cm ³)	1.5	2.5
Tensile strength (MPa)	500	2000-3000
Tensile modulus (GPa)	50	70-75
Elongation at brake %	2	2.5-3
Fiber diameter (µm)	20	25
Fiber length (cm)	100	—
Cellulose (%)	64-71	—

formance of the honeycomb sandwich structure using the flax/glass hybrid composite as an FS material with a honeycomb core. Therefore, this study is aimed at investigating the tensile, edgewise compression, and flexural (3-point bending) properties of the hybrid FS sandwich structure made from flax and glass composites. The effects of fiber type, their ratios in the hybrid composites, and fiber volume fraction on the mechanical properties were analyzed with experimental and normalized results.

2. Experimental Details

2.1. Material. Flax and E-glass reinforcement were utilized in woven mats to fabricate the composites FS as shown in Figure 1. The flax fabric and glass fiber were procured in woven mats from the Easy Composite, UK. Table 1 shows the individual properties of the fibers [8, 18]. The Epoxamite® 100 epoxy resin with slow hardener 103 was used as a matrix. The specifications of this epoxy resin are reported in the literature [19]. The aluminium honeycomb 5052 grade was used as the core material with cell size (distance between two opposite cell walls) and thickness of 3.2 mm and 8 mm, respectively. The aluminium honeycomb core and the epoxy adhesive film were acquired from Hexcore industries based in Jiangsu, China. The areal density and standard shear strength of the adhesive film are 300 g.m⁻² and 15 MPa, respectively.

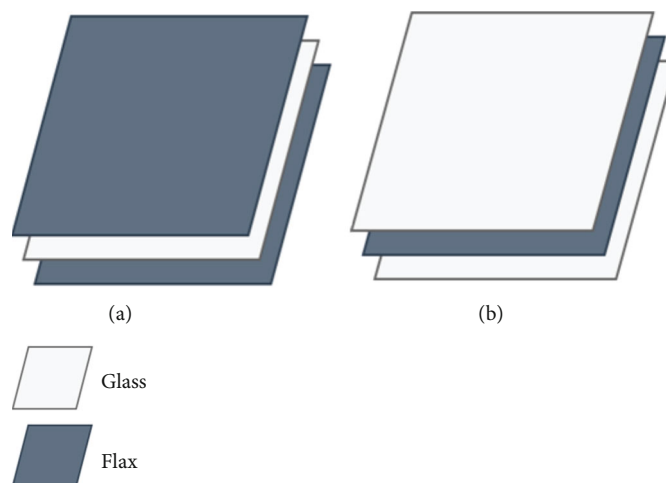


FIGURE 2: Fabric stacking sequence of composite laminates: (a) H1 hybrid and (b) H2 hybrid.

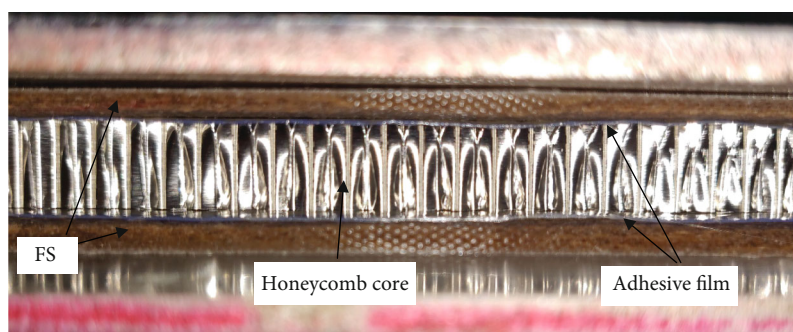


FIGURE 3: Curing of the composite sandwich structure.

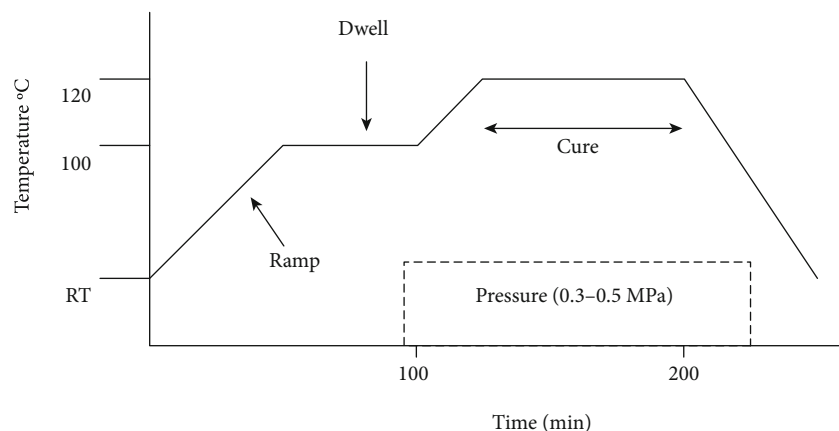


FIGURE 4: Curing profile of composite structures in hot-press.

2.2. Sandwich Structure Fabrication. The honeycomb core sandwich structures were fabricated using the precure technique. This precure fabrication process was comprised of two stages. In the initial process, the composite FS were fabricated, followed by FS bonding with the core using adhesive film in the subsequent process. The hybrid and nonhybrid composite FS were precured in the vacuum infusion process with various stacking sequences of the flax and glass fabric plies, as shown in Figure 2.

The peel-ply treated surface of the precure composite FS was used for secondary bonding with the core. The epoxy adhesive film was applied to the peel-ply treated surface of the FS to fabricate the sandwich structure, as described by Farooq et al. [20]. The whole assembly was placed in hot-press for bonding and curing of the adhesive film, as shown in Figure 3. The curing profile of the sandwich structure in the hot-press is given in Figure 4. The intermediate dwell time was taken at 100°C for one hour, followed by curing at 120°C [4]. The

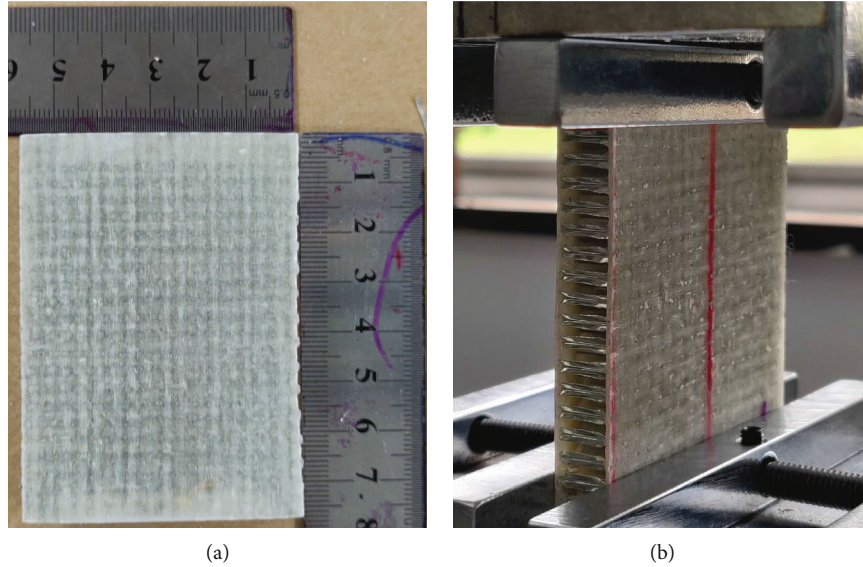


FIGURE 5: Edgewise compression test: (a) actual specimen size and (b) experimental setup.

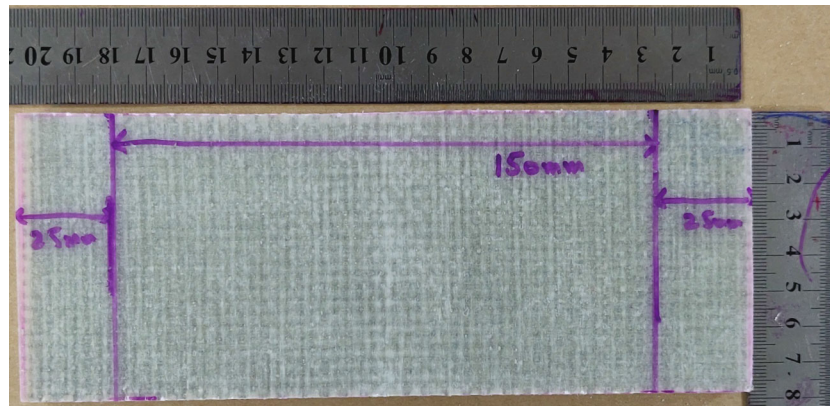


FIGURE 6: specimen prepared for flexural testing (3-point loading).

required specimens as per standard size for testing were cut from the fabricated panel of 300 mm × 300 mm.

2.3. Characterization. The tensile properties of flax, glass, and hybrid composites FS were performed to determine the strength and modulus of the FS materials. According to the ASTM D3039, the tensile test was performed with a crosshead speed of 2 mm/min [21]. The 150 mm span length and 25.4 mm width of each composite FS type were prepared for the tensile test as per standard guidelines. The modulus of elasticity of each composite FS was calculated by the ratio of change in stress to the change in strain from the slope of the chord between 0.1% and 0.3% strain. The edgewise compression test was conducted to determine the ultimate compression strength of the sandwich structures as per standard ASTM C364 with a crosshead speed of 0.5 mm/min [22]. The specimen size and experimental set-up for the edgewise compression test are given in Figure 5.

The flexural test (3-point loading) was performed to determine the facing stress of the sandwich structure. The specimen dimensions were taken as per ASTM C393

standard configuration with a crosshead displacement of 3 mm/min [23]. The specimen size for the flexural test was taken as standard configuration given in ASTM C393. The actual specimen for the flexural test is shown in Figure 6.

The specimens of each type were tested five times at loading conditions, and their average values and standard derivation were calculated as per standard. The mechanical testing (tensile, edgewise compression and flexural) was carried out on the Instron 3382 Universal testing machine. The experimental density of the composite specimens was computed using a digital densimeter by measuring the weight of the samples in the air and water according to the ASTM D792 standard [24]. The fiber volume fraction of each cured composite FS was calculated using equation (1) [13]. The thickness, fiber volume fraction, and density of each composite FS are given in Table 2.

$$V_f = \frac{(w_f/\rho_f)}{\left[\frac{(w_f/\rho_f)}{(\rho_f)} + \frac{(w_r/\rho_r)}{(\rho_r)} \right]}, \quad (1)$$

TABLE 2: Properties of composite laminates.

FS laminate	FS thickness (mm)	Total fiber volume fraction V_f	Fiber weight fraction (%)		FS density ($\text{g}\cdot\text{cm}^{-3}$)
			Glass	Flax	
Flax	$1.1 \pm (0.05)$	0.26	0	100	$1.17 \pm (0.02)$
H1	$1.3 \pm (0.05)$	0.297	57	43	$1.30 \pm (0.02)$
H2	$1.1 \pm (0.05)$	0.326	75	25	$1.45 \pm (0.03)$
Glass	$0.8 \pm (0.05)$	0.415	100	0	$1.66 \pm (0.03)$

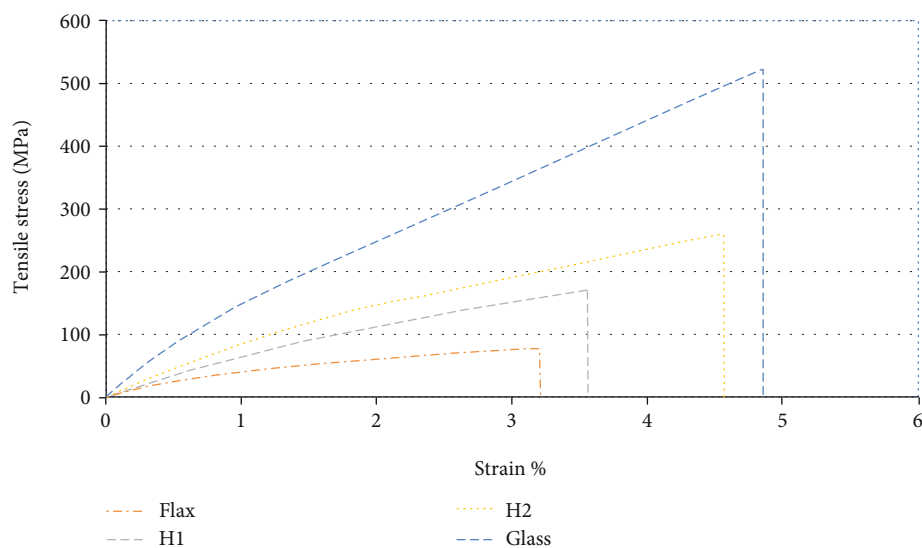


FIGURE 7: Stress-strain curves of tensile loading.

TABLE 3: Tensile force, strength, and modulus of the composite laminates.

FS laminate	Avg. ultimate load (kN)	Tensile strength (MPa)	Normalized tensile strength (MPa)	Avg. modulus (GPa)	Normalized modulus (GPa)
Flax	$2.64 \pm (0.12)$	$94.6 \pm (3.4)$	151.0	$5.3 \pm (0.13)$	8.45
H1	$6.02 \pm (0.32)$	$182.3 \pm (9.9)$	254.8	$7.5 \pm (0.96)$	10.5
H2	$6.74 \pm (.51)$	$241.2 \pm (18.4)$	303.4	$10.5 \pm (1.53)$	13.2
Glass	$9.14 \pm (0.78)$	$449.8 \pm (36.8)$	449.8	$15.5 \pm (1.11)$	15.5

where V_f is the volume fraction of fiber, w_f is the weight of fiber, w_r is the weight of resin, ρ_f is the density of fiber, and ρ_r is the density of the resin.

3. Results and Discussion

3.1. Tensile Test. The stress-strain curves of the glass, flax, and hybrid composites are illustrated in Figure 7. It showed that the glass fiber composite showed higher failure strain compared to the flax composite. The hybrid composite H2 showed higher elongation than H1 because of the higher volume fraction of glass fiber in the H2 hybrid composite. The possible explanation of the higher elongation in the glass composite was higher elongation at break of glass than flax

fiber, as given in Table 1. These findings are supported by similar results concluded by Zhang et al. [10].

The tensile force, strength, and modulus of all composite laminates are given in Table 3. The experimental results showed that the hybrid composites significantly improved the tensile strength and modulus compared to the flax composite. The tensile strength was improved by around 92.7% and 155% in H1 and H2 hybrid composites, respectively. The hybrid composite H1 and H2 showed improved tensile modulus by 42% and 98%, respectively. The higher tensile strength and modulus of H2 hybrid composite compared to H1 indicated that the results were improved by increasing the glass fiber volume content in the hybrid composites. The results showed that the glass fiber composite had the highest tensile strength and modulus compared to flax and

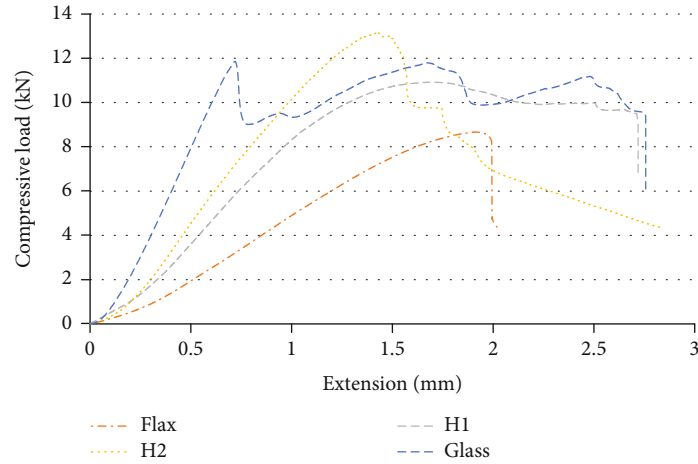


FIGURE 8: Load-extension curves of edgewise compression.

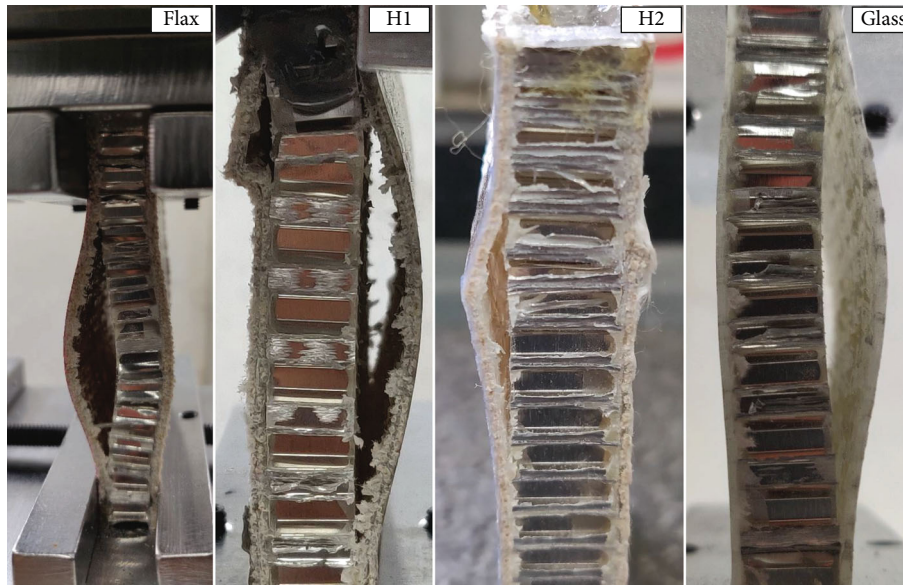


FIGURE 9: Failure mode of sandwich structures through edgewise compression.

hybrid composites due to the higher total fiber volume since the glass fiber carried most of the load. The experimental results of tensile strength and modulus were normalized with the common fiber volume fraction to compare better while the samples have different total fiber volume fractions. The results were normalized by multiplying the ratio of the common fiber volume fraction of the glass composite (0.415) to the actual fiber volume of the composite using equation (2) and equation (3), respectively [13]. The normalized tensile strengths of flax and hybrid composites were improved compared to the experimental results, as given in Table 3. The results showed that the normalized tensile strength was increased with the increasing glass fiber volume ratio in the hybrid composites. The normalized H2 hybrid composite improved tensile strength by 19% compared to the H1 hybrid composite. The glass fiber composite still showed the higher normalized tensile strength compared to flax and hybrid composites. The possible reason was due to the better strength of glass than flax fiber, as given in Table 1.

TABLE 4: Edgewise compression force and strength of the composite sandwich structure.

FS laminate	Avg. load (kN)	Compression strength (MPa)	Normalized compression strength (MPa)
Flax	$8.9 \pm (0.29)$	$58.1 \pm (1.93)$	89.3
H1	$11.3 \pm (0.46)$	$79.1 \pm (3.2)$	112.6
H2	$12.8 \pm (0.55)$	$106.3 \pm (4.57)$	133.1
Glass	$13.0 \pm (0.44)$	$148.4 \pm (5.07)$	148.4

Table 3 showed the improvement in the tensile modulus of flax and hybrid composites when the results were normalized. The H2 hybrid composite attained 85% of the tensile modulus of the glass fiber composite when the results were normalized to the same glass fiber volume. However, the glass composite still showed the higher modulus when the

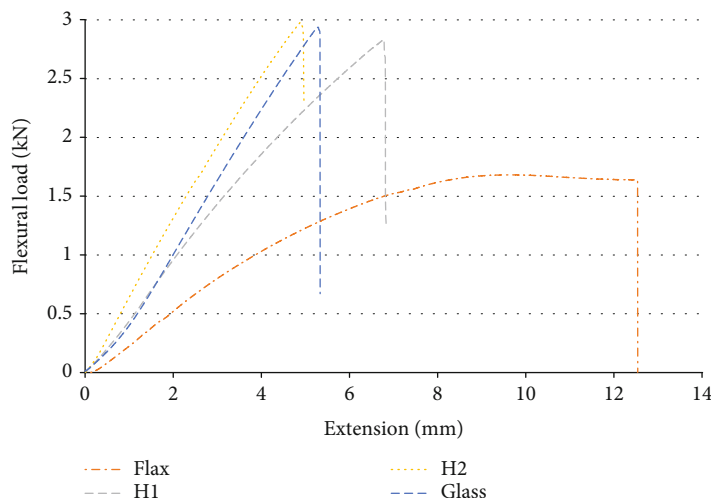


FIGURE 10: Load-extension curves of the flexural test.

composites were normalized to the same fiber volume fraction due to better fiber-matrix adhesion of glass than flax fiber [11].

$$\sigma_n = \frac{\sigma}{V_f} \times V_{f_c} \quad (2)$$

$$E_n = \frac{E}{V_f} \times V_{f_c} \quad (3)$$

where σ_n is the normalized strength, σ is the strength of the composite (MPa), E_n is the normalized modulus (GPa), E is the modulus of the composite (GPa), V_f is the actual fiber volume, and V_{f_c} is the common fiber volume fraction.

3.2. Edgewise Compression Strength. The edgewise compression or inplane compression test was conducted to evaluate the performance of the sandwich structure through the compression loading applied on the edges of FS. The compression performance is the relevant design parameter because the bending strength of the sandwich structure is affected by the poor compression performance [25]. Figure 8 shows the load-extension curves of flax, glass, and hybrid composites through compression loading. The flax composite curve revealed a linear elastic behavior and showed abrupt failure due to the adhesive failure between FS and core. The glass and hybrid composites showed similar elastic performance followed by the softening phase before failure. The face wrinkling initiated the failure in glass and hybrid composites due to matrix cracking in the composite FS, followed by FS debonding, as shown in Figure 9.

The average edgewise compression force and strength are given in Table 4. It indicated that the experimental results of edgewise compression strength were improved by increasing the glass fiber volume content. The compression strength was enhanced by 25% and 68% by H1 and H2, respectively, compared with the flax composite. The glass fiber composite showed the highest compression strength than flax and hybrid composites due to the higher fiber volume fraction and better stiffness of glass than flax fiber. The experimental results of the hybrid composites were normalized to the same

TABLE 5: Flexural load and facing stress of the composite sandwich structures.

FS laminate	Avg. load (kN)	Avg. facing stress (MPa)	Normalized facing stress (MPa)
Flax	1.61 ± (0.057)	80.5 ± (2.86)	128.4
H1	2.80 ± (0.12)	116 ± (4.66)	165.4
H2	2.82 ± (0.22)	140.8 ± (11.3)	178.2
Glass	3.06 ± (0.19)	218 ± (13.7)	218

glass fiber volume using equation (2), as described in tensile testing. The compression strength of the flax and hybrid composites was achieved higher when the results were normalized (Table 4). The normalized compression strength of the H2 hybrid composite showed comparable results by approaching 92% compression strength of the glass fiber composite.

3.3. Flexural Test. The peak loads reached by each sandwich structure are shown in the load-extension curves (Figure 10). The failure extension through the bending of sandwich structures was significantly affected by the stacking sequence and relative fiber volume ratio of glass fiber in composite FS. The glass and H2 hybrid composites that possessed the outer glass fiber layer in FS showed more resistance to the bending load than H1 and flax composites. This behavior was due to the high stiffness of glass compared to flax fiber [13].

Table 5 shows the flexural load and flexural facing stress of the sandwich structures. The experimental results indicated that the facing stress of the hybrid composites was improved with increasing the glass fiber content. The H1 and H2 hybrid composites showed the improved facing stress by around 44% and 75%, respectively, compared with the flax composite. The glass fiber composite showed higher flexural facing stress than flax and hybrid composites due to the higher total fiber volume fraction. The flexural facing stress of flax and hybrid composites was normalized as described in tensile using equation (2) to compare the same fiber

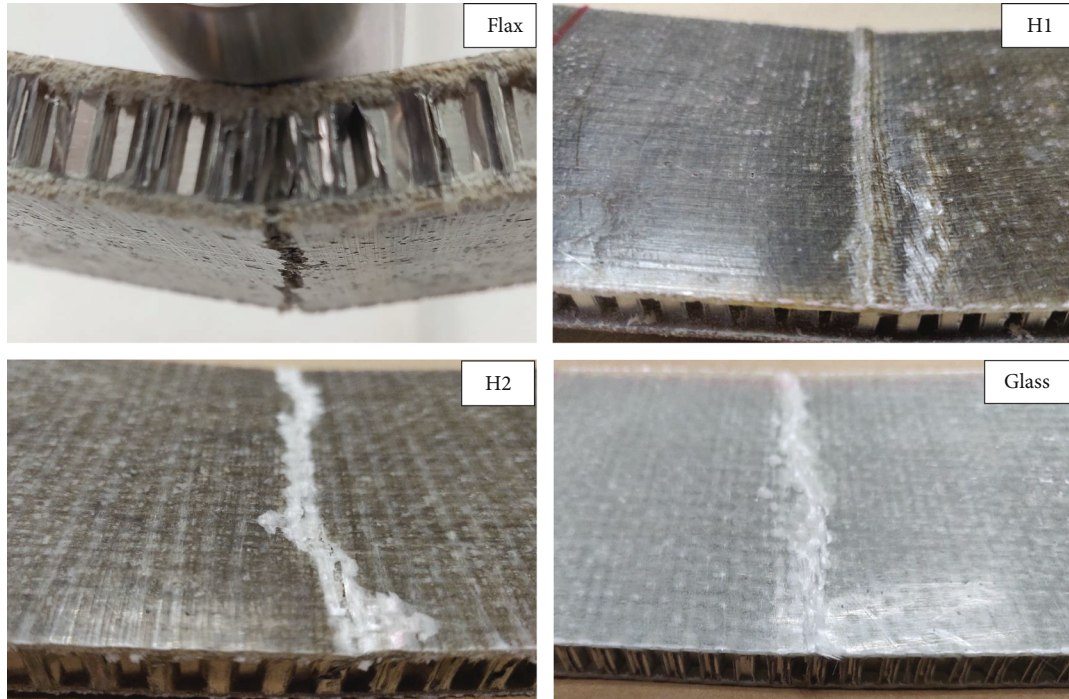


FIGURE 11: Collapse mode of sandwich structures subjected to the flexural test.

TABLE 6: Dimensions and flexural stiffness of the composite sandwich structures.

FS laminate	Width, b (mm)	Sandwich structure thickness, d (mm)	Flexural stiffness, D (N.m ²)	Weight of sandwich panel (g.cm ⁻²)	Specific flexural stiffness (N.m ² /(g.cm ⁻²))
Flax	75	10.2 ± (0.05)	18.19 ± (0.23)	0.45	40.2
H1	75	10.6 ± (0.05)	31.93 ± (1.04)	0.46	69.3
H2	75	10.2 ± (0.05)	36.12 ± (2.87)	0.44	82.0
Glass	75	9.6 ± (0.05)	36.10 ± (1.73)	0.38	95

volume fraction composites. The experimental facing stress of hybrid composites was achieved higher when the results were normalized to the same glass fiber volume, as given in Table 5. The normalized results indicated that the facing stress was improved by increasing the glass fiber ratio in the hybrid composites, which was due to the better strength of glass fiber than flax fiber. The normalized H2 hybrid composite showed improved facing stress by approaching 82% facing stress of the glass composite.

Figure 11 shows the fractured sandwich structures subjected to the three-point flexural loading. This type of failure in a sandwich structure is caused by face yielding, and it generally occurs when the FS materials exceed their allowable stress or strain [26]. The failures observed in glass and hybrid composites were due to compression or upper FS failure, while the flax composite showed lower FS failure. The possible reason for the lower FS failure was due to the lower tensile strain of the flax composite compared to the glass and hybrid composites, as discussed in the tensile testing.

The flexural stiffness of the sandwich structures was calculated using equation (4) as per ASTM D7250 [27]. Table 6 shows the flexural stiffness of the sandwich structure.

The flexural stiffness of the glass and H2 hybrid composite showed similar results using the same number of reinforcement layers in composite FS. In contrast to the previous research reported by CoDyre et al. [16] that the similar flexural stiffness of one layer of the glass composite FS sandwich structure was achieved using the three layers of flax fiber. The higher FS thickness of the H2 composite (1.1 mm) compared to the glass composite (0.8 mm) balanced the lower modulus to achieve the similar flexural stiffness. The flax and H1 hybrid composite showed lower flexural stiffness than glass and H2 hybrid composites, but the difference was not significant. The comparable flexural thickness of the flax and H1 hybrid composite was due to the higher thickness of flax and H1 sandwich structures [17].

The specific flexural stiffness was calculated by the ratio of actual flexural stiffness to the areal density or weight of the sandwich structure since the glass, and hybrid composites had different density and FS thickness. The areal density of the sandwich structure was calculated by adding the weight of FS, core, and adhesive film. The glass fiber composite FS had lower weight than that of hybrid composites due to the lower thickness of FS. The glass composite sandwich

structure exhibited higher stiffness to weight ratio because of the lower areal density and higher modulus of glass composite FS. The relative ratio glass fiber volume showed a significant effect on the specific flexural stiffness of hybrid composites FS. The hybrid laminates with the outer glass fiber layer (H2) that had higher specific flexural by around 18% compared to H1, as given in Table 6.

$$D = \frac{E_f(d^3 - C^3)b}{12}, \quad (4)$$

where D is the flexural stiffness, E_f is the FS modulus, d is the sandwich structure thickness, c is the core thickness, and b is the width of the specimen.

4. Conclusion

The mechanical properties of the hybrid composite FS sandwich structures were analyzed at different loading conditions (tensile, edgewise compression, and flexural) for different fiber volume ratios of flax and glass fibers. The overall mechanical properties of composite FS and sandwich structures were improved with the increasing glass fiber content. The H2 hybrid composites using glass in the outer layer showed improved tensile strength and modulus by around 155% and 98%, respectively, compared with the flax composite FS. The H2 hybrid composite achieved 85% modulus value of the glass composite when the results were normalized to the same glass fiber volume. The edgewise compression strength was improved around 68% by the H2 hybrid FS, compared with the flax composite sandwich structure. The normalized H2 hybrid composite achieved a 90% compression strength of the glass composite. The flexural facing stress of the sandwich structure was increased up to 75% by H2 hybrid FS compared to flax composite facing stress. The H2 hybrid composite achieved about 82% of the flexural facing stress of the glass fiber composite when the results were normalized. The H2 hybrid composite showed similar flexural stiffness to glass composite with only a 6% increase in the H2 hybrid sandwich thickness than the glass composite sandwich structure. However, the specific flexural stiffness (flexural stiffness to weight ratio) results showed that the glass fiber composite had 15% higher specific flexural stiffness than the H2 hybrid sandwich structure.

Data Availability

All data included in this study are available from the corresponding author upon request.

Conflicts of Interest

The authors declare that they have no conflicts of interest.

Acknowledgments

The authors would like to thank and sincere appreciation to the Aerospace Manufacturing Research Centre (AMRC) and Department of Aerospace, Universiti Putra Malaysia,

for providing the lab facility to conduct this study. The Universiti Putra Malaysia funded this research work under FRGS (5540205).

References

- [1] V. Birman and G. A. Kardomateas, "Review of current trends in research and applications of sandwich structures," *Composites: Part B*, vol. 142, pp. 221–240, 2018.
- [2] K. B. Shin, J. Y. Lee, and S. H. Cho, "An experimental study of low-velocity impact responses of sandwich panels for Korean low floor bus," *Composite Structures*, vol. 84, no. 3, pp. 228–240, 2008.
- [3] B. V. Ramnath, K. Alagarraja, and C. Elanchezian, "Review on sandwich composite and their applications," *Materials Today: Proceedings*, vol. 16, pp. 859–864, 2019.
- [4] S. M. Grove, E. Popham, and M. E. Miles, "An investigation of the skin/core bond in honeycomb sandwich structures using statistical experimentation techniques," *Composites. Part A, Applied Science and Manufacturing*, vol. 37, no. 5, pp. 804–812, 2006.
- [5] N. Mohd Nurazzi, A. Khalina, S. M. Sapuan, A. H. A. M. Dayang Laila, M. Rahmah, and Z. Hanafee, "A review: fibres, polymer matrices and composites," *Pertanika J Sci Technol*, vol. 25, pp. 1085–1102, 2017.
- [6] M. Pervaiz and M. M. Sain, "Carbon storage potential in natural fiber composites," *Resources, Conservation and Recycling*, vol. 39, no. 4, pp. 325–340, 2003.
- [7] H. M. Akil, M. F. Omar, A. A. M. Mazuki, S. Safiee, Z. A. M. Ishak, and A. Abu Bakar, "Kenaf fiber reinforced composites: a review," *Materials and Design*, vol. 32, no. 8-9, pp. 4107–4121, 2011.
- [8] K. L. Pickering, M. G. A. Efendy, and T. M. Le, "A review of recent developments in natural fibre composites and their mechanical performance," *Composites Part A: Applied Science and Manufacturing*, vol. 83, pp. 98–112, 2016.
- [9] M. R. Sanjay, G. R. Arpitha, and B. Yogesha, "Study on mechanical properties of natural - glass fibre reinforced polymer hybrid composites: a review," *Mater Today Proc*, vol. 2, no. 4-5, pp. 2959–2967, 2015.
- [10] Y. Zhang, Y. Li, H. Ma, and T. Yu, "Tensile and interfacial properties of unidirectional flax/glass fiber reinforced hybrid composites," *Composites Science and Technology*, vol. 88, pp. 172–177, 2013.
- [11] E. H. Saidane, D. Scida, M. Assarar, H. Sabhi, and R. Ayad, "Hybridisation effect on diffusion kinetic and tensile mechanical behaviour of epoxy based flax-glass composites," *Composites. Part A, Applied Science and Manufacturing*, vol. 87, pp. 153–160, 2016.
- [12] M. Ramesh and P. Sudharsan, "Experimental investigation of mechanical and morphological properties of flax-glass fiber reinforced hybrid composite using finite element analysis," *SILICON*, vol. 10, no. 3, pp. 747–757, 2018.
- [13] E. Selver, N. Ucar, and T. Gulmez, "Effect of stacking sequence on tensile, flexural and thermomechanical properties of hybrid flax/glass and jute/glass thermoset composites," *Journal of Industrial Textiles*, vol. 48, no. 2, pp. 494–520, 2018.
- [14] A. Mancuso, G. Pitarresi, and D. Tumino, "Mechanical behaviour of a green sandwich made of flax reinforced polymer facings and cork core," *Procedia Eng*, vol. 109, pp. 144–153, 2015.

- [15] E. Kandare, P. Luangtriratana, and B. K. Kandola, "Fire reaction properties of flax/epoxy laminates and their balsa-core sandwich composites with or without fire protection," *Composites. Part B, Engineering*, vol. 56, pp. 602–610, 2014.
- [16] L. CoDyre, K. Mak, and A. Fam, "Flexural and axial behaviour of sandwich panels with bio-based flax fibre-reinforced polymer skins and various foam core densities," *Journal of Sandwich Structures and Materials*, vol. 20, no. 5, pp. 595–616, 2018.
- [17] P. Sadeghian, D. Hristozov, and L. Wroblewski, "Experimental and analytical behavior of sandwich composite beams: comparison of natural and synthetic materials," *Journal of Sandwich Structures and Materials*, vol. 20, no. 3, pp. 287–307, 2018.
- [18] M. M. Davoodi, S. M. Sapuan, D. Ahmad, A. Ali, A. Khalina, and M. Jonoobi, "Mechanical properties of hybrid kenaf/glass reinforced epoxy composite for passenger car bumper beam," *Materials and Design*, vol. 31, no. 10, pp. 4927–4932, 2010.
- [19] A. Hamdan, F. Mustapha, K. A. Ahmad, A. S. M. Rafie, M. R. Ishak, and A. E. Ismail, "The effect of customized woven and stacked layer orientation on tensile and flexural properties of woven kenaf fibre reinforced epoxy composites," *International Journal of Polymer Science*, vol. 2016, 11 pages, 2016.
- [20] U. Farooq, M. S. Ahmad, S. A. Rakha, N. Ali, A. A. Khurram, and T. Subhani, "Interfacial mechanical performance of composite honeycomb sandwich panels for aerospace applications," *Arabian Journal for Science and Engineering*, vol. 42, no. 5, pp. 1775–1782, 2017.
- [21] ASTM standard, "D3039M-08 (2008) Standard test method for tensile properties of polymer matrix composite materials," *ASTM International, West Conshohocken, PA*, vol. 15, no. 3, 2017.
- [22] ASTM C364 / C364M-16, "Standard Test Method for Edgewise Compressive Strength of Sandwich Constructions," *ASTM International, West Conshohocken, PA*, vol. 15, no. 3, 2016.
- [23] ASTM C393 / C393M-20, "Standard Test Method for Core Shear Properties of Sandwich Constructions by Beam Flexure," *ASTM International, West Conshohocken, PA*, vol. 15, no. 3, 2020.
- [24] ASTM D792-20, "Standard Test Methods for Density and Specific Gravity (Relative Density) of Plastics by Displacement," *ASTM International, West Conshohocken, PA*, vol. 8, no. 1, 2020.
- [25] M. J. Sharba, Z. Leman, M. T. H. Sultan, M. R. Ishak, and M. A. A. Hanim, "Tensile and compressive properties of woven kenaf/glass sandwich hybrid composites," *International Journal of Polymer Science*, vol. 2016, 6 pages, 2016.
- [26] A. Petras and M. P. F. Sutcliffe, "Failure mode maps for honeycomb sandwich panels," *Composite Structures*, vol. 44, no. 4, pp. 237–252, 1999.
- [27] ASTM D7250 / D7250M-20, "Standard Practice for Determining Sandwich Beam Flexural and Shear Stiffness," *ASTM International, West Conshohocken, PA*, vol. 1503, 2020.

Review Article

Jatropha Oil as a Substituent for Palm Oil in Biobased Polyurethane

Mohamad Ridzuan Amri,¹ Syeed Saifulazry Osman Al-Edrus ¹, Chuah Teong Guan ^{1,2},
Faizah Md Yasin,^{2,3} and Lee Seng Hua¹

¹Institute of Tropical Forestry and Forest Product, Universiti Putra Malaysia, 43400 Serdang, Selangor, Malaysia

²Department of Chemical and Environmental Engineering, Faculty of Engineering, Universiti Putra Malaysia, 43400 Serdang Selangor, Malaysia

³Institute of Advanced Technology, Universiti Putra Malaysia, 43400 Serdang, Selangor, Malaysia

Correspondence should be addressed to Syeed Saifulazry Osman Al-Edrus; saifulazry@upm.edu.my and Chuah Teong Guan; chuah@upm.edu.my

Received 29 November 2020; Revised 29 December 2020; Accepted 28 January 2021; Published 17 February 2021

Academic Editor: Mehdi Salami-Kalajahi

Copyright © 2021 Mohamad Ridzuan Amri et al. This is an open access article distributed under the Creative Commons Attribution License, which permits unrestricted use, distribution, and reproduction in any medium, provided the original work is properly cited.

Polyurethanes (PUs) are unique polymers that can be tailored to suit certain applications and are increasingly used in many industrial fields. Petrochemicals are still used as the main compound to synthesize PUs. Today, environmental concerns arise in the research and technology innovations in developing PUs, especially from vegetable polyols which are having an upsurge. These are driven by the uncertainty and fluctuations of petroleum crude oil price and availability. Jatropha has become a promising substituent to palm oil so as to reduce the competition of food and nonfood in utilizing this natural resource. Apart from that, jatropha will solve the problem related to the European banning of palm oil. Herein, we review the literature on the synthesis of PUs using different vegetable oils and compare it with jatropha oil and its nanocomposites reinforced with cellulose nanocrystals. Given the potential of vegetable oil PUs in many industrial applications, we expect that they will increase commercial interest and scientific research to bring these materials to the market soon.

1. Introduction

For a century, mankind has exploited so many nonrenewable resources, mainly petrochemicals. Today, most of the polymer markets are petrochemical-based and have been extensively converted in numerous ways, including household raw materials for industry, generating energy, and intermediate and derivative products. This exploitation process uses a vast amount of energy and leads to various effects on the environment and ecosystems due to toxic substances. On the another hand, issues related to fluctuation and depletion supply of oil, which have pushed academicians as well as industries to find suitable biobased polymers to be used instead of petrochemical-based polymers to reduce the dependency on petroleum oil. Biorenewable polymer derived from biomass is the most possible substituent to the petro-

chemical polymer. Malaysia produces more than 160 million tonnes of biomass yearly and expects to grow in the future, and those biomasses include palm oil, timber waste, coconut trunk fibers, rice husks, sugarcane waste, and municipal waste [1]. Plant-based and agriculture-based biomasses are the largest natural resources and abundantly available in Malaysia [1]. In general, biorenewable polymers created from biomass can be categorized into 3 main types: (1) polymers directly synthesized from plant-based biomass, (2) polymers synthesized from biobased monomers, and (3) polymer products from naturally or genetically modified animals/organisms [2]. Malaysia is blessed with underutilized biomass due to its unique tropical whether suitable for agriculture activities. Thus, palm oil plantation is widely planted in Malaysia and generates a substantial amount of waste every year. This waste includes empty fruit bunches, mesocarp

fibers, palm oil fronds, palm kernel shell, palm oil trunks, and palm oil mill effluent. However, only 23% of palm oil biomass is used as a source of energy for the boiler in a palm oil mill, and the remaining 75% is underutilized and abandoned on site [3]. This value shows a stable supply of plant-based biomass which contains polysaccharides and lipids/oil to be utilized and exploited for diversified products.

Cellulose is important to human civilization and has been utilized in all kinds of practical applications for centuries. With the discovery of cellulose, its structure, morphology, and chemical composition were unknown. Improvements have been made over time, mainly through the selection and processing of its original sources and harvesting. The molecular structure of cellulose did not bring any meaning until its discovery at the beginning of the nineteenth century. Cellulose consists of linear polysaccharides with repeating units of disaccharides of *D glucose*. The *D glucose* is linked with β -1,4 linkage and intramolecular or intermolecular hydrogen bonding between the adjacent glucose units to form a linear chain. In plants, the majority of cell walls consist of lignin, cellulose, and hemicellulose, where they present about 10-25%, 35-50%, and 20-25% of the dry weight of lignocellulosic biomass, respectively [4]. Examples of lignocellulosic biomass that contain high cellulose composition are jute, hardwood, softwood, and pinecone biomass.

Today, the research trend has moved toward nanosized fillers for biopolymer composites. The biopolymer composite is widely used from low-cost household products to high-end industrial production. As cellulose is one of the natural and most abundant fibers, the cellulose fiber-reinforced polymer composite has gained much attention from academicians as well as industrialists. Cellulose-reinforced polymer composite has advantages and relevant properties such as non-abrasiveness, nontoxicity, biodegradability, low density, combustibility, and less production course compared to other synthetic polymers [4]. Despite its advantages, it has some disadvantages like poor interfacial adhesion and high water adsorption. Due to this, industrials are not interested in the production of cellulose fiber-reinforced processes. Even though this issue can be solved by chemical modification of the cellulose fiber itself, but the recent trend of research is now focused more on the extraction of nanocellulose material from cellulosic fibers for the fabrication of nanocellulose fiber biocomposite application. Review of the extraction and production of nanoscale cellulose materials has been made extensively in the last decade, but their application as reinforcement fillers is a relatively new research field. When compared with cellulose, the nanocellulose material has a high surface ratio, is light weight, and is higher in strength and stiffness.

A recent study conducted by Kim et al. shows that by adding cellulose nanofibrils from 1-50 wt% of waterborne polyurethane, the thermal and mechanical properties of the composite film improve significantly as the loading of cellulose nanofibrils increases [5]. Same trends were also observed in the work conducted by Zhang et al. and Kaushik et al. in which 1-15% of CNF in the starch natural polymer was incorporated [6, 7]. It is proven that, by all past studies conducted, cellulose nanofibers can increase the mechanical

properties and are suitable to be used as reinforcement filler for biopolymers.

In Malaysia, the agriculture sector contributes about 7.3% (RM 99.5 billion) to Malaysia's gross domestic product (GDP) in 2018; meanwhile, palm oil was the major contributor to the GDP of the agriculture sector by as much as 37.9%. This achievement is due to Malaysia having produced millions of tonnes of crude palm oil and palm kernel oil throughout the year 2018. However, to utilize this availability of natural resources, some issues arise as using edible oil to serve nonfood products is not appropriate. The use of edible oil as a feedstock will increase and create competition and conflicts of interest in terms of demand and supply between food and nonfood industries. This will affect the price growth and insufficient supply of palm oil. Apart from that, there is an issue arising about the banning of international trade of palm oil by the European Union from commodity countries such as Malaysia and Indonesia. This banning is aimed at reducing tropical deforestation and forest degradation in developing countries to limit global warming and preserve biodiversity [8]. It is estimated that globally between 2001 and 2015, about 27% of all forest disturbance was commodity-driven, and palm oil production is one of the examples that are implicated in countries such as Indonesia and Malaysia [9, 10]. Realizing this, since 2017, Malaysia had moved to the plantation of *Jatropha curcas* for nonedible oil production purposely to serve nonfood product production and avoid tropical deforestation and forest degradation.

Polyurethane (PU) is one of the possible products that can be created from vegetables. PU is a green material, a high-performance elastomer, and has been applied in a wide range of engineering fields such as automotive, construction, and electrical appliances [11]. PU has various properties and can be tailor-made to suit each research application by selecting different monomers and chain extenders for synthesis or by blending special reinforcement materials. Recently, many studies reveal the use of vegetable oil especially jatropha oil for the production of polyols and polyurethane, such as producing jatropha oil-based polymer via epoxidation and ring-opening [12], polyurethane as a wood adhesive [13], jatropha oil-based polyurethane as nonaqueous solid polymer electrolyte [14], and jatropha oil-based waterborne polyurethane dispersion [15]. Briefly, this paper will review and compare a few chemical processes and their parameters to produce a vegetable-based polyol as an intermediate for biobased polyurethane. As biobased polyurethane is weak in terms of mechanical and thermal properties, we will review the potential of nanocellulose materials as reinforcement and highlight its enhancement in terms of thermal and mechanical, and lastly, we highlight the finding of numerous studies which show promising nanocomposite film-reinforced cellulose nanomaterials. Overall, the overview is illustrated in Figure 1.

2. Vegetable Oil-Based Polyurethane

Polyurethanes (PUs) are a unique class of polymers which exhibit an excellent range of properties and applications in elastomers, adhesives, sealants, and foams [16-18]. PU is synthesized by the reaction between isocyanate and polyol.

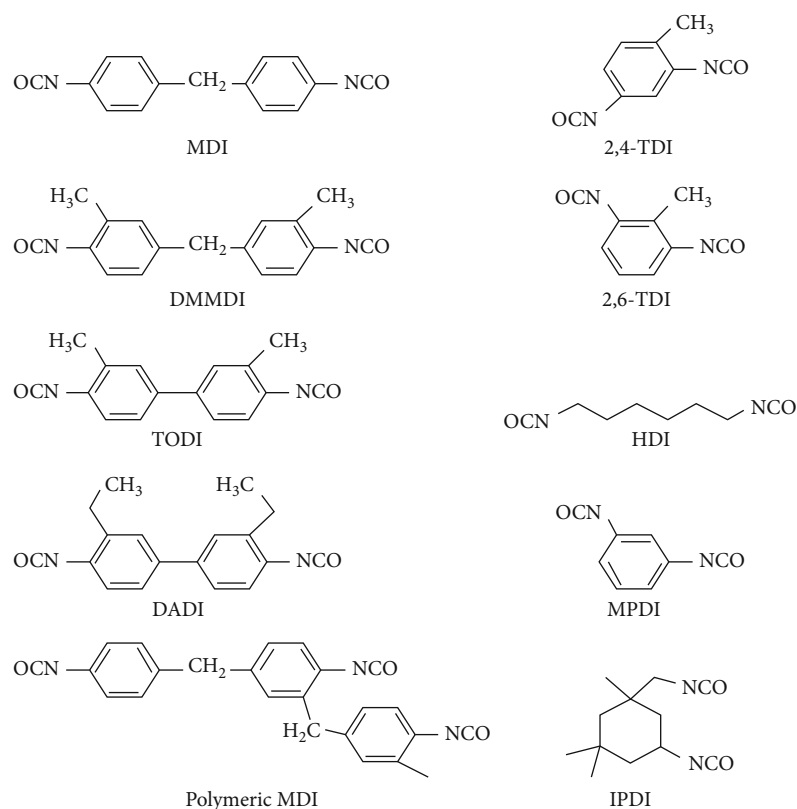


FIGURE 1: Overall flowchart.

Sometimes, low molecular weight diols or amines are used to increase the PU molecular weight. The specific application requires a specific character of polymer. The structure of the resulting polymers can be adjusted to manually selecting and controlling appropriate reacting components. A variety of polyols are widely available; meanwhile, only a few polyisocyanates are commercially available [19]. Figure 2 shows some commonly used isocyanates for PU synthesis. Properties of the created PUs are highly dependent on the selection of polyols. Vegetable oil-based polyols act as soft amorphous segments that provide flexibility to the created PU, while cyclic isocyanates act as hard segments providing mechanical strength. These combinations of hard and soft segments give an excellent combination of properties to the created PU, including degradation, mechanical strength, elasticity, and toughness [20]. Besides that, the selection of suitable vegetable oil as a soft segment of polyurethane gives a significant impact to its properties. As of today, soybean oil is the world's largest vegetable oil used by industries for various applications. As for Malaysia, it is still dependent on palm oil. *Jatropha* oil is a promising candidate to replace palm oil for polyurethane production in Malaysia. This is because its chemical composition is much better than palm oil. The chemical composition is summarized in Table 1.

2.1. Vegetable Oil-Based Polyol Prepared by Epoxidation/Oxirane Ring-Opening and Their Resulting PUs. Of all common vegetable oils, castor oil naturally contains hydroxyl

groups which makes it the absolute choice to produce PU. However, the resource of castor oil is only available in the American region and is not suitable to be planted in Malaysia. The most commercially used synthesis method of vegetable-based polyols is by epoxidation and the ring-opening method. Epoxidation and ring-opening have become the main reaction route for the synthesis of vegetable-based polyols because of its advantages in terms of economic and safety, as the reaction can be performed at a lower temperature which is between 25°C and 80°C. On another hand, hydroformylation requires expensive catalysts and needs to be conducted at high pressure and temperature, 14-28 MPa and 90-120°C, respectively. Meanwhile, ozonolysis produced polyols with a lower hydroxyl number with a maximal functionality of 3. Here, the recent advances related to epoxidation and the ring-opening reaction of vegetable oil will be reviewed. Comparison between these methods is summarized in Table 2 and reviewed in detail in this section.

Several research groups have conducted a systematic study on the kinetics of ring-opening reactions. Guo et al. [23] reported that epoxidized palm oil was successfully ring-opened by acetic acid without a catalyst and showed that its activation energy was 40.28 kJ/mol. Zhang et al. showed a comparable result of activation energy with Guo et al. [24] by using the same ring opener but used soybean oil instead of palm oil. On another hand, Zhang et al. [25] utilized the natural hydroxyl group located at the castor oil fatty acid chain

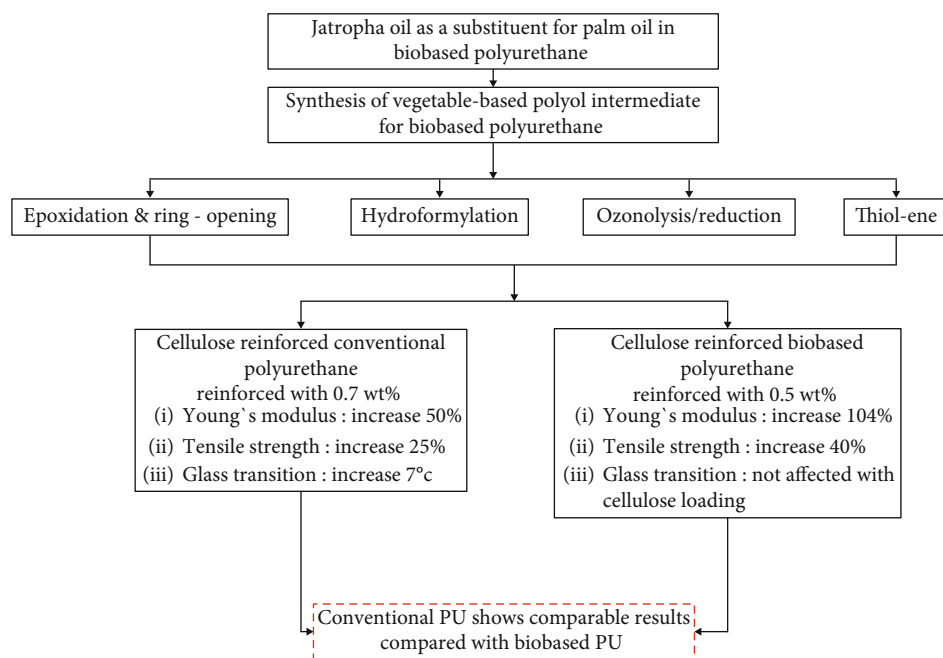


FIGURE 2: Chemical structure of commonly used isocyanates [24].

TABLE 1: Chemical composition comparison of fatty acid profile.

Fatty acid	Jatropha oil ^a	Palm oil ^{a,b}	Coconut oil ^b	Sunflower oil ^b	Soybean oil ^b	Pongamia oil ^b
Caprylic acid (C8:0)	—	—	8	—	—	—
Capric acid (C10:0)	—	—	8	—	—	—
Lauric acid (C12:0)	—	—	48	0.5	—	—
Myristic acid (C14:0)	0.38	3.5	16.0	0.2	0.1	—
Palmitic acid (C16:0)	16.0	39.5	40.3	8.5	4.8	11.0
Palmitoleic acid (16:1)	1-3.5	—	—	0.8	0.1	—
Stearic acid (C18:0)	6-7	3.5	3.1	2.5	5.7	4.0
Oleic acid (C18:1)	42-43.5	46	43.3	6.5	20.6	23.4
Linoleic acid (C18:2)	33-34.5	7.5	13.2	2.0	66.2	53.2
Linolenic acid (C18:3)	0.8	—	—	0.8	7.8	—

^aTaken from Verma and Gaur [21]; ^btaken from Koh and Mohd Ghazi [22].

TABLE 2: Comparison of commonly used methods for vegetable oil-based polyols.

	Epoxidation/ring-opening	Ozonolysis/reduction	Hydroformylation	Thiol-ene
Number of steps	2	2	2	1
Functionality	Secondary, tunable	Terminal, 3	Primary, tunable	Primary, tunable
OH value	70-320	228-260	150-200	223
MW	Variable (>1000)	500-700 ^a	900-1100 ^a	1070-1440 ^a
Viscosity	High	Low	Medium	Medium
Reaction temperature	Variable (50-170)	RT	120	Low or RT
Reaction time	Long	Medium	—	Short

^aTaken from [31]. RT: room temperature; MW: molecular weight.

as a ring opener for epoxidized soybean oil with the presence of 1,8-diazabicycloundec-7-ene as a catalyst and showed that the activation energy was 72.2 kJ/mol. Based on this finding, it can be concluded that higher activation energy is due to the

steric effect of long carbon chains. As a solution for high activation energy, a suitable catalyst and reaction temperature can be used to lower it down and thus achieve faster reaction time.

Another type of ring opener that is widely used is water and alcohol (mono-/polyhydroxy) and is widely catalyzed by phosphoric acid, sulphuric acid, fluoroboric acid, and Lewis acid [23, 26]. Using a different ring opener, which is methanol glycol and 1,2-propanediol, Ni et al. [27] produced a soybean oil-based polyol with OH number in the range of 148 to 240 mg KOH/g. What makes the OH number important is because it correlates with the crosslink density between isocyanate and polyol. PUs with glassy properties were usually created from polyols with OH numbers above 170 mg KOH/g (high crosslink density) while PUs with OH numbers below 170 mg KOH/g were rubbery (low crosslink density). In addition, as the OH number increases, the glass transition temperature and mechanical properties increase [28]. Hazmi et al. [12] successfully synthesized jatropha oil-based polyols with OH numbers ranging from 171 to 179 mg KOH/g by using methanol as a ring opener. The authors used 50% concentrated hydrogen peroxide during the solvent-free epoxidation process and determined that concentrated hydrogen peroxide accelerated the epoxidation reaction, thus resulting in the maximum value of oxirane oxygen content and minimum side reaction. However, another study conducted by Saalah et al. [15] which used 30% hydrogen peroxide and methanol as the ring opener shows that concentrated hydrogen peroxide does not affect the OH number but affects only the reaction time. The authors successfully synthesized jatropha oil-based polyols with OH numbers varying from 138 to 217 mg KOH/g with the minimum side reaction proven by FTIR spectra. Zieleniewska et al. [29] used diethylene glycol as a ring opener for epoxidized rapeseed oil, followed by the synthesis of a porous polyurethane scaffold. The authors concluded that this scaffold is a good potential candidate as a substrate for bone tissue culture based on simulated body fluid testing. A suitable candidate is due to bioactivity and degradation behavior.

Apart from using chemical hydroxyl groups, water also was used as a ring opener as it is a cheap, highly available, and green nucleophilic reagent. Gaikwad et al. [30] reported that epoxidation and ring-opening process can be done in a single step by using a mixture of formic acid and hydrogen peroxide, in which water acts as a ring opener. Meanwhile, Kim et al. [5] synthesized palm oil-based polyols using tetrafluoroboric acid as a catalyst and water as a ring opener through epoxidation and ring-opening process. The created polyurethane exhibited a tensile strength of 6.05 MPa, elongation at break 62.05%, and a glass transition temperature of 25°C. The mechanical and thermal properties of vegetable-based polyol PUs synthesized via epoxidation and different types of ring-opening are summarized in Table 3. Hence, it is concluded that the properties of PU are influenced by the formulation of the polyol hydroxyl number, ring opener, and type of isocyanate.

In contrast, polyols prepared by ozonolysis/reduction produce primary alcohol which is more reactive compared to secondary alcohol produced by epoxidation and ring-opening [32]. During hydrolysis, unsaturated carbon reacted with ozone and unstable ozonide is formed. At this stage, polyols can be produced in 3 simple steps. Unstable ozonide leads to cleavage of the unsaturated carbon in the fatty acid

chains, followed by reduction to an aldehyde, and lastly to alcohol [33–37]. In addition, the resulting PU from this ozonolysis step is a rigid PU due to the hydroxyl group being located at the end of the fatty acid chain [38]. Three different models of ozonolysis from 3 different vegetable oils were successfully developed by Husic et al. [39]. Those vegetable oils were triolein oil, canola oil, and soybean oil. Based on that model, the functionalities of these polyols were 3.0, 2.8, and 2.5, and the T_g of the resulting PU were 53°C, 36°C, and 22°C, respectively. Based on this, different and residual saturated fatty acid PUs from canola and triolein polyol were glassy as shown by its elongation at break which was 51% and 25%, respectively. In contrast, the elongation of PU from soybean is 176% indicating that it is a hard rubber. The functionality of polyols prepared by epoxidation/ring-opening can be tunable by varying the choice of vegetable oil with different epoxy content and ring-opening agent. Meanwhile, polyols obtained by ozonolysis/reduction are limited to a maximum of three hydroxyl groups per triglyceride [24].

Apart from ozonolysis/reduction, vegetable oil-based polyols with primary alcohol can also be produced by hydroformylation of unsaturated carbon into aldehyde using syngas in the presence of catalyst followed by reduction into hydroxyls by hydrogenation [29]. Catalysts used are rhodium with a conversion rate of about 95% but costly [40]. Based on studies conducted by Petrović et al. [41], the authors prepared crude alga oil-based polyol by hydroformylation with rhodium as catalyst $\text{Rh}(\text{CO})_2$ and compared the results with alga polyols prepared by ozonolysis and epoxidation. Epoxidation produced polyols with brown color with a hydroxyl value of around 150 mg KOH/g. PU produced from this process led to a red colored transparent sheet with T_g of -39°C, a good tensile strength of 6.8 MPa, and 38% elongation at break. Hydroformylation produced polyols with black color with an OH value of 150 mg KOH/g. A black film was prepared with the properties of T_g of -36°C, tensile strength of 8.1 MPa, and elongation at break of 28%. Polyol from ozonolysis is light colored but with a low hydroxyl value. This low hydroxyl number indicated that this polyol made from ozonolysis was not suitable for polyurethane application due to the low unsaturation of algal oil.

Thiol-ene reaction provides direct conversion of vegetable oil to polyol with less side reaction, high yields, and high conversion rate [42–44]. Thiol-ene reactions consist of 3 steps: (1) formation of free radicals by thermal initiation or photoirradiation, (2) formation of thiyl radicals by transferring free radicals to the sulphur atom, and (3) anti-Markovnikov addition of thiyl radicals to double bonds [45]. Desroches et al. [46] studied the effect of radiation intensity, thiol/double bond ratio, and the number of double bonds per chain on the optimization of rapeseed oil polyols. The glass transition and thermal stability were comparable to those of a commercial polyol Desmophen 1150 (OH value: 165 mg KOH/g). However, the drawback of this method is the low reactivity of internal double bonds of vegetable oils, which make the thiol-ene rate for vegetable oil-based polyol limited. Tables 2 and 4 summarize the difference in each process parameter and the mechanical and thermal properties of biobased polyol produced from different vegetable oils.

TABLE 3: Mechanical and thermal properties of vegetable-based polyol polyurethane synthesized via epoxidation and ring-opening.

	Ring opener	Polyols Epoxidized vegetable oil	OH number (mg KOH/g)	DSC T_g ($^{\circ}$ C)	PUs		Modulus (MPa)	Reference
					Tensile strength (MPa)	Elongation at break (%)		
Alcohol	Methanol	Jatropha oil	161-217	—	4	84.9	27.9	[15]
	Methanol	Jatropha oil	171-176	—	—	—	—	[12]
	Methanol	Jatropha oil	—	—	0.41	341	1.31	[2]
	Glycol	Soybean	195-240	60-75	11.1-116.9	32.8-36.4	—	[47]
Acid	Lactic acid	Soybean oil	309.6	9.6-20.4	9.3-27.1	74.1-110.7	4.4-12.7	[48]
	Phthalic acid	Palm oil	73-80	—	—	—	—	[49]
	Acetic acid	Soybean	—	43	23.7	7.4	977	[49]
Amine	Propanolamine	Soybean	317	29	9.3	140.8	—	[50]
	Diethyl amine	Soybean	67.8	26	7.8	24.7	184.7	[51]

3. Cellulose as Versatile Fiber Reinforcement for Polymer Composite

Today, most composites were reinforced with synthetic fibers and have been applied in multiple applications such as aircraft and automation industries. However, the biggest disadvantage of synthetic fiber is its nonbiodegradability; the manufacturing process releases carbon dioxide which brings impact on the environment, and it always depends on nonrenewable resources. Therefore, inorganic biofiller has attracted much attention as it is renewable. Most documented works focused on lignin and cellulose. Here, the recent advances related to cellulose as a versatile reinforcement for polymer-based composites will be reviewed.

Based on the work conducted by Pei et al. [52], polyurethane/cellulose nanocrystal nanocomposites with ultrahigh tensile strength were successfully synthesized. Polytetramethylene glycol was used as a polyol. A cellulose nanocrystal was covalently bonded to a hard segment of polyurethane. The authors concluded that this bonded cellulose with hard segment polyurethane is important to stiffening and toughens the thermoplastic polyurethane. In addition, with the addition of only 1 wt% cellulose nanocrystals, the authors obtained a polyurethane nanocomposite with a tensile strength of 61.5 MPa, strain-to-failure of 994.2%, and Young's modulus of 42.4 MPa. Meanwhile, Kupka et al. [53] utilized cellulose nanocrystals (CNCs) as nanofiller in a polyurethane matrix. In this work, CNCs modified by grafting polyethylene glycol (PEG) on the CNC surface (CNC-PEG) were used and compared with CNCs in the native state. The authors concluded that CNC-PEG composites showed an improved modulus up to 50% and strength up to 25% compared to CNCs by incorporating only 0.24 vol% of CNC-PEG. The matrix T_g increased by up to 7° C with just 0.7 vol% of CNC-PEG, indicating reduced polymer mobility close to CNC-PEG surface arising from excellent CNC-PEG dispersion and strong interfacial interactions. TEM showed excellent dispersion of CNC-PEG in the PU matrix compared to CNC, presumably due to better interactions between the matrix and the CNC-PEG surface. Interestingly, the cellulose

used by both Pei et al. [52] and Kupka et al. [53] was from the acid hydrolysis of Whatman No. 1 cellulose filter paper, and the same casting method was used. In brief, CNC was extracted from cotton 20 g Whatman No. 1 cellulose paper by acid hydrolysis, using 175 ml of 64 wt% sulphuric acid for 1 hour at 45° C. Then, the suspension was washed with deionized water, and the resultant precipitate was rinsed and dialyzed against water. The microcrystallites were further dispersed by ultrasonic treatment to create cellulose crystals of colloidal dimension. The detail parameters were described in the literature [52].

Khadivi et al. [54] studied the relationship of cellulose and polyurethane nanocomposite toward microphase separation. By adding CNCs, nanoparticles prevented the formation of hydrogen bonding between PU chains affected by the presence of hydroxyl groups on the surface of CNCs. The addition of CNC made significant changes in the microphase separation of PU such as the size of phases and morphology and creates smaller droplets with irregular shapes. The authors concluded that the addition of CNCs improved the tensile modulus of nanocomposites compared to neat PU due to the hard nature of CNCs and its reinforcement effect in the matrix, increasing the crosslinking density due to the reaction of hydroxyls on the surface of CNC with isocyanate groups. Nanocellulose was fabricated using acid hydrolysis of microcrystalline cellulose, and PEG was used as a polyol. Kim et al. [5] studied the influence of cellulose nanofibrils on the microstructures and physical properties of waterborne polyurethane-based nanocomposite films. Based on the authors work, the glass transition temperature of soft segments ($T_{g,SS}$) decreased slightly with increase of the CNF content, whereas the $T_{g,HS}$ values of WPU hard segments increased significantly with the increment of the CNF content up to ~ 7 wt%, which is caused by the presence of specific interactions between CNFs and WPU hard segments. For thermal degradation, the degradation temperature of both soft and hard segments increases as CNF increases. Interestingly, the final residues of the nanocomposite films at 800° C increased from 1 wt% to 19 wt% as CNF increases. However, no mechanical property change was reported.

TABLE 4: Mechanical and thermal properties of biobased polyols produced from different vegetable oils. These polyols were then used to synthesize PU.

Polyol		Pu						References
Type of reaction	Vegetable oil	OH value	Isocyanate	Glass transition temperature (T_g) ($^{\circ}$ C)	Tensile strength (MPa)	Elongation at break (%)	Young's modulus (MPa)	
EPO & RO	Jatropha	138-217	IPDI	NF ^a	1.8-4.0	85-325	1-28	[15]
	Sunflower	402	HDI & IPDI	46-86	1.6-4.1	10.6-56.6	52.1-302.3	[55]
	Soybean	309	HDI	9.6-24.9	9.3-27.1	74.1-110.7	NF ^a	[48]
	Soybean	61-97	MDI	65-75	11-32	101-310	NF ^a	[56]
	Soybean, castor, linseed, canola, & grapeseed	109-173	IPDI	22.9-54.5	0.4-29.1	11-98	0.8-495	[57]
	Soybean	158-283	MDI	22-62	3.4-39.7	15-35	32-351	[58]
	Soybean	NF ^a	MDI	43-52	23.7-35.9	6.1-7.4	954-1284	[59]
	Canola and sunflower	259-286	MDI	86-101	55-60	5.6-6.4	1.5-1.73	[60]
	Soybean	148-237	TDI	83.6	6.3-38.1	14.5-19.6	NF ^a	[28]
	Soybean	124-183	IPDI	24-69	3.5-20.1	104.0-232.7	5.6-303.7	[61]
RO	Soybean, linseed, corn, and peanut	139-163	IPDI	-9 to 13	2.4-7.5	312-343	5.20-16.1	[62]
	Soybean	99-460	IPDI	50-82	4.5-13.8	16-109	13-299	[63]
	Soybean	63-81	IPDI	-23 to 26	4.6-12.4	8.4-46	NF ^a	[63]
	Soybean	160	IPDI	6.6-14.4	11.6	232.7	5.8	[25]
	Soybean	317	HDI	24.36-28.69	2.74-27.76	140-168	NF ^a	[50]
	Soybean & linseed	353-434	MDI	23.7-52.3	19.7-35.1	9.5-90.4	NF ^a	[25]
	Soybean & linseed	150-215	IPDI	19.0-56.3	8.6-17.2	62-210	67.2-315	[64]
Palm	60-100	IPDI	NF ^a	0.05-0.07	51-74	0.09-0.2	[65]	
Thiol	Rapeseed	165-223	HDI & MDI	25 to -25	NF ^a	NF ^a	NF ^a	[46]
	Castor and soybean	203-278	MDI	100-150	13.07	NF ^a	NF ^a	[66]
	Soybean	199	MDI	41	15.7	471	471	[67]
	Soybean	119-198	MHI	12-17	8.1-16.8	605-800	605-800	[68]
	Jojoba	NF ^a	HDI & MDI	-18 to -43	NF ^a	NF	NF	[69]
	Castor	218-290	XDI, MDI, & HDI	16-54	2.5-43.9	4-112	4-112	[70]
	Castor	NF ^a	IPDI	18-41	6-24	45-401	45-401	[71]
	Linseed, Olive, grapeseed, castor, canola, & corn	190-305	IPDI	23-50	1-11	3-204	3-204	[72]
	Olive, linseed, rice bran, & grapeseed	190-305	IPDI	8.7-56.9	4.7-50.7	15-331	15-331	[73]

Abbreviations: IPDI: isophorone diisocyanate; XDI: m-xylylene diisocyanate; TDI: toluene diisocyanate; HDI: hexamethylene-1,6-diisocyanate; MDI: methylene diphenyl diisocyanate; MHI: 4,4'-methylenebis (cyclohexyl isocyanate). ^aThe corresponding data was not reported by authors.

In conclusion, the types of polyol for conventional-based does not bring any significant effect toward the properties of polyurethane; however, it eases the synthesis process as its chemical structure is a straight line compared to nonconventional based. What is important is the hydroxyl number. High hydroxyl number will contribute to the high crosslink between isocyanate and polyol which will result in its good mechanical properties. The higher crosslink density in PUs made with polyols with OH numbers above 170 mg KOH/g resulted in glassy

properties, while PUs with lower crosslink densities with hydroxyl numbers lower than 170 mg KOH/g were rubbery [24]. Apart from that, it is proven that cellulose does help to strengthen the mechanical properties of the nanocomposite film as per the above discussion. However, too much CNC loading leads to agglomeration in the PU matrix. The optimum loading for CNC is about 0.5 wt%. Based on the work conducted by Khadivi et al. [54], 0.5 wt% showed microphase mixing in which CNC is well dispersed and placed between HS-rich regions. Cellulose is

used in a wide range of applications. Table 5 shows a short review on cellulose nanocomposites in different industries.

4. Cellulose as Versatile Fiber Reinforcement for Biobased Polyurethane Composite

Gao et al. [84] developed waterborne castor oil-based PU nanocomposites with cellulose nanocrystals as reinforcement. The resulting PU shows that the tensile strength and Young's modulus of the composites increased by 125% and 104%, respectively, with 1 wt% nanocrystals. This is due to their rigid nature and high aspect ratio (nanosize) and the strong hydrogen bonding between the filler and the PU matrix. Authors also highlighted that an increase in cellulose content led to self-aggregation and a decrease in properties; however, the incorporation of cellulose does not significantly affect the T_g . Floros et al. [85] used cellulose with loading rate of 0-2.5 wt% to reinforce inside the oleic acid-based thermoplastic PU. Authors report that reinforcement of cellulose did not affect T_g , crystallization behavior, and melting temperature. Authors stated that with 0.5 wt%, cellulose loading shows an increase in elongation at break and tensile strengths of 50% and 40%, respectively. Apart from that, He et al. [86] compare cellulose with dialdehyde cellulose at loading levels of 0-25 wt% as reinforcement for soybean oil-based thermosetting polyurethane composite via the casting method. The authors concluded that oxidized cellulose shows better performance than cellulose due to higher interfacial bonding and small particle size. Saralegi et al. [87] reported that the addition of 0.5 wt% cellulose nanocrystals to castor oil-based PU did not affect the shape fixity but improved the shape recovery from 50 to 100% because of the hard phase crystallinity of cellulose. Mosiewicki et al. [88] used micro/nanocellulose to reinforce rapeseed oil-based PU foam. The incorporation of cellulose increased the mechanical properties, water absorption, and rigidity of the resulting foams.

When discussing about biobased materials, the toxicity level of the materials is quite important to study. Based on work conducted by Rezaei Hosseinabadi et al. [89], the authors studied the cytotoxicity level between vegetable oil-based (castor oil) and petroleum-based (polycaprolactone) PU without reinforcement of the nanocellulose. Cytotoxicity of the PU sample was performed by the MTT assay. MTT assay was conducted in cultured L-929 cells on 3, 5, and 7 days. It is reported that cellular viability of polycaprolactone (PCL) is higher compared to castor oil-based PU, and cytotoxicity of PCL-based PU was significantly lower compared to castor oil-based PU. The authors explained that ester linkages in PCL-based PU are highly biocompatible with microorganisms. Apart from biocompatible properties, structure crystallinity and hydrophilicity properties of the films contributed to better cytotoxicity. These enhanced characteristics result in better cell growth and adhesion. It is supported by static contact angle where PCL-based PU (5.67%) is more hydrophilic compared to castor oil-based

PU (0.76%). However, the authors explained that they were very significantly different ($p < 0.05$) between vegetable-based and petroleum-based PUs in terms of cell viability and cytotoxicity. In fact, it is reported that with the addition of nanocellulose, the nanocomposite film obtained will have a better cytotoxicity level. As reported by Khadivi et al. [90], concentration of viable cells increases as reinforced CNC loading increases on polydimethylsiloxane- (PDMS-) based PU nanocomposite films. The CNC was incorporated using the prepolymer method. The cytotoxicity studied from the samples was determined by in vitro cell culturing via seeding human fibroblast (FBS) cells on sample films. It is noted that cell toxicity was inversely proportional to the concentration of viable cells. Based on the authors' work, cell viability was increased from 50-60% to 90-100% as CNC increases from 0.1 to 2 wt%. In general, the authors explained that sources of cytotoxicity of the polymer resulted from the presence of impurities, polymer degradation, and interaction of the polymer with intracellular processes as well as cell membrane. Therefore, the authors concluded that moderate cytotoxicity resulted from interaction with intracellular processes or/and interactions of polymers with cell membranes as all monomers completely reacted in the reaction synthesis which lead to no molecule impurities, and no degradation of the polymer happens at lower temperatures which is supported by FTIR and TGA analyses, respectively. On the other hand, Xu et al. [91] studied about the influence of different cotton cellulose nanofiber (c-CNF) loading and degree functionalisation of amino-terminated polydimethylsiloxane (H_2N -PDMS- H_2N) on the cytotoxicity level of polycarbonate diol- (PCDL-) based PU nanocomposite films. 2 sets of samples were successfully prepared; (1) influence of c-CNF was studied by using 0 and 5 wt% CNF while the molecular weight of H_2N -PDMS- H_2N was fixed at 1000 and (2) degree of functionalisation was observed by using 2000 and 4000 molecular weights of H_2N -PDMS- H_2N while c-CNF loading was fixed at 5 wt%. Incorporation of c-CNF was prepared by the prepolymer method. It is observed that on sample set (1), cell viability increases as much as 3.7% when loading of c-CNF increases from 0 to 5 wt%. This finding shows good agreement with work conducted by Khadivi et al. [90]. Next, by increasing the molecular weight of H_2N -PDMS- H_2N from 1000 to 4000 with fixed 5 wt% c-CNF, the finding shows increase in cell viability value by as much as 23.1%. This is due to H_2N -PDMS- H_2N which introduces excellent biocompatibility properties toward the polymer matrix which supports more cell adhesion and growth. Overall, there is very small difference in terms of cell viability and cytotoxicity between vegetable-based and petroleum-based PUs. Both CNC and CNF help to increase cell viability and better cytotoxicity of nanocomposite films as loading of cellulose increases, and lastly, cell viability and cytotoxicity can be further improved by introducing biocompatible monomer inside the polymer matrix of nanocomposites. An example of monomer is H_2N -PDMS- H_2N . Therefore, it is supported that both vegetable oil- and petroleum oil-based PU nanocomposite films can be utilized in medical and food packaging applications as they achieved high cell viability by as much as 90-100%.

TABLE 5: Cellulose nanocomposite application in different industries.

Application field	Product features	References
Paper & packaging	Intelligent packaging	[74, 75]
	Transparent packaging	[76]
	Ultraviolet screening packaging	[77]
Barrier properties	Shelf-life extension	[78]
	Downgauging of films	
	Oxygen scavenger	
Electronics/metallic particles	Time-temperature integrator	[79]
	Freshness indicator	
	Gas and leakage detector	
	Sensors for food monitoring	
Medical	Signal processor for biochemical pathways	[4]
	Drug delivery and controlled release	
	Scaffold in tissue engineering	
Composites & plastics	Implants	[80]
	Shelf-life extension	[81]
	Heat resistance	[82]
Aerogel	Dimensional stability	[83]
	Self-healing material	

5. Conclusion

Vegetable oil is an excellent feedstock for biobased polymeric materials. As for now, several technologies have been developed to synthesize these valuable resources into polymer composites, monomers, and polymers with properties comparable to conventional polymers made from petrochemicals. The use of biorenewable feedstocks offers a solution towards volatility in oil price and disruption in oil supplies. For Malaysia, *Jatropha* oil offers protection against the crisis over the ban issue of import of palm oil into European countries. *Jatropha* oil shows promising properties as its chemical composition is the same as soybean oil which has been widely utilized in biopolyurethane production. Most of the manufacturers have little initiative to change to biobased plastic because the price of oil is low for now. However, it is predicted by economists that future economic and regulatory conditions will likely cause the cost of fossils to rise. In some regions of the world which lack petroleum reserves and access to refineries, the utilization of vegetable oil for agricultural production may open up to new economic development. A great challenge for vegetable oil-based polymers is in its property gap compared to conventional petroleum-based polymers. As highlighted in this review, a lot of research has been conducted to narrow these property differences. Chemical modification can contribute to the improvement in the mechanical, chemical, and thermal properties. Furthermore, filler sizing could also play an important role. Nano-

filler is loaded into vegetable oil-based polymer matrices to increase the performance and render new properties to extend their application area. Some of these fillers can be derived from renewable sources from agriculture or industrial by-product which lead to stable and sustainable polymer composites and can reduce the price of these materials. Even though a lot of research has been made, several challenges still exist. Those challenges include the controversy on polymers made up of food-grade vegetable oil. This food-grade vegetable oil has a problem in controlling its quality due to the heterogeneous nature of vegetable oil. The composition of vegetable oil varies between one another based on many different growth factors, including geographical location, environmental conditions, cultivar selection, and processing techniques. As highlighted throughout this review, different strategies have been developed to synthesize biobased polyols from vegetable oil with one good goal of meeting the cost and property requirements of the marketplace. The mechanical and thermal properties of PU were the most improved properties when reinforced with cellulose, which are the two important criteria for the market to adopt. However, the thermal and mechanical properties need continuous improvement. Tremendous research effort has been made to match the performance of vegetable oil-based PU with petroleum-based, as discussed in this review. Further research and innovation are required to produce cost-effective and high-quality vegetable oil-based PUs and broaden their application since vegetable oil appears to be a bright future. Novel PUs synthesized using biobased and renewable materials with improved mechanical and thermal properties are expected to fill the market shelf soon as research efforts in this field are continuously increasing, and *Jatropha* oil seems the most relevant of all vegetable oils as reviewed.

Data Availability

No data were used to support this study.

Conflicts of Interest

The authors declare that they have no conflicts of interest.

Acknowledgments

The support of this research by the Malaysian Ministry of Higher Education and Universiti Putra Malaysia under the granted GP-IPM (9667100), FRGS (03-01-19-2193FR), and INTROP HICOE (6369110) are gratefully acknowledged.

References

- [1] M. Ozturk, N. Saba, V. Altay et al., "Biomass and bioenergy: an overview of the development potential in Turkey and Malaysia," *Renewable and Sustainable Energy Reviews*, vol. 79, pp. 1285–1302, 2017.
- [2] S. O. A. SaifulAzry, T. G. Chuah, M. T. Paridah, M. M. Aung, and E. S. Zainudin, "17. Green nanocomposites from cellulose nanowhiskers and *Jatropha* oil-based polyurethane," in

- Cellulose-Reinforced Nanofibre Composites*, pp. 391–400, Elsevier Ltd, 2017.
- [3] N. James Rubinsin, W. R. W. Daud, S. K. Kamarudin et al., "Optimization of oil palm empty fruit bunches value chain in Peninsular Malaysia," *Food and Bioproducts Processing*, vol. 119, pp. 179–194, 2020.
 - [4] A. Sharma, M. Thakur, M. Bhattacharya, T. Mandal, and S. Goswami, "Commercial application of cellulose nanocomposites - a review," *Biotechnology Reports*, vol. 21, no. 2018, article e00316, 2019.
 - [5] M. S. Kim, K. M. Ryu, S. H. Lee, Y. C. Choi, and Y. G. Jeong, "Influences of cellulose nanofibril on microstructures and physical properties of waterborne polyurethane-based nanocomposite films," *Carbohydrate polymers*, vol. 225, article 115233, 2019.
 - [6] C. Zhang, S. S. Nair, H. Chen, N. Yan, R. Farnood, and F. Li, "Thermally stable, enhanced water barrier, high strength starch bio-composite reinforced with lignin containing cellulose nanofibrils," *Carbohydrate polymers*, vol. 230, article 115626, 2020.
 - [7] A. Kaushik, M. Singh, and G. Verma, "Green nanocomposites based on thermoplastic starch and steam exploded cellulose nanofibrils from wheat straw," *Carbohydrate Polymers*, vol. 82, no. 2, pp. 337–345, 2010.
 - [8] E. A. Wilman, "Market redirection leakage in the palm oil market," *Ecological Economics*, vol. 159, pp. 226–234, 2019.
 - [9] K. M. Carlson, R. Heilmayr, H. K. Gibbs et al., "Effect of oil palm sustainability certification on deforestation and fire in Indonesia," *Proceedings of the National Academy of Sciences of the United States of America*, vol. 115, no. 1, pp. 121–126, 2018.
 - [10] P. G. Curtis, C. M. Slay, N. L. Harris, A. Tyukavina, and M. C. Hansen, "Classifying drivers of global forest loss," *Science*, vol. 361, no. 6407, pp. 1108–1111, 2018.
 - [11] R. De Chen, C. F. Huang, and S. Hsu, "Composites of waterborne polyurethane and cellulose nanofibers for 3D printing and bioapplications," *Carbohydrate Polymers*, vol. 212, no. 1, pp. 75–88, 2019.
 - [12] A. S. A. Hazmi, M. M. Aung, L. C. Abdullah, M. Z. Salleh, and M. H. Mahmood, "Producing *Jatropha* oil-based polyol via epoxidation and ring opening," *Industrial Crops and Products*, vol. 50, pp. 563–567, 2013.
 - [13] M. M. Aung, Z. Yaakob, S. Kamarudin, and L. C. Abdullah, "Synthesis and characterization of *Jatropha* (*Jatropha curcas* L.) oil-based polyurethane wood adhesive," *Industrial Crops and Products*, vol. 60, pp. 177–185, 2014.
 - [14] S. R. Mustapa, M. M. Aung, A. Ahmad, A. Mansor, and L. TianKhoon, "Preparation and characterization of *Jatropha* oil-based polyurethane as non-aqueous solid polymer electrolyte for electrochemical devices," *Electrochimica Acta*, vol. 222, pp. 293–302, 2016.
 - [15] S. Saalah, L. C. Abdullah, M. M. Aung et al., "Waterborne polyurethane dispersions synthesized from *Jatropha* oil," *Industrial Crops and Products*, vol. 64, pp. 194–200, 2015.
 - [16] M. Desroches, M. Escouvois, R. Auvergne, S. Caillol, and B. Boutevin, "From vegetable oils to polyurethanes: synthetic routes to polyols and main industrial products," *Polymer Reviews*, vol. 52, no. 1, pp. 38–79, 2012.
 - [17] G. Lligadas, J. C. Ronda, M. Galia, and V. Cádiz, "Renewable polymeric materials from vegetable oils: a perspective," *Materials Today*, vol. 16, no. 9, pp. 337–343, 2013.
 - [18] M. A. Mosiewicki and M. I. Aranguren, "A short review on novel biocomposites based on plant oil precursors," *European Polymer Journal*, vol. 49, no. 6, pp. 1243–1256, 2013.
 - [19] D. K. Chattopadhyay and D. C. Webster, "Thermal stability and flame retardancy of polyurethanes," *Progress in Polymer Science*, vol. 34, no. 10, pp. 1068–1133, 2009.
 - [20] V. K. Balla, K. H. Kate, J. Satyavolu, P. Singh, and J. G. D. Tadimeti, "Additive manufacturing of natural fiber reinforced polymer composites: processing and prospects," *Composites Part B: Engineering*, vol. 174, article 106956, 2019.
 - [21] K. C. Verma and A. K. Gaur, "*Jatropha curcas* L.: substitute for conventional energy," *World Journal of Agricultural Sciences*, vol. 5, no. 5, pp. 552–556, 2009.
 - [22] M. Y. Koh and T. I. M. Ghazi, "A review of biodiesel production from *Jatropha curcas* L. oil," *Renewable and Sustainable Energy Reviews*, vol. 15, no. 5, pp. 2240–2251, 2011.
 - [23] R. Guo, C. Ma, S. Sun, and Y. Ma, "Kinetic study on oxirane cleavage of epoxidized palm oil," *Journal of the American Oil Chemists' Society*, vol. 88, no. 4, pp. 517–521, 2011.
 - [24] C. Zhang, T. F. Garrison, S. A. Madbouly, and M. R. Kessler, "Recent advances in vegetable oil-based polymers and their composites," *Progress in Polymer Science*, vol. 71, pp. 91–143, 2017.
 - [25] C. Zhang, Y. Xia, R. Chen, S. Huh, P. A. Johnston, and M. R. Kessler, "Soy-castor oil based polyols prepared using a solvent-free and catalyst-free method and polyurethanes therefrom," *Green Chemistry*, vol. 15, no. 6, pp. 1477–1484, 2013.
 - [26] Y. Guo, J. H. Hardesty, V. M. Mannari, and J. L. Massingill, "Hydrolysis of epoxidized soybean oil in the presence of phosphoric acid," *Journal of the American Oil Chemists' Society*, vol. 84, no. 10, pp. 929–935, 2007.
 - [27] B. Ni, L. Yang, C. Wang, L. Wang, and D. E. Finlow, "Synthesis and thermal properties of soybean oil-based waterborne polyurethane coatings," *Journal of Thermal Analysis and Calorimetry*, vol. 100, no. 1, pp. 239–246, 2010.
 - [28] C. S. Wang, L.-T. Yang, B.-L. Ni, and G. Shi, "Polyurethane networks from different soy-based polyols by the ring opening of epoxidized soybean oil with methanol, glycol, and 1,2-propanediol," *Journal of Applied Polymer Science*, vol. 114, no. 1, pp. 125–131, 2009.
 - [29] M. Zieleniewska, M. Auguścik, A. Prociak, P. Rojek, and J. Ryszkowska, "Polyurethane-urea substrates from rapeseed oil-based polyol for bone tissue cultures intended for application in tissue engineering," *Polymer Degradation and Stability*, vol. 108, pp. 241–249, 2014.
 - [30] M. S. Gaikwad, V. V. Gite, P. P. Mahulikar, D. G. Hundiware, and O. S. Yemul, "Eco-friendly polyurethane coatings from cottonseed and Karanja oil," *Progress in Organic Coatings*, vol. 86, pp. 164–172, 2015.
 - [31] B. Nohra, L. Candy, J. F. Blanco, C. Guerin, Y. Raoul, and Z. Mouloungui, "From petrochemical polyurethanes to bio-based polyhydroxyurethanes," *Macromolecules*, vol. 46, no. 10, pp. 3771–3792, 2013.
 - [32] Y.-C. Tu, P. Kiatsimkul, G. Suppes, and F.-H. Hsieh, "Physical properties of water-blown rigid polyurethane foams from vegetable oil-based polyols," *Journal of Applied Polymer Science*, vol. 105, no. 2, pp. 453–459, 2007.
 - [33] P. S. Bailey, "The reactions of ozone with organic compounds," *Chemical Reviews*, vol. 58, no. 5, pp. 925–1010, 1958.

- [34] R. Criegee, "Mechanism of ozonolysis," *Angewandte Chemie International Edition in English*, vol. 14, no. 11, pp. 745–752, 1975.
- [35] M. He, Y. Sun, H. Cao, D. Han, and J. Hu, "Theoretical study of the ozonolysis of allyl acetate: mechanism and kinetics," *Structural Chemistry*, vol. 23, no. 1, pp. 201–208, 2012.
- [36] J. Li, D. Han, H. Cao, M. Li, and M. He, "Theoretical study on the mechanism and kinetics for the ozonolysis of vinyl propionate," *Structural Chemistry*, vol. 25, no. 1, pp. 285–291, 2014.
- [37] T. S. Omonov, E. Kharraz, and J. M. Curtis, "Ozonolysis of canola oil: a study of product yields and ozonolysis kinetics in different solvent systems," *Journal of the American Oil Chemists' Society*, vol. 88, no. 5, pp. 689–705, 2011.
- [38] Z. S. Petrović, W. Zhang, and I. Javni, "Structure and properties of polyurethanes prepared from triglyceride polyols by ozonolysis," *Biomacromolecules*, vol. 6, no. 2, pp. 713–719, 2005.
- [39] S. Husic, I. Javni, and Z. S. Petrović, "Thermal and mechanical properties of glass reinforced soy-based polyurethane composites," *Composites Science and Technology*, vol. 65, no. 1, pp. 19–25, 2005.
- [40] T. Vanbesien, F. Hapiot, and E. Monflier, "Hydroformylation of vegetable oils and the potential use of hydroformylated fatty acids," *Lipid Technology*, vol. 25, no. 8, pp. 175–178, 2013.
- [41] Z. S. Petrović, O. Bilić, A. Zlatanić et al., "Polyols and polyurethanes from crude algal oil," *Journal of the American Oil Chemists' Society*, vol. 90, no. 7, pp. 1073–1078, 2013.
- [42] G. B. Bantchev, J. A. Kenar, G. Biresaw, and M. G. Han, "Free radical addition of butanethiol to vegetable oil double bonds," *Journal of Agricultural and Food Chemistry*, vol. 57, no. 4, pp. 1282–1290, 2009.
- [43] C. E. Hoyle and C. N. Bowman, "Thiol-ene click chemistry," *Angewandte Chemie International Edition*, vol. 49, no. 9, pp. 1540–1573, 2010.
- [44] A. B. Lowe, "Thiol-ene "click" reactions and recent applications in polymer and materials synthesis," *Polymer Chemistry*, vol. 1, no. 1, pp. 17–36, 2010.
- [45] M. Ionescu, D. Radojčić, X. Wan, Z. S. Petrović, and T. A. Upshaw, "Functionalized vegetable oils as precursors for polymers by thiol-ene reaction," *European Polymer Journal*, vol. 67, pp. 439–448, 2015.
- [46] M. Desroches, S. Caillol, V. Lapinte, R. Auvergne, and B. Boutevin, "Synthesis of biobased polyols by thiol-ene coupling from vegetable oils," *Macromolecules*, vol. 44, no. 8, pp. 2489–2500, 2011.
- [47] Y. Wang, H. Tian, and L. Zhang, "Role of starch nanocrystals and cellulose whiskers in synergistic reinforcement of waterborne polyurethane," *Carbohydrate Polymers*, vol. 80, no. 3, pp. 665–671, 2010.
- [48] S. Miao, L. Sun, P. Wang, R. Liu, Z. Su, and S. Zhang, "Soybean oil-based polyurethane networks as candidate biomaterials: synthesis and biocompatibility," *European Journal of Lipid Science and Technology*, vol. 114, no. 10, pp. 1165–1174, 2012.
- [49] K. P. Ang, C. S. Lee, S. F. Cheng, and C. H. Chuah, "Synthesis of palm oil-based polyester polyol for polyurethane adhesive production," *Journal of Applied Polymer Science*, vol. 131, no. 6, pp. 1–8, 2014.
- [50] S. Miao, S. Zhang, Z. Su, and P. Wang, "Synthesis of bio-based polyurethanes from epoxidized soybean oil and isopropanolamine," *Journal of Applied Polymer Science*, vol. 127, no. 3, pp. 1929–1936, 2013.
- [51] H. Bakhshi, H. Yeganeh, S. Mehdipour-Ataei, M. A. Shokrgozar, A. Yari, and S. N. Saeedi-Eslami, "Synthesis and characterization of antibacterial polyurethane coatings from quaternary ammonium salts functionalized soybean oil based polyols," *Materials Science and Engineering: C*, vol. 33, no. 1, pp. 153–164, 2013.
- [52] A. Pei, J. M. Malho, J. Ruokolainen, Q. Zhou, and L. A. Berglund, "Strong nanocomposite reinforcement effects in polyurethane elastomer with low volume fraction of cellulose nanocrystals," *Macromolecules*, vol. 44, no. 11, pp. 4422–4427, 2011.
- [53] V. Kupka, F. Ansari, H. Tang et al., "Well-dispersed polyurethane/cellulose nanocrystal nanocomposites synthesized by a solvent-free procedure in bulk," *Polymer Composites*, vol. 40, no. S1, pp. E456–E465, 2019.
- [54] P. Khadivi, M. Salami-Kalajahi, H. Roghani-Mamaqani, and R. Lotfi Mayan Sofla, "Fabrication of microphase-separated polyurethane/cellulose nanocrystal nanocomposites with irregular mechanical and shape memory properties," *Applied Physics A: Materials Science & Processing*, vol. 125, no. 11, pp. 1–10, 2019.
- [55] I. Omrani, A. Farhadian, N. Babanejad, H. K. Shendi, A. Ahmadi, and M. R. Nabid, "Synthesis of novel high primary hydroxyl functionality polyol from sunflower oil using thiol-ene reaction and their application in polyurethane coating," *European Polymer Journal*, vol. 82, pp. 220–231, 2016.
- [56] F. Yu, P. Saha, P. W. Suh, and J. K. Kim, "Green polyurethane from dimer acid based polyether polyols: synthesis and characterization," *Journal of Applied Polymer Science*, vol. 132, no. 5, pp. 1–9, 2015.
- [57] C. Zhang, S. A. Madbouly, and M. R. Kessler, "Biobased polyurethanes prepared from different vegetable oils," *ACS applied materials & interfaces*, vol. 7, no. 2, pp. 1226–1233, 2015.
- [58] K. Karadeniz, Y. Çalikoğlu, and M. Y. Sen, "A novel polyurethanes from epoxidized soybean oil synthesized by ring opening with bifunctional compounds," *Polymer Bulletin*, vol. 74, no. 7, pp. 2819–2839, 2017.
- [59] S. Caillol, M. Desroches, G. Boutevin, C. Loubat, R. Auvergne, and B. Boutevin, "Synthesis of new polyester polyols from epoxidized vegetable oils and biobased acids," *European Journal of Lipid Science and Technology*, vol. 114, no. 12, pp. 1447–1459, 2012.
- [60] X. Kong, G. Liu, H. Qi, and J. M. Curtis, "Preparation and characterization of high-solid polyurethane coating systems based on vegetable oil derived polyols," *Progress in Organic Coatings*, vol. 76, no. 9, pp. 1151–1160, 2013.
- [61] C. Zhang, R. Ding, and M. R. Kessler, "Reduction of epoxidized vegetable oils: a novel method to prepare bio-based polyols for polyurethanes," *Macromolecular Rapid Communications*, vol. 35, no. 11, pp. 1068–1074, 2014.
- [62] T. F. Garrison and M. R. Kessler, *Plant Oil-Based Polyurethanes*, Elsevier Inc., 2015.
- [63] H. Bakhshi, H. Yeganeh, and S. Mehdipour-Ataei, "Synthesis and evaluation of antibacterial polyurethane coatings made from soybean oil functionalized with dimethylphenylammonium iodide and hydroxyl groups," *Journal of Biomedical Materials Research Part A*, vol. 101, no. 6, pp. 1599–1611, 2013.
- [64] R. Chen, C. Zhang, and M. R. Kessler, "Polyols and polyurethanes prepared from epoxidized soybean oil ring-opened by polyhydroxy fatty acids with varying oh numbers," *Journal of Applied Polymer Science*, vol. 132, no. 1, pp. 1–10, 2014.

- [65] F. H. Yeoh, C. S. Lee, Y. B. Kang, S. F. Wong, and S. F. Cheng, "One-pot synthesis of palm oil-based polyester polyol for production of biodegradable and biocompatible polyurethane," *Journal of Applied Polymer Science*, vol. 135, no. 44, article 46861, pp. 1–16, 2018.
- [66] P. Alagi, Y. J. Choi, J. Seog, and S. C. Hong, "Efficient and quantitative chemical transformation of vegetable oils to polyols through a thiol-ene reaction for thermoplastic polyurethanes," *Industrial Crops and Products*, vol. 87, pp. 78–88, 2016.
- [67] Y. Feng, H. Liang, Z. Yang et al., "A solvent-free and scalable method to prepare soybean-oil-based polyols by thiol-ene photo-click reaction and biobased polyurethanes therefrom," *ACS Sustainable Chemistry & Engineering*, vol. 5, no. 8, pp. 7365–7373, 2017.
- [68] P. Alagi, Y. J. Choi, and S. C. Hong, "Preparation of vegetable oil-based polyols with controlled hydroxyl functionalities for thermoplastic polyurethane," *European Polymer Journal*, vol. 78, pp. 46–60, 2016.
- [69] C. Mokhtari, F. Malek, S. Caillol, and C. Negrell, "Synthesis of bio-based polyurethanes from Jojoba oil," *European Journal of Lipid Science and Technology*, vol. 120, no. 3, 2018.
- [70] M. Ionescu, D. Radojčić, X. Wan, M. L. Shrestha, Z. S. Petrović, and T. A. Upshaw, "Highly functional polyols from castor oil for rigid polyurethanes," *European Polymer Journal*, vol. 84, pp. 736–749, 2016.
- [71] M. Comí, G. Lligadas, J. C. Ronda, M. Galià, and V. Cádiz, "Synthesis of castor-oil based polyurethanes bearing alkene/alkyne groups and subsequent thiol-ene/yne post-modification," *Polymer*, vol. 103, pp. 163–170, 2016.
- [72] H. Liang, Y. Feng, J. Lu et al., "Bio-based cationic waterborne polyurethanes dispersions prepared from different vegetable oils," *Industrial Crops and Products*, vol. 122, pp. 448–455, 2018.
- [73] Y. Shen, J. He, Z. Xie, X. Zhou, C. Fang, and C. Zhang, "Synthesis and characterization of vegetable oil based polyurethanes with tunable thermomechanical performance," *Industrial Crops and Products*, vol. 140, article 111711, 2019.
- [74] H. P. S. Abdul Khalil, Y. Davoudpour, C. K. Saurabh et al., "A review on nanocellulosic fibres as new material for sustainable packaging: process and applications," *Renewable and Sustainable Energy Reviews*, vol. 64, pp. 823–836, 2016.
- [75] H. M. C. Azeredo, M. F. Rosa, and L. H. C. Mattoso, "Nanocellulose in bio-based food packaging applications," *Industrial Crops and Products*, vol. 97, pp. 664–671, 2017.
- [76] S. Boufi, I. González, M. Delgado-Aguilar, Q. Tarrès, M. À. Pèlach, and P. Mutjé, "Nanofibrillated cellulose as an additive in papermaking process: a review," *Carbohydrate Polymers*, vol. 154, pp. 151–166, 2016.
- [77] S. H. Osong, S. Norgren, and P. Engstrand, "Processing of wood-based microfibrillated cellulose and nanofibrillated cellulose, and applications relating to papermaking: a review," *Cellulose*, vol. 23, no. 1, pp. 93–123, 2016.
- [78] N. Lavoine, I. Desloges, A. Dufresne, and J. Bras, "Microfibrillated cellulose - its barrier properties and applications in cellulosic materials: a review," *Carbohydrate Polymers*, vol. 90, no. 2, pp. 735–764, 2012.
- [79] M. Kaushik and A. Moores, "Review: nanocelluloses as versatile supports for metal nanoparticles and their applications in catalysis," *Green Chemistry*, vol. 18, no. 3, pp. 622–637, 2016.
- [80] Y. Xue, Z. Mou, and H. Xiao, "Nanocellulose as a sustainable biomass material: structure, properties, present status and future prospects in biomedical applications," *Nanoscale*, vol. 9, no. 39, pp. 14758–14781, 2017.
- [81] M. H. Mousa, Y. Dong, and I. J. Davies, "Recent advances in bionanocomposites: preparation, properties, and applications," *International Journal of Polymeric Materials and Polymeric Biomaterials*, vol. 65, no. 5, pp. 225–254, 2016.
- [82] I. Siró and D. Plackett, "Microfibrillated cellulose and new nanocomposite materials: a review," *Cellulose*, vol. 17, no. 3, pp. 459–494, 2010.
- [83] K. J. De France, T. Hoare, and E. D. Cranston, "Review of hydrogels and aerogels containing nanocellulose," *Chemistry of Materials*, vol. 29, no. 11, pp. 4609–4631, 2017.
- [84] Z. Gao, J. Peng, T. Zhong, J. Sun, X. Wang, and C. Yue, "Bio-compatible elastomer of waterborne polyurethane based on castor oil and polyethylene glycol with cellulose nanocrystals," *Carbohydrate Polymers*, vol. 87, no. 3, pp. 2068–2075, 2012.
- [85] M. Floros, L. Hojabri, E. Abraham et al., "Enhancement of thermal stability, strength and extensibility of lipid-based polyurethanes with cellulose-based nanofibers," *Polymer Degradation and Stability*, vol. 97, no. 10, pp. 1970–1978, 2012.
- [86] M. He, J. Zhou, H. Zhang, Z. Luo, and J. Yao, "Microcrystalline cellulose as reactive reinforcing fillers for epoxidized soybean oil polymer composites," *Journal of Applied Polymer Science*, vol. 132, no. 36, pp. 6–13, 2015.
- [87] A. Saralegi, M. L. Gonzalez, A. Valea, A. Eceiza, and M. A. Corcuera, "The role of cellulose nanocrystals in the improvement of the shape-memory properties of castor oil-based segmented thermoplastic polyurethanes," *Composites Science and Technology*, vol. 92, pp. 27–33, 2014.
- [88] M. A. Mosiewicki, P. Rojek, S. Michałowski, M. I. Aranguren, and A. Prociak, "Rapeseed oil-based polyurethane foams modified with glycerol and cellulose micro/nanocrystals," *Journal of Applied Polymer Science*, vol. 132, no. 10, pp. 9–12, 2015.
- [89] S. Rezaei Hosseinabadi, A. Parsapour, S. Nouri Khorasani et al., "Wound dressing application of castor oil- and CAPA-based polyurethane membranes," *Polymer Bulletin*, vol. 77, no. 6, pp. 2945–2964, 2020.
- [90] P. Khadivi, M. Salami-Kalajahi, and H. Roghani-Mamaqani, "Evaluation of *in vitro* cytotoxicity and properties of polydimethylsiloxane-based polyurethane/crystalline nanocellulose bionanocomposites," *Journal of Biomedical Materials Research Part A*, vol. 107, no. 8, pp. 1771–1778, 2019.
- [91] C. A. Xu, B. Nan, M. Lu et al., "Effects of polysiloxanes with different molecular weights on *in vitro* cytotoxicity and properties of polyurethane/cotton-cellulose nanofiber nanocomposite films," *Polymer Chemistry*, vol. 11, no. 32, pp. 5225–5237, 2020.

Review Article

Potential Application of Green Composites for Cross Arm Component in Transmission Tower: A Brief Review

M. R. M. Asyraf ¹, M. R. Ishak ^{1,2,3}, S. M. Sapuan ^{3,4}, N. Yidris ¹, R. A. Ilyas ^{5,6},
M. Rafidah,⁷ and M. R. Razman ⁸

¹Department of Aerospace Engineering, Universiti Putra Malaysia, 43400 UPM Serdang, Selangor, Malaysia

²Aerospace Malaysia Research Centre (AMRC), Universiti Putra Malaysia, 43400 UPM Serdang, Selangor, Malaysia

³Laboratory of Biocomposite Technology, Institute of Tropical Forestry and Forest Products (INTROP), Universiti Putra Malaysia, 43400 UPM Serdang, Selangor, Malaysia

⁴Advanced Engineering Materials and Composites Research Centre (AEMC), Department of Mechanical and Manufacturing Engineering, Universiti Putra Malaysia, 43400 UPM Serdang, Selangor, Malaysia

⁵School of Chemical and Energy Engineering, Faculty of Engineering, Universiti Teknologi Malaysia, 81310 UTM Johor Bahru, Johor, Malaysia

⁶Centre for Advanced Composite Materials, Universiti Teknologi Malaysia (CACM), 81310 UTM Johor Bahru, Johor, Malaysia

⁷Department of Civil Engineering, Universiti Putra Malaysia, 43400 UPM Serdang, Selangor, Malaysia

⁸Research Centre for Sustainability Science and Governance (SGK), Institute for Environment and Development (LESTARI), Universiti Kebangsaan Malaysia, 43600 UKM Bangi, Selangor, Malaysia

Correspondence should be addressed to M. R. M. Asyraf; asyrafritz96@gmail.com and M. R. Ishak; mohdridzwan@upm.edu.my

Received 29 September 2020; Revised 9 November 2020; Accepted 11 November 2020; Published 3 December 2020

Academic Editor: Yulin Deng

Copyright © 2020 M. R. M. Asyraf et al. This is an open access article distributed under the Creative Commons Attribution License, which permits unrestricted use, distribution, and reproduction in any medium, provided the original work is properly cited.

Recently, advanced technologies exploit materials from nonrenewable resources such as petroleum, natural gas, metal ores, and minerals. Since the depletion of these resources and environmental issues, it has brought attention to researchers to progress in the development of biodegradable materials from green composites. Most biofibres and biopolymers are obtained from agricultural waste products either from stem, leaf, stalk, or fruit. Nowadays, green composites with well-regulated life span have been widely discussed in numerous fields and applications. Some studies have shown that biofibres and biopolymers have comparable mechanical, thermal, and physical properties with glass fibre and other synthetic polymers. Thus, researchers are progressively narrowing down the development of green composite materials in many high strength applications, such as house deck and automotive components. This review focuses on the background of green composites (natural fibres and biopolymers), the manufacturing processes, potential applications in cross arm structures, and testing evaluations. This article also focuses on the specific current cross arm configurations and the pultrusion process to form squared hollow section beams. Many open issues and ideas for potential applications of green composites are analysed, and further emphases are given on the development of environmentally friendly material structures. Hence, the article is expected to deliver a state-of-art review on manufacturability and perspectives of natural fibre reinforced biopolymer composite cross arms for transmission towers.

1. Introduction

Currently, the growth of environmental concerns in manufacturing new materials among researchers and corporate sectors has increased; thus, the idea is to substitute the current material with more environmentally friendly fibres and resins [1, 2]. Petroleum has been widely used for decades

in order to power various transportation systems and also to produce many synthetic plastics such as polyester. However, they can last only for another 5–6 decades at the current rate of global consumption [3]. Another issue associated with petroleum consumption is the emission of greenhouse gases, such as methane and carbon dioxide, which contribute to global warming [4]. This issue has increased awareness of

the finiteness of fossil energy resources, leading to the development of new materials that are entirely based on renewable resources. Mass production of petroleum plastics has also led to a significant reduction of landfill capacities across the globe. This issue has led many nations to create new legislations and laws regarding plastic waste control, which educate the society to be more conscious on environmental issues. Subsequently, this phenomenon will drive many manufacturers and retailers to capitalise their finance on the development of green and sustainable products with acceptable costs to reduce the impact of global warming. Thus, the rising awareness among the public on the abundance of synthetic plastics as well as their effects towards the environment has brought an urgency to develop a technology based on biodegradable materials with acceptable properties [5].

In order to fabricate materials from used products, consumption of energy, raw materials, and cost would increase. Thus, several actions have been taken by scientists to find suitable alternative material sources. Renewable resources such as plants, animals, and minerals are the advantageous alternative sources on the condition of subsequent processing with low energy requirements [6]. A solution to the aforementioned statement is implementing naturally available fibrous resources from agricultural wastes. On top of that, plants could benefit the urban society in many ways, including as energy-saving structures in building structures and thermal insulation. In this case, there are several advantages of applying plant fibre in structural composite applications, such as thermal regulation of structures, protection from weather, and protection from direct sunlight. To ensure the advantages are grasped accordingly, it is necessary to consider suitability of the structures, types of plants, and locations in the plants, as well as questions of keeping the plants [7–10]. Thus, from the above statement, the plants' waste products not only can be harvested to become new materials but also can act as a sustainable and energy-saving agent for urban building environment.

Previously, the aviation industry was the first forerunner of producing polymeric composite products [11]. This material has been implemented in various applications including the energy sector due to its ability in high mechanical strength and stiffness as well as lightweight property [12–14]. These applications include the application of pultruded E-glass fibre reinforced unsaturated polyester cross arms in transmission towers [15] and wind turbines [16]. Specifically for cross arms, the pultruded glass fibre reinforced polymer (PGFRP) composite is the most suitable material next to Chengal wood due to its ability to arc-quench lightning strikes [17]. Moreover, the PGFRP cross arms are able to withstand constant loading of insulators and cables in long term [18, 19]. The synthetic polymeric composites have caused many major problems especially in recycling at the end of their life span. Moreover, the implementation of landfill disposal of used synthetic polymeric composites is not a suitable option due to the growth of environmental awareness among the society. This has pushed the government in implementing stricter regulations and law of landfill disposal [20]. In order to solve this issue, the application of alternatives for petroleum-based composites, such as renewable

composite materials, has shown a significant effort to improve the current environmental quality [21, 22].

Green composites are the next generation of biocomposite material where natural fibre reinforced biodegradable polymer forms a lightweight and strong structure material [2, 23]. Hence, this review article focuses on the potential of natural fibre reinforced biopolymer composites (NFRBCs) in a cross arm structure for transmission tower application. NFRBCs or green composites could potentially replace the current synthetic composite in cross arm application due to their properties including high mechanical strength and excellent biocompatibility, and they have gained more attention and a growing field in material technology. A general review on green composites composed of plant fibre and bioplastic was done by several researchers [23–26]. Although there is a numerous amount of literature available on bio-based composite materials, there is lack of extensive review articles that specifically focus on manufacturability and application of green composites for cross arm beam application. This work highlights on the current research that has been carried out in the field of green composites. Further elaborations on the natural fibre, biopolymer, manufacturing process of green composites, and its potential applications on cross arm structures will be discussed in the subsequent subtopics.

2. Green Composites

Composite materials are divided into several classifications, such as (1) fibre reinforced composites, (2) particle reinforced composites, and (3) structural composites [20]. Green composites are one of the subsets of composite materials composed of both fibre and polymer originating from nature or recycled resources [27]. These materials include plant fibres, such as flax, kenaf, sugar palm fibres, recycled wood, or even waste paper-based fibres [28–31]. In order to select the most appropriate biofibre and biopolymer in a composite, several factors are essential to be fulfilled including tensile stiffness and strength, fibre treatments, thermal stability, elongation at failure, and fatigue and creep resistance properties [32–35]. For green composite products, they can be fabricated through various processes which employ the analysis and optimization methods in composite technology. The processes include mixing, wetting, and saturating the fibre and resin together in order to achieve better bonding of firm composite structure. This would later contribute to better mechanical performance, thermal stability, and heat reaction [21, 28].

The current applications of natural fibre reinforced biopolymer composites are emerging in many sectors. Table 1 shows the progresses of green composites in many sectors including transportation, construction, sports, electronics, household, and material handling and storage [24, 36]. In addition, the rising demands for the advanced materials with tailored physical and mechanical properties have made the natural fibres as the most attractive composite materials for high-performance applications.

2.1. Natural Fibre: Plant Cellulosic Fibre. Rapid depletion of fossil fuel resources alongside the growth of environmental

TABLE 1: Common applications of natural fibre reinforced composites in various industrial sectors [100–108].

Sector	Application
Electronics	Laptop cases and mobile
Sports	Ball, snowboard, bicycle frame, fork, seat post, and boats
Transportation	Door panel, engine rubber insulation, engine cover, floor mat, dashboard, car spoiler, hand-brake, steering, pedal components, parcel shelves, interior carpet, and body panels
Building and construction	Bridge, railing, false ceiling, partition boards, windows, door frames, mobile structures, wall, and floor
Household	Mug pad, chairs, coffee table, shoe rack, suitcases, food tray, partitions, safety helmet, ropes, fencing elements, showers, bath units, and pipes
Materials handling and storage	Post-boxes, biogas containers, fuel container, and storage silos

awareness due to excessive production of man-made fibres is the main drive to substitute them with natural fibres as green composites. The natural fibres have attracted the researchers and industries, since it is sustainable in nature. These fibres are categorized based on their origins, such as plants, geological processes (mineral), and animals [37, 38]. Among these natural fibre origins, the plants are most widely implemented as reinforcement in composite materials. Figure 1 displays the classifications of natural fibres.

Nowadays, plant-based fibres have progressively replaced synthetic fibres as reinforcement agents in composite materials for various industrial applications and household products. This is due to researchers' and manufacturers' interests with the ecological advantages and low capital cost during manufacturing process [39–41]. These fibres have extra advantages over synthetic fibres, such as cheap, high strength, ease of handling, low fossil-fuel energy requirements, and can deliver high mechanical properties. A report from Karus [42] discussed on 4.3×10^6 kg of cellulosic fibre being utilized by the automobile industries every year as reinforcing agents in composites. For plant fibre, they are divided into several types depending on where they are extracted. Figure 2 displays various subdivisions of plant cellulosic fibres [30].

The increasing usage of plant-based fibres can be attributed to their affordability, availability, biodegradability, renewability, recyclability, and processability [43–45]. Additionally, plant fibres can also benefit the composite industry in many ways, such as permit better tensile strength and stiffness, good insulation performance, lightweight, consume less energy during fabrication, and less health risk especially respiratory diseases [46, 47]. Based on the aforementioned statements, most plant-based fibres demonstrate that they are the prominent candidates to substitute man-made (synthetic) fibres in most sectors in the composite industry. Table 2 shows the comparison between plant-based fibres and man-made fibres.

All mentioned plant fibres are termed as nonwood fibres. Currently, many developers and scientists have narrowed the implementation of nonwood fibres to assist the effort of preventing deforestation. In this case, the depletion of wood timber in wood-plastic composites for construction has caused a massive destruction of biodiversity. For example, Malaysia has reported that around 14.4% of its tropical forests have been lost from 2000 to 2012, in which the land area covers

about 47, 278 km² [48]. Thus, the application of nonwood fibre seems to be a solution for this issue to substitute synthetic fibres. These nonwood natural fibres have good comparable values with synthetic fibres such as glass fibres. Table 3 depicts the comparison of tensile properties of glass fibres and other well-known natural fibres.

However, the main problem associated with plant fibre-green composites is low thermal stability in order to be applied for engineering applications. Hence, it is essential to improve the thermal stability of plant fibres using modifications to produce better performance of green composites to be used in wider applications. According to Ramesh [49], the dynamic mechanical properties and thermal stability are dependent on the fibre weight fraction of the composites. Meanwhile, the modified plant fibre-based green composites that show losses of modulus peaks are widened due to improved fibre/matrix adhesion [50]. In another study conducted by Belhassan et al. [51], thermal behaviour of the improved green composites was comparable with the synthetic fibre composites. This can be proven based on their morphological analysis which depicted that the interaction between untreated plant fibres with their matrices was poor due to the occurrence of fibre debonding, fibre pull-out, matrix fracture, and fibre fracture.

2.2. Biopolymer. Polymer is a chemical substance made up from a number of repetitive subunits. According to Ramesh [52], the exploitation of biopolymer is the most prominent aspect compared to plant fibre to ensure environmental sustainability. Since they have a wide range of behaviours, both synthetic and natural polymers are vital materials in many sectors from the industrial scale to household products [53]. In general, plastics are composed of a long chain of polymers formed by the addition of polymerization reactions and condensation processes [54, 55]. From these processes, they can be formed either in thermosetting or thermoplastic polymers. These polymers are obtained from petroleum-based (synthetic polymer) and renewable-based (biopolymer) resources. Bio-based plastics are made up from renewable and natural resources such as plant oils, latex, starch, and animal fats. On the other hand, biodegradable plastic means that it can be decayed by action of living organisms (fungi and bacteria) into water, carbon dioxide, and biomass. Figure 3 shows the demonstration of conventional and bio-based polymer.

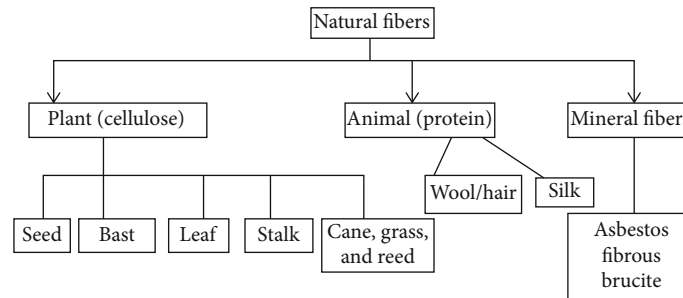


FIGURE 1: Classifications of natural fibres.

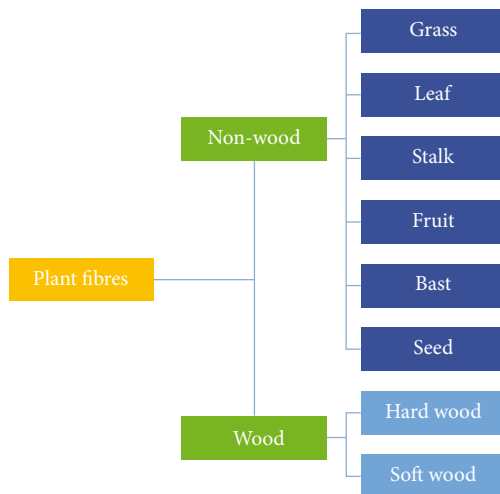


FIGURE 2: Classification of plant cellulosic fibres.

Typically, polymer has a significant ability to resist chemical reaction as well as both electric and thermal insulators. They are also lightweight which also possess good mechanical properties in terms of stiffness and strength. Table 4 shows the list of mechanical and physical properties of biopolymers and synthetic polymers. On top of that, they can be manufactured in various ways either in open or closed moulding techniques. They have a limitless range of characteristics and colours, and they can be used to produce items that have no alternatives from other materials [56].

3. Manufacturing of Green Composites

In common practices, green composites from both polymer and fibre can be fabricated from various manufacturing processes either in open or closed moulding systems. Open moulding fabrication process involves hand layup, spray layup, and filament winding. This process exposes both resin and fibre to air as they cure or harden [57]. Open moulding is usually applied to a composite product, which is large, and has a complex shape, whereby the design option is virtually limitless. However, the problem of this fabrication technique is that it has low volumes, which contribute to higher moulding costs of automated processes. Apart from open moulding system, closed moulding is another common manufacturing process of composite products applied in enclosed and heated cavity for curing using pressure pump or vacuum

[58]. The examples of closed moulding techniques are compression moulding, resin transfer moulding, pultrusion, injection moulding, hot pressing, and vacuum infusion moulding [59]. These manufacturing techniques enable product developers to produce better parts faster and consistent with lesser waste. At the end of the process, the end products have good surface finishes, which eliminate post-work activities. Nevertheless, manufacturers have to bear the initial capital cost of tools and equipment. Figure 4 depicts the classifications of fabrication processes of green composite products.

There are several criteria needed to be fulfilled using these conventional manufacturing processes as these are primarily designed from synthetic composites. Thus, pretreatment process, either chemically or physically, is required for natural fibres to improve interfacial adhesion with their matrix in composite laminates [60, 61]. Pretreatment of fibres improves fibre-matrix interfacial interactions, improving processability and properties of green composites. Specifically for cross arm beam fabrication process, pultrusion process is implemented as the product is in symmetrical square shape in the long beam section. The following subtopic elaborates on the specific process of pultrusion of composite products.

3.1. Current Fabrication Method: Pultrusion. Pultrusion is a fabrication process of composite profile by impregnating the fibre with thermosetting matrix and is pulled via heated die [62]. In general, this fabrication technique has the capability to operate continuously in order to produce symmetrical section profile such as cross arm (Figure 5) with high volume rate.

In the pultrusion process, it can be categorized into three main zones, which are pulling zone, heat transfer zone, and pressure zone [63]. Initially, a thermosetting resin bath with appropriate viscosity is ready to impregnate the fibre from the creel by pulling them towards the basin as shown in Figure 6. Guide plates are applied in the system to direct the fibre inside the resin bath for impregnation process. The resin bath contains thermoset resins along with its filler, colouring pigment, catalyst, release agent, stabilizers, and ultraviolet ray to initiate the curing process of impregnated resin. After that, the fibres are pulled out via preform guides to remove excess resin before going inside heated die for curing. This heated die is also called the curing zone. Within the heated die, it is divided into two zones, which are low

TABLE 2: Comparison of natural fibres to man-made fibres [109].

Attributes	Natural fibre	Man-made fibre
Raw material cost	Low	High
Manufacturing cost	Low	High
Weight/density	Light	Heavy
Disposal	Highly degradable	Takes thousand years to be composed
Availability	Widely available	Depleted from time by time
Renewability	Yes	No
Recyclability	Yes	No
Energy usage	Low	High
Health risk	No	Yes

TABLE 3: Comparison between glass fibres with various plant fibres [90, 110–118].

Fibre	Tensile strength (MPa)	Elongation at break	Tensile modulus (GPa)
Banana	355.0	5.3	33.8
Jute	400.0-800.0	1.8	10.0-30.0
Bagasse	20.0-290.0	1.1	19.7-27.1
Coir	220.0	15.0-25.0	6.0
Abaca	980.0	—	—
Cotton	400.0	3.0-10.0	12.0
Flax	800.0-1500.0	1.2-1.6	60.0-80.0
Kenaf (bast)	295.0	2.7-6.9	—
Sisal	60.0-700.0	2.0-3.0	38.0
Hemp	550.0-900.0	1.6	70.0
Pineapple	170.0-1627.0	1.0-3.0	82.0
Sugar palm	42.1	9.8	10.4
Ramie	500.0	2.0	44.0
Oil palm (empty fruit bunch)	248.0	2.5	3.2
Henequen	3.0-4.7	—	—
S-glass	4570.0	2.8	86.0
E-glass	4570.0	2.8	86.0

temperature for gelation and high temperature for curing action. In this part of the pultrusion, the die is heated by the heater that embeds thermocouple sensor to ensure the temperature is sufficient enough for curing. Moreover, the thermocouple sensor also functions to avoid the die from overheating which could flaw the composite profile.

Typically, the pultrusion of composite profiles apply continuous unidirectional fibres impregnated with low viscosity thermosetting resin [62]. Later, the resin would be in rubbery state from liquid state. This transition point is called as gelation point, which later solidifies to form solid pultruded profile [64, 65]. Overall, the movement of pultrusion line is controlled by pneumatic controller system that instructs the hydraulic clamp to pull the profiles through cutter as displayed in Figure 6. Moreover, the hydraulic clamp is installed with rubber to grip and protect the composite profiles. The pulling speed is controlled using a programming control system, and it can be easily monitored and controlled in the monitor screen.

3.2. Other Potential Advance Fabrication Method: Filament Winding. Filament winding is another advanced manufacturing method which implements impregnated fibre with polymer resin thoroughly onto the rotating mandrel. The winding angle, patterns, and rotation number are automatically controlled by a computerised system. In terms of application to transmission lines, this method could produce better beams for cross arm members in latticed tower [66, 67].

In general, there are three types of winding patterns in this manufacturing process, which are hoop, helical, and polar windings as shown in Figure 7 [29]. Morozov [68] found out that mechanical properties of thin-walled filament wind structure depend on its winding patterns. The stress and strain distributions are affected by the size of the triangular mosaic units and their numbers per unit of length in both longitudinal (hoop) and circumferential (helical) directions. Thus, it is suggested that the cross arm beams to be fabricated, to implement hoop and helical windings to ensure

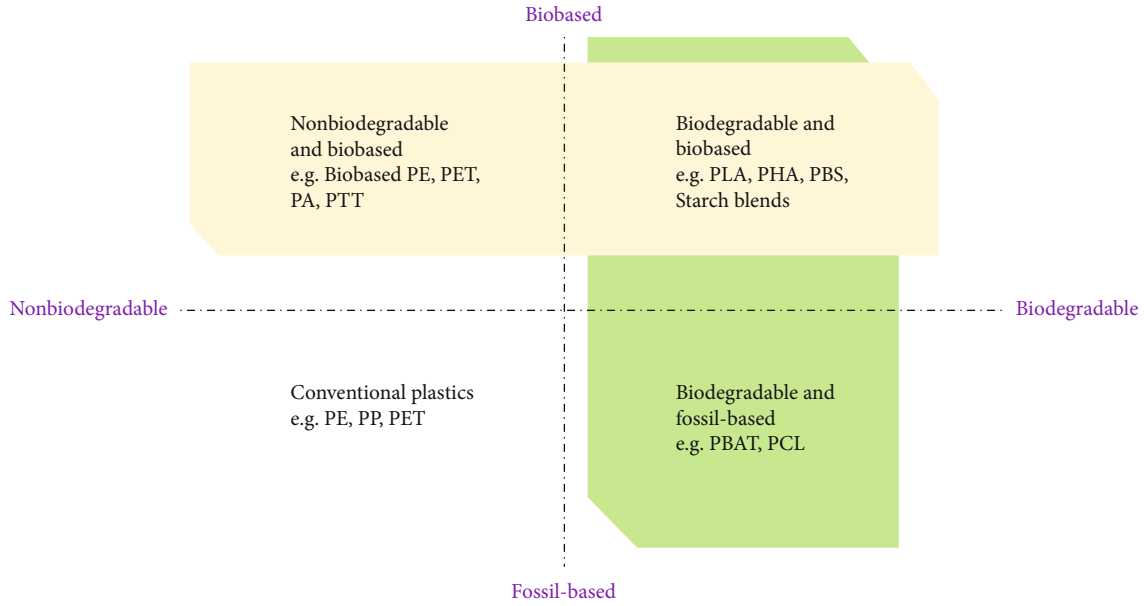


FIGURE 3: Classification of polymers.

TABLE 4: Comparison of man-made petroleum-based polymers with biopolymers [119–122].

Polymers	Tensile strength (MPa)	Elongation at break (%)	Tensile modulus (GPa)
Petroleum-based polymer			
Polyester	41.4-89.7	2.6	2.06-4.11
Low-density polyethylene (LDPE)	190.0	190.0	0.21
High-density polyethylene (HDPE)	20.3	380.0	0.91
Poly(ethylene terephthalate) (PET)	55.0	130.0	2.70
Epoxy	26.0	2.33	1.21
Biopolymer			
Poly(lactic acid) (PLA)	49.6	2.4	3.60
Poly(hydroxyalkanoate)s (PHA)s	17.0-40.0	5.0-680.0	0.20-3.50
Poly(3-hydroxybutyrate) (PHB)	36.4	2.1	2.99
B-lactoglobulin + glycerol	4.9	11.4	0.15

well-distribution of stress from dead weights of electric cables and insulators as well as dynamic loading from winds.

Another advantage of implementing filament winding for cross arm beam fabrication is they can manufacture these beams with their core structures simultaneously. This manufacturing technique allows the beams to have more coherent thickness distribution along with their core structures. Further elaboration on reinforcement of core structure of cross arm will further be discussed in the next subsection.

3.3. Potential Reinforcement of Core Structure in Cross Arm Beam to Enhance Its Strength. Core structure can be defined as a thin-walled composite structure that contains aluminium, NOMEX, and natural fibre composites (NFCs) cores which join them by using either adhesive or brazing. Figure 8 displays the laminated wood timber which acts as a core structure inside pultruded glass fibre reinforced polymer composite (PGFRPC) square hollow section. There are various types of cores used to reinforced beams such as balsa wood, honeycomb, NOMEX, foam, and corrugated and tetrahedral truss core. The facing of the thin-walled structure is usually thinner than the core to ensure the produced material is stiff and strong [69, 70]. In common practices, the composite filled core structures have various functions and applications depending on durability, manufacturing and raw material costs, and availability. For instance, graphite-epoxy and carbon-epoxy are the facings that enclose the NOMEX or aluminium honeycomb core for aerospace structures in order to resist extreme environment conditions [71]. Meanwhile, in marine and civil structure sectors, the typical facings implemented are glass-epoxy or glass-vinyl ester reinforced with close-cell or open-cell foam [72, 73]. Balsa with various densities has typically become a choice for sandwich structure's core in ship application [69].

From the aforementioned statement, honeycomb core structure is one of the potential improvements associated to have high durability and longer service for cross arm structure. This could be due to honeycomb core to be lightweight as well as has high bending strength and stiffness [74, 75]. The innovation of honeycomb sandwich structure has been paid generous attention, and this has led to the development of filled-type, embedded, tandem, and hierarchical [76, 77] as displayed in Figure 9. From the previous studies [78, 79], it can be seen that the filled sandwich structure has currently attracted researchers because of its simple configuration and ease of manufacturing. In order to optimize the

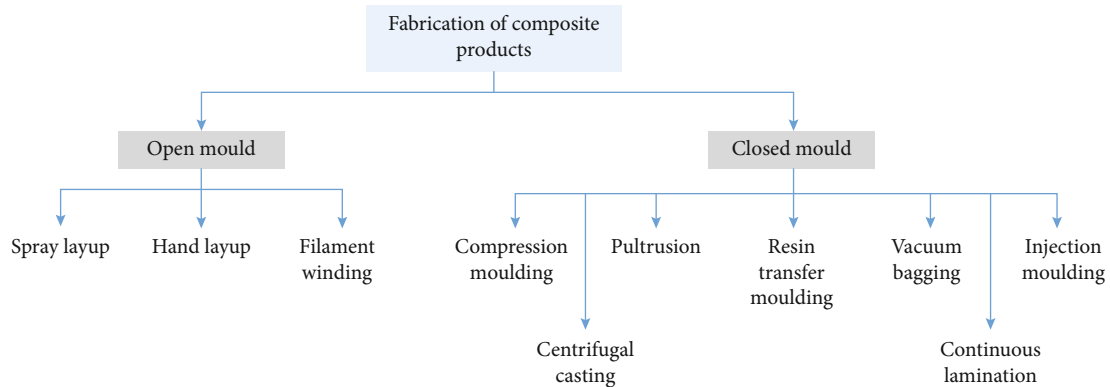


FIGURE 4: General classification of green composites fabrication processes.



FIGURE 5: Cross arm beams in stockpiles after pultrusion for distribution.

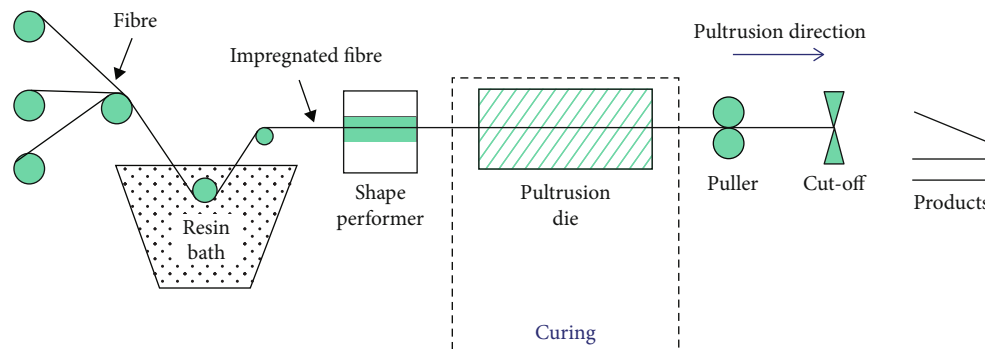


FIGURE 6: Schematic diagram of pultrusion process of pultruded composite.

composite filled core structure, various fillers have been investigated to seek the optimal combination including foam, honeycomb, lattice-filled, and balsa wood [80–82]. Another way to fabricate composite filled structure is by embedding the honeycomb cell with foam, tubes, or even other polymer materials using the concept of a container instead of a filler [83]. For tandem honeycomb structure, it is considered to combine several segments with a separator between each segment. The idea of a separator is using it to distinguish segments from each other and to deliver interactions between them [84].

4. PGFRP Composite: Current Cross Arm's Material

Based on previous literature, the current cross arm in transmission tower used pultruded glass fibre reinforced polymer (PGFRP) composites [85, 86]. Previously, Chengal wood cross arm was applied to the transmission tower since 1963 due to its ability to arc quench lightning strikes and has better mechanical performance [87, 88]. However, the wooden cross arm seemed to degrade and started to fail due to natural wood defect and attack from termites and microbes [89].

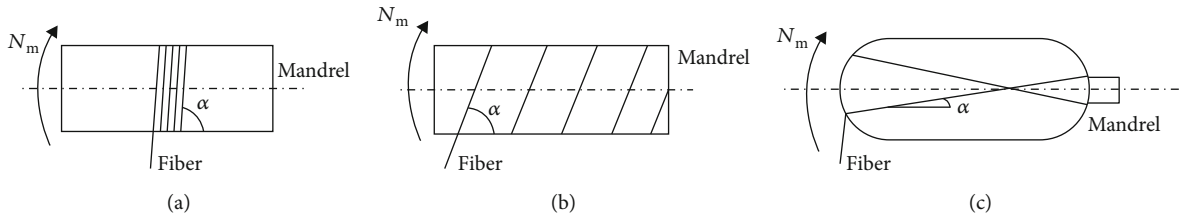


FIGURE 7: Types of winding patterns: (a) hoop, (b) helical, and (c) polar windings [29].

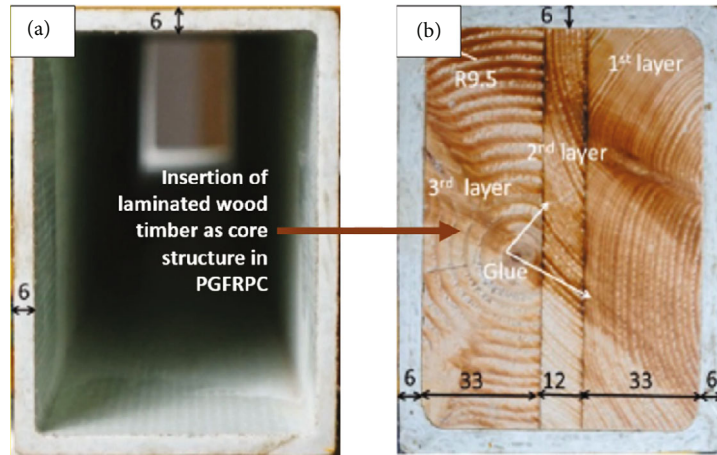


FIGURE 8: Sandwich composite structure layout.

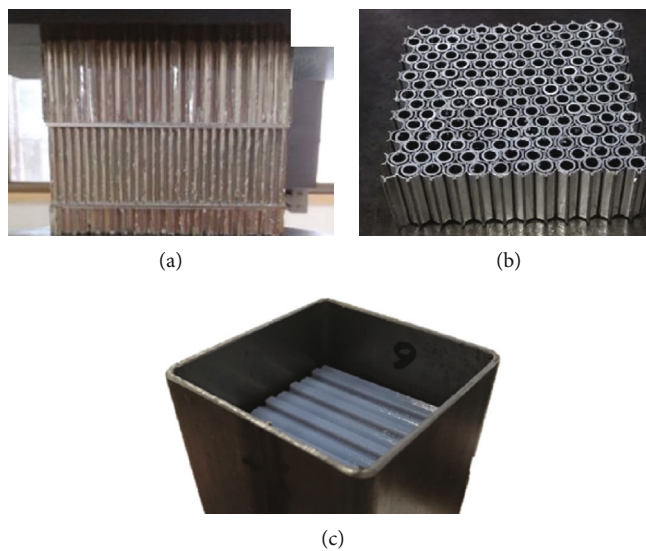


FIGURE 9: Innovation of honeycomb structures. (a) Tandem honeycomb structure. (b) Embedded honeycomb structure. (c) Honeycomb-filled structure.

This has led researchers and engineers to conduct a research to shift wooden cross arms to PGFRP cross arms.

In general, the PGFRP composites have become the successor for wooden cross arms due to good tensile strength and stiffness, lightweight property, better bending strength and stiffness, as well as good electrical and thermal insulation

properties [90, 91]. The PGFRP composite is made up of E-glass fibre reinforced with unsaturated polyester (UPE) resin with ratio of 37 : 63 in order to achieve optimum mechanical performance [92]. The PGFRP composite also seems to be lightweight as both densities of E-glass fibre and unsaturated polyester are less, of around 2580 and 1350 kg/m³,

TABLE 5: Comparison between PGFRP composites and structural steel used in cross arms system [86].

Properties	PGFRP composite	Structural steel
Density (kg/m^3)	1800	7850
Poisson ratio, $\nu_{xy} = \nu_{yz} = \nu_{xz}$	0.28	0.3
Shear modulus, $\nu_{xy} = \nu_{yz} = \nu_{xz}$ (MPa)	4000	76923
Young modulus in x , E_x (MPa)	16000	200000
Young modulus in y , E_y (MPa)	4800	200000
Young modulus in z , E_z (MPa)	1440	200000

respectively. The overall mechanical and physical properties of PGFRP composite and structural steel are demonstrated in Table 5.

In terms of surface finish, the PGFRP composite has homogenous, fine, and unidirectional fibre along its polymer laminate. The optimal configurations for PGFRP composite, specifically for cross arm beams, five layers of E-glass fibre are laminated with various orientations and thicknesses in order to attain high mechanical and structural properties [86]. Table 6 elaborates the fabric orientations and its thickness layers to form pultruded square profile of cross arm beams.

5. Potential Applications of Green Composites in Cross Arm Structures

Natural fibre reinforced biopolymer composites are vital potential prospects of green technologies based on numerous findings emphasized in this review. One of these interesting inventions of the green composites is the simplicity of processing with various types of biopolymers. Other than that, the highlighted findings in this review also found that green composites have great potential as alternative composite materials for cross arm beams (Figure 10) due to their lightweight property and low cost. Other cross arm application in transmission tower is as bracing arm as shown in Figure 11. Currently, the ongoing research used wooden bracing arms to reinforce cross arm structure for better structural and long-term mechanical performances [93]. Thus, it is highly suggested to apply pultruded green composites as a replacement candidate for both cross arm beams and bracing arms.

Based on the previous paragraph, the green composites have high potential to substitute the PGFRP cross arms (Figure 10) and wooden bracing arms (Figure 11) as new materials in transmission tower applications. However, comprehensive studies have to be carried out for fabricated green composite cross arms with additional members in terms of mechanical and electrical insulation performances. The test evaluations include mechanical quasistatic test, creep test, and electrical resistance test before the newly fabricated green composite cross arms compute their services in electrical suspension towers.

TABLE 6: Fabric orientation and fibre thickness of PGFRP composite [86].

PGFRP composite layer	Fabric orientation ($^\circ$)	Thickness (mm)
Fifth (Inner)	45	0.7
Forth	0	3.6
Third	90	0.7
Second	-45	0.5
First (Outer)	45	0.5

6. Test Evaluation

6.1. Creep Test. To extend the description of the loading mechanisms at prolonged time of pultruded green composite cross arms in such applications, many research works have emphasized on creep experiments in both coupon-scale and full-scale cross arms [33]. This creep test is conducted to investigate the strength of the structure and material, failure mode, elasticity, and viscoelasticity under constant load in long-term period [12, 32]. The creep strain, creep compliance, stress-independent material constant, creep failure, and creep life are the interesting topics, especially for cross arm structures. Thus, related previous studies from creep responses of cross arm structures are highlighted to give a clear picture for any potential evaluation before being commercialised in the energy sector.

Currently, recent research works have been conducted especially in providing testing facilities to evaluate long-term mechanical performances of cross arms. According to Asyraf et al. [94, 95], two conceptual designs of creep test rigs, specifically for cross arm structures, have been developed in order to set up a platform for creep testing in three-point flexural and cantilever beam tests. This research team has designed both test rigs using hybridization of TRIZ, Morphological chart, and Analytic Network Process to generate ideas, refine attributes and characteristics, as well as design selection. Along these processes, both computer-aided drawing (CAD) and finite element analysis (FEA) tools were used to compute the process systematically and optimize the designs based on actual scenarios based on the structural principles [96].

Other than that, many creep studies and long-term mechanical performance comparisons of cross arm's coupons have been conducted. For instance, Johari et al. [18] have evaluated the influence of calcium carbonate (CaCO_3) on creep response of PGFRP composite cross arms. In the research, the conventional creep and time-temperature superposition (TTSP) methods were evaluated, and it was found that the CaCO_3 did not influence the long-term performance of the pultruded laminates. Moreover, both pultruded composites (with and without CaCO_3) had the same creep life of about 25 years.

All in all, it is noteworthy that the evaluation of creep performances and responses in both conventional and accelerated creep techniques are highly important for new green composite cross arm structures. Moreover, before coming to the experimental stage, the test facilities have to be

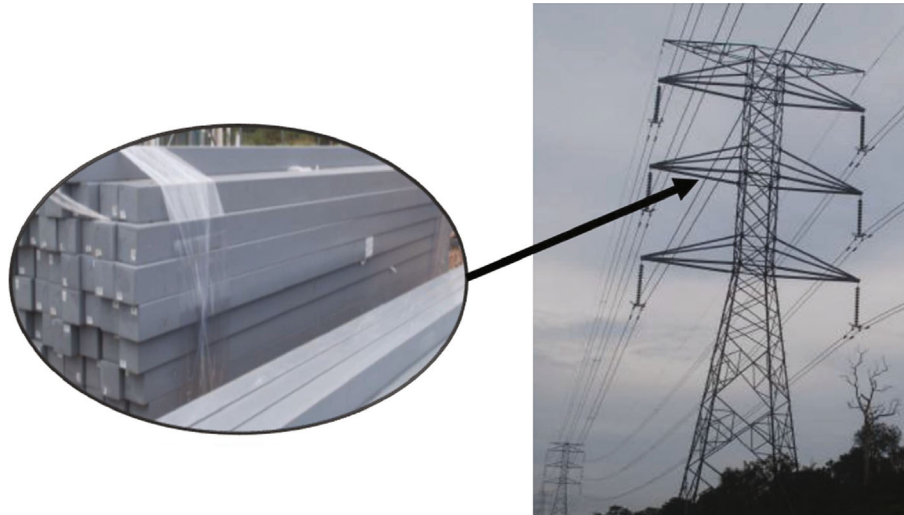


FIGURE 10: Potential application of green composite in cross arm beams.

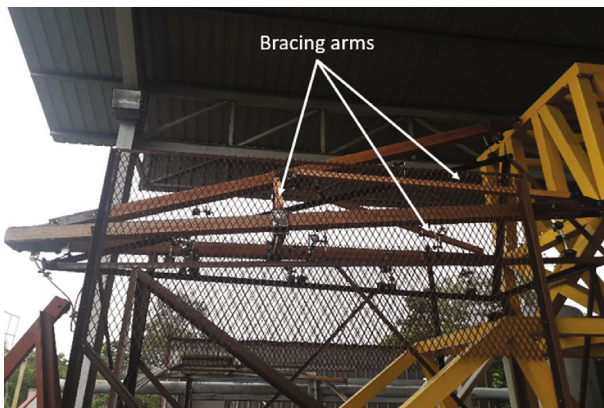


FIGURE 11: Potential application of green composite in bracing arms.

designed and developed to execute the specialised tests and analyses for structural evaluations.

6.2. Quasistatic Mechanical Test. In the past 20 years, many research activities have been executed to address the mechanical strength and performances of PGFRP composite beams. Since PGFRP cross arms are made up of pultrusion and in square hollow shape, it helps the structures to be low self-weight and has corrosion resistance capability. However, the cross-section geometry in the cross arm beams has caused a very complex behaviour as it is subjected to multiaxis compression forces. This phenomenon may induce a concentric compression due to immediate loading action, which subsequently causes a buckling reaction. Hence, a series of quasistatic mechanical tests and analyses is required to ensure the fabricated green composite cross arms fulfil the mechanical property standards as their predecessors (wood and PGFRP composites).

An earlier study conducted by Cardoso et al. [13] developed a comprehensive mathematical formulation to govern the mechanical strength of PGFRP square hollow composite

under buckling action. From this research, PGFRP composites with longer length and lower strength specimen were exposed to higher potential of failure during postbuckling stage. Postbuckling was observed on the behaviour and interaction between crushing and local and global buckling.

In another study, Sharaf et al. [93] have also designed and examined full-scale wooden cross arms using quasistatic mechanical tests in both normal and broken wire conditions. The findings proved that the design of wooden cross arms experienced deflection and were exposed in broken wire condition, which was higher than normal wire condition. Afterwards, Sharaf et al. [97] developed a conceptual design of cross arm structure with the incorporation of bracing arms. A simple computational simulation using finite element analysis was executed to identify the best design with the most optimal mechanical and structural performances.

Thus, the previous literature shows that it is necessary to evaluate quasistatic mechanical properties of green composite cross arms and to guarantee the newly fabricated cross arms to be at least at par with PGFRP composite.

6.3. Electrical Capacity Test. From the view of electrical capacity of cross arms, it is essential for any cross arms to have their voltage stress, relative permittivity, volume conductivity, and current density examined. This is required in order to ensure continuous electrical supply to end users for urban and rural areas [98, 99]. These aspects are vital for cross arm structures to avoid experiencing any structural failures which could cause disruptions along the transmission line [91]. Some failures that cross arms might experience are being burnt by the electrical tracking and forming a charred path, creating some cavities which reveal the PGFRP composite structure as shown in Figure 12. From an analysis conducted by Rawi et al. [17], the cross arm located at the top of transmission tower experienced the highest peak voltage during lightning that stroke the earth wire of the cross arms. This was due to distance from the stricken point to the cross arms.



FIGURE 12: Surface tracking of PGFRP composite cross arm beams.

7. Conclusions

This manuscript presents a brief review on the potential of manufacturing cross arm components from natural fibre reinforced biopolymer composites. This green composite material has attracted the attention of many researchers and industrial sectors due to its excellent mechanical ability, and the material itself is a part of green technology. In the most recent research works reviewed, several natural fibres seem to be at par with synthetic fibre in terms of mechanical performance. In particular, flax and pineapple fibres have comparable tensile strength and stiffness values to glass fibre. Moreover, the physical, thermal, and mechanical properties of natural fibres can be enhanced either via physical or chemical treatments, which improve interfacial adhesion between fibre and its resin. Meanwhile, several biopolymers have the potential to replace the current synthetic polymers, such as PLA, PHA, and PHB. These biopolymers could be good candidates to be applied in structural applications especially as cross arm beams. Since the cross arms are made via pultrusion process, it is suggested that the natural fibre reinforced biopolymers could be conducted via the same process with the same configuration in order to develop green composite cross arms. In addition, it is useful to enhance their intrinsic properties and significantly improve the green composite cross arms developed from treated natural fibres. However, there are several properties that need to be identified and evaluated, such as creep, fatigue, and quasistatic mechanical performance, since green composite cross arms are new in this field. Hence, further exploration on more advanced processing techniques for natural fibre reinforced biopolymer composite cross arms is necessary to be conducted in order to replace the conventional cross arms in transmission towers.

Data Availability

The data used to support the findings of this study are included within the article.

Conflicts of Interest

The authors declare no conflict of interest in the article.

Acknowledgments

The authors are very thankful to the Department of Aerospace Engineering, Faculty of Engineering, Universiti Putra Malaysia (UPM), for providing space and facilities for this project. Moreover, all authors were also very thankful to Jabatan Perkhidmatan Awam (JPA) via Excellent Graduate Award Scholarship Award (PPC2019) and Kursi Rahmah Nawawi for providing financial aids to the first author to carry out this research project. This work was supported by the Fundamental Research Grant Scheme (FRGS/1/2019/TK05/02/11) with VOT No. 5540205 from Ministry of Higher Education, Malaysia, and partly from Universiti Kebangsaan Malaysia through a research grant, Dana Pecutan Penerbitan-LESTARI UKM [PP/LESTARI/2020] and XX-2018-008.

References

- [1] M. Ramesh, K. Palanikumar, and K. H. Reddy, "Mechanical property evaluation of sisal-jute-glass fiber reinforced polyester composites," *Composites Part B: Engineering*, vol. 48, pp. 1–9, 2013.
- [2] M. J. John and S. THOMAS, "Biofibres and biocomposites," *Carbohydrate Polymers*, vol. 71, no. 3, pp. 343–364, 2008.
- [3] R. F. Aguilera, R. G. Eggert, G. Lagos Cruz-Coke, and J. E. Tilton, "Depletion and the future availability of petroleum resources," *Energy Journal*, vol. 30, no. 141, p. 174, 2009.
- [4] H. Ritchie and M. Roser, *CO₂ and Greenhouse Gas Emissions*, 2020, <https://ourworldindata.org/co2-and-other-greenhouse-gas-emissions>.
- [5] M. Ramesh, K. Palanikumar, and K. H. Reddy, "Plant fibre based bio-composites: sustainable and renewable green materials," *Renewable and Sustainable Energy Reviews*, vol. 79, pp. 558–584, 2017.
- [6] R. Drochytka, J. Zach, A. Korjenic, and J. Hroudová, "Improving the energy efficiency in buildings while reducing the waste using autoclaved aerated concrete made from power industry waste," *Energy and Buildings*, vol. 58, pp. 319–323, 2013.
- [7] N. H. Wong, D. K. W. Cheong, H. Yan, J. Soh, C. L. Ong, and A. Sia, "The effects of rooftop garden on energy consumption of a commercial building in Singapore," *Energy and Buildings*, vol. 35, no. 4, pp. 353–364, 2003.

- [8] W. J. Stec, A. H. C. Van Paassen, and A. Maziarz, "Modelling the double skin façade with plants," *Energy and Buildings*, vol. 37, no. 5, pp. 419–427, 2005.
- [9] M. Ottel , K. Perini, A. L. A. Fraaij, E. M. Haas, and R. Raiteri, "Comparative life cycle analysis for green facades and living wall systems," *Energy and Buildings*, vol. 43, no. 12, pp. 3419–3429, 2011.
- [10] G. P rez, L. Rinc n, A. Vila, J. M. Gonz lez, and L. F. Cabeza, "Behaviour of green facades in Mediterranean Continental climate," *Energy Conversion and Management*, vol. 52, no. 4, pp. 1861–1867, 2011.
- [11] J. Nickel and U. Riedel, "Activities in biocomposites," *Materials Today*, vol. 6, no. 4, pp. 44–48, 2003.
- [12] M. R. M. Asyraf, M. R. Ishak, S. M. Sapuan, N. Yidris, and R. A. Ilyas, "Woods and composites cantilever beam: a comprehensive review of experimental and numerical creep methodologies," *Journal of Materials Research and Technology*, vol. 9, no. 3, pp. 6759–6776, 2020.
- [13] D. C. T. Cardoso, K. A. Harries, and E. D. M. Batista, "Compressive strength equation for GFRP square tube columns," *Composites Part B: Engineering*, vol. 59, pp. 1–11, 2014.
- [14] R. Rahman and S. Z. F. S. Putra, "Tensile properties of natural and synthetic fiber-reinforced polymer composites," in *Mechanical and Physical Testing of Biocomposites, Fibre-Reinforced Composites and Hybrid Composites*, M. Thariq, N. Saba, and M. Jawaid, Eds., pp. 81–102, Woodhead Publishing Series, 2019.
- [15] A. N. Johari, M. R. Ishak, Z. Leman, M. Z. M. Yusoff, and M. R. M. Asyraf, "Creep behaviour monitoring of short-term duration for fiber-glass reinforced composite cross-arms with unsaturated polyester resin samples using conventional analysis," *Journal of Mechanical Engineering and Sciences*, vol. 14, no. 3, 2020.
- [16] A. N. Johari, M. R. Ishak, Z. Leman et al., "Fabrication and cut-in speed enhancement of savonius vertical axis wind turbine (SVAWT) with hinged blade using fiberglass composites," in *Seminar Enau Kebangsaan*, pp. 978–983, Institute of Tropical Forestry and Forest Products (INTROP), Universiti Putra Malaysia, Bahau, Negeri Sembilan, Malaysia, 2019.
- [17] I. M. Rawi, M. S. A. Rahman, M. Z. A. Ab Kadir, and M. Izadi, "Wood and fiberglass crossarm performance against lightning strikes on transmission towers," in *International Conference on Power Systems Transient (IPST)*, pp. 1–6, Sungkyunkwan University, Seoul, Republic of Korea, 2017.
- [18] A. N. Johari, M. R. Ishak, Z. Leman, M. Z. M. Yusoff, and M. R. M. Asyraf, "Influence of CaCO₃ in pultruded glass fibre/unsaturated polyester composite on flexural creep behaviour using conventional and TTSP methods," *Polimery*, vol. 65, no. 10, pp. 46–54, 2020.
- [19] A. Alhayek, A. Syamsir, V. Anggraini, Z. C. Muda, and N. M. Nor, "Numerical modelling of glass fiber reinforced polymer (GFRP) cross arm," *International Journal of Recent Technology and Engineering*, vol. 8, no. 4, pp. 6484–6489, 2019.
- [20] R. A. Ilyas and S. M. Sapuan, "Biopolymers and biocomposites: chemistry and technology," *Current Analytical Chemistry*, vol. 16, no. 5, pp. 500–503, 2020.
- [21] R. A. Ilyas, S. M. Sapuan, A. Atiqah et al., "Sugar palm (Arenga pinnata [Wurmb.] Merr) starch films containing sugar palm nanofibrillated cellulose as reinforcement: Water barrier properties," *Polymer Composites*, vol. 41, no. 2, pp. 459–467, 2020.
- [22] R. A. Ilyas, S. M. Sapuan, M. N. F. Norraahim et al., "Nanocellulose/starch biopolymer nanocomposites: Processing, manufacturing, and applications," in *Advanced Processing, Properties, and Applications of Starch and Other Bio-Based Polymers*, F. M. Al-Oqla and S. M. Sapuan, Eds., pp. 65–88, Elsevier Inc., Amsterdam, Netherland, 2020.
- [23] M. L. Sanyang, S. M. Sapuan, M. Jawaid, M. R. Ishak, and J. Sahari, "Recent developments in sugar palm (Arenga pinnata) based biocomposites and their potential industrial applications: a review," *Renewable and Sustainable Energy Reviews*, vol. 54, pp. 533–549, 2016.
- [24] E. Zini and M. Scandola, "Green composites: an overview," *Polymer Composites*, vol. 32, no. 12, pp. 1905–1915, 2011.
- [25] F. P. La Mantia and M. Morreale, "Green composites: a brief review," *Composites Part A: Applied Science and Manufacturing*, vol. 42, no. 6, pp. 579–588, 2011.
- [26] G. Koronis, A. Silva, and M. Fontul, "Green composites: a review of adequate materials for automotive applications," *Composites Part B: Engineering*, vol. 44, no. 1, pp. 120–127, 2013.
- [27] X. Cao, Y. Chen, P. R. Chang, M. Stumborg, and M. A. Huneault, "Green composites reinforced with hemp nanocrystals in plasticized starch," *Journal of Applied Polymer Science*, vol. 109, no. 6, pp. 3804–3810, 2008.
- [28] R. Ilyas, S. M. Sapuan, M. S. N. Atikah et al., "Effect of hydrolysis time on the morphological, physical, chemical, and thermal behavior of sugar palm nanocrystalline cellulose (Arenga pinnata (Wurmb.) Merr)," *Textile Research Journal*, 2020.
- [29] M. R. M. Asyraf, M. Rafidah, M. R. Ishak et al., "Integration of TRIZ, morphological chart and ANP method for development of FRP composite portable fire extinguisher," *Polymer Composites*, vol. 41, no. 7, pp. 2917–2932, 2020.
- [30] R. A. Ilyas, S. M. Sapuan, M. R. M. Asyraf et al., "Introduction to biofiller reinforced degradable polymer composites," in *Biofiller Reinforced Biodegradable Polymer Composites*, S. M. Sapuan, R. Jumaidin, and I. Hanafi, Eds., CRC press, Boca Raton, USA, 2020.
- [31] R. Siakeng, M. Jawaid, H. Ariffin, and S. M. Sapuan, "Mechanical , Dynamic , and Thermomechanical Properties of Coir / Pineapple Leaf Fiber Reinforced Poly(lactic Acid Hybrid Biocomposites)," *Polymer Composites*, vol. 40, no. 5, pp. 1–12, 2018.
- [32] M. R. M. Asyraf, M. R. Ishak, S. M. Sapuan et al., "Creep test rig for cantilever beam: fundamentals, prospects and present views," *Journal of Mechanical Engineering and Sciences*, vol. 14, no. 2, pp. 6869–6887, 2020.
- [33] M. R. M. Asyraf, M. R. Ishak, M. R. Razman, and M. Chandrasekar, "Fundamentals of creep, testing methods and development of test rig for the full-scale crossarm: a review," *Jurnal Teknologi*, vol. 81, no. 4, pp. 155–164, 2019.
- [34] P. R. Vieira, E. M. L. Carvalho, J. D. Vieira, and R. D. Toledo Filho, "Experimental fatigue behavior of pultruded glass fibre reinforced polymer composite materials," *Composites Part B: Engineering*, vol. 146, pp. 69–75, 2018.
- [35] C. N. A. Jaafar, M. A. M. Rizal, and I. Zainol, "Effect of kenaf alkalization treatment on morphological and mechanical properties of epoxy/silica/kenaf composite," *International Journal of Engineering & Technology*, vol. 7, no. 4.35, pp. 258–263, 2018.
- [36] K. Goda and Y. Cao, "Research and development of fully green composites reinforced with natural fibers," *Journal of*

- Solid Mechanics and Materials Engineering*, vol. 1, no. 9, pp. 1073–1084, 2007.
- [37] M. L. Sanyang, S. M. Sapuan, M. Jawaid, M. R. Ishak, and J. Sahari, “Effect of sugar palm-derived cellulose reinforcement on the mechanical and water barrier properties of sugar palm starch biocomposite films,” *BioResources*, vol. 11, no. 2, pp. 4134–4145, 2016.
- [38] R. A. Ilyas, M. S. Sapuan, M. N. Norizan et al., “Macro to nanoscale natural fiber composites for automotive components: research, development, and application,” in *Biocomposite and Synthetic Composites for Automotive Applications*, M. S. Sapuan and R. A. Ilyas, Eds., Woodhead Publishing Series, Amsterdam, Netherland, 2020.
- [39] L. Yan, N. Chouw, and X. Yuan, “Improving the mechanical properties of natural fibre fabric reinforced epoxy composites by alkali treatment,” *Journal of Reinforced Plastics and Composites*, vol. 31, no. 6, pp. 425–437, 2012.
- [40] A. K. Bledzki and J. Gassan, “Composites reinforced with cellulose based fibres,” *Progress in Polymer Science*, vol. 24, no. 2, pp. 221–274, 1999.
- [41] J. George, M. S. Sreekala, and S. Thomas, “A review on interface modification and characterization of natural fiber reinforced plastic composites,” *Polymer Engineering & Science*, vol. 41, no. 9, pp. 1471–1485, 2001.
- [42] M. Karus, “Market and economy of natural and wood fibre reinforced plastics,” *Proc of SusCompNet 9: Sustainability and biocomposites-A one day seminar*, Risø National Laboratory, Denmark, 2005.
- [43] O. Faruk, A. K. Bledzki, H. P. Fink, and M. Sain, “Progress report on natural fiber reinforced composites,” *Macromolecular Materials and Engineering*, vol. 299, no. 1, pp. 9–26, 2014.
- [44] M. L. Sanyang, R. A. Ilyas, S. M. Sapuan, and R. Jumaidin, “Sugar palm starch-based composites for packaging applications,” in *Bionanocomposites for Packaging Applications*, pp. 125–147, Springer, 2017.
- [45] M. R. Ishak, S. M. Sapuan, Z. Leman, M. Z. A. Rahman, U. M. K. Anwar, and J. P. Siregar, “Sugar palm (*Arenga pinnata*): its fibres, polymers and composites,” *Carbohydrate Polymers*, vol. 91, no. 2, pp. 699–710, 2013.
- [46] A. Bismarck, S. Mishra, and T. Lampke, “Plant fibers as reinforcement for green composites,” in *Natural Fibers, Biopolymers, and Biocomposites*, pp. 52–128, CRC Press, 2005.
- [47] M. R. Ketabchi, M. E. Hoque, and M. Khalid Siddiqui, “Critical concerns on manufacturing processes of natural fibre reinforced polymer composites,” in *Manufacturing of Natural Fibre Reinforced Polymer Composites*, S. M. Sapuan, M. Jawaid, N. Yusoff, and M. E. Hoque, Eds., pp. 125–138, Springer International Publishing, Cham, Switzerland, 2015.
- [48] R. A. Butler, “Malaysia has the world’s highest deforestation rate,” <https://news.mongabay.com/wildtech/2013/11/malaysia-has-the-worlds-highest-deforestation-rate-reveals-google-forest-map/>.
- [49] M. Ramesh, “Flax (*Linum usitatissimum* L.) fibre reinforced polymer composite materials: a review on preparation, properties and prospects,” *Progress in Materials Science*, vol. 102, pp. 109–166, 2019.
- [50] M. Ramesh, “Kenaf (*Hibiscus cannabinus* L.) fibre based biomaterials: a review on processing and properties,” *Progress in Materials Science*, vol. 78–79, pp. 1–92, 2016.
- [51] R. Belhassen, S. Boufi, F. Vilaseca et al., “Biocomposites based on Alfa fibers and starch-based biopolymer,” *Polymers for Advanced Technologies*, vol. 20, no. 12, pp. 1068–1075, 2009.
- [52] M. Ramesh, C. Deepa, L. R. Kumar, M. R. Sanjay, and S. Siengchin, “Life-cycle and environmental impact assessments on processing of plant fibres and its bio-composites: a critical review,” *Journal of Industrial Textiles*, 2020.
- [53] A. K. Mohanty, M. Misra, and L. T. Drzal, “Sustainable biocomposites from renewable resources: opportunities and challenges in the green materials world,” *Journal of Polymers and the Environment*, vol. 10, no. 1/2, pp. 19–26, 2002.
- [54] W. Lu, H. Lin, D. Wu, and G. Chen, “Unsaturated polyester resin/graphite nanosheet conducting composites with a low percolation threshold,” *Polymer*, vol. 47, no. 12, pp. 4440–4444, 2006.
- [55] D. Zindani, S. Kumar, S. R. Maity, and S. Bhowmik, “Mechanical characterization of bio-epoxy green composites derived from sodium bicarbonate treated Punica granatum short fiber agro-waste,” *Journal of Polymers and the Environment*, 2020.
- [56] P. A. Fowler, J. M. Hughes, and R. M. Elias, “Biocomposites: technology, environmental credentials and market forces,” *Journal of the Science of Food and Agriculture*, vol. 86, no. 12, pp. 1781–1789, 2006.
- [57] D. Francia, G. Caligiana, A. Liverani, L. Frizziero, and G. Donnici, “PrinterCAD: a QFD and TRIZ integrated design solution for large size open moulding manufacturing,” *International Journal on Interactive Design and Manufacturing*, vol. 12, no. 1, pp. 81–94, 2018.
- [58] R. Crutchlow, “Changing from open to closed moulding,” *Reinforced Plastics*, vol. 48, no. 8, pp. 40–41, 2004.
- [59] N. S. B. Yusof, S. M. Sapuan, M. T. H. Sultan, and M. Jawaid, “Manufacturing process selection of “green” oil palm natural fiber reinforced polyurethane composites using hybrid TEA criteria requirement and AHP method for automotive crash box,” *Journal of Renewable Materials*, vol. 8, no. 6, pp. 647–660, 2020.
- [60] M. Jacob, S. Joseph, L. A. Pothan, and S. Thomas, “A study of advances in characterization of interfaces and fiber surfaces in lignocellulosic fiber-reinforced composites,” *Composite Interfaces*, vol. 12, no. 1–2, pp. 95–124, 2005.
- [61] P. V. Joseph, K. Joseph, and S. Thomas, “Short sisal fiber reinforced polypropylene composites: the role of interface modification on ultimate properties,” *Composite Interfaces*, vol. 9, no. 2, pp. 171–205, 2002.
- [62] A. M. Fairuz, S. M. Sapuan, E. S. Zainudin, and C. N. A. Jaafar, “Polymer composite manufacturing using a pultrusion process: a review,” *American Journal of Applied Sciences*, vol. 11, no. 10, pp. 1798–1810, 2014.
- [63] S. M. Moschiar, M. M. Reboredo, J. M. Kenny, and A. Vázquez, “Analysis of pultrusion processing of composites of unsaturated polyester resin with glass fibers,” *Polymer Composites*, vol. 17, no. 3, pp. 478–485, 1996.
- [64] H. Y. Yeh and S. C. Yang, “Building of a composite transmission tower,” *Journal of Reinforced Plastics and Composites*, vol. 16, no. 5, pp. 414–424, 1997.
- [65] I. Baran, C. C. Tutum, M. W. Nielsen, and J. H. Hattel, “Process induced residual stresses and distortions in pultrusion,” *Composites Part B: Engineering*, vol. 51, pp. 148–161, 2013.
- [66] W. Huchang and W. Xueming, “Material selection for transmission tower made of fiber reinforced plastics,” *Electrical Power Construction*, vol. 32, no. 2, pp. 1–5, 2011.

- [67] S. Ibrahim, D. Polyzois, and S. K. Hassan, "Development of glass fiber reinforced plastic poles for transmission and distribution lines," *Canadian Journal of Civil Engineering*, vol. 27, no. 5, pp. 850–858, 2000.
- [68] E. V. Morozov, "The effect of filament-winding mosaic patterns on the strength of thin-walled composite shells," *Composite Structures*, vol. 76, no. 1–2, pp. 123–129, 2006.
- [69] V. Birman and G. A. Kardomateas, "Review of current trends in research and applications of sandwich structures," *Composites Part B: Engineering*, vol. 142, pp. 221–240, 2018.
- [70] SAE International, *Composite Materials Handbook, Volume 6. Structural Sandwich Composites*, SAE International, 2013.
- [71] R. Roy, S. J. Park, J. H. Kweon, and J. H. Choi, "Characterization of Nomex honeycomb core constituent material mechanical properties," *Composite Structures*, vol. 117, no. 1, pp. 255–266, 2014.
- [72] Y. Fu and P. Sadeghian, "Flexural and shear characteristics of bio-based sandwich beams made of hollow and foam-filled paper honeycomb cores and flax fiber composite skins," *Thin-Walled Structures*, vol. 153, article 106834, 2020.
- [73] A. Önder and M. Robinson, "Investigating the feasibility of a new testing method for GFRP/polymer foam sandwich composites used in railway passenger vehicles," *Composite Structures*, vol. 233, article 111576, 2020.
- [74] F. E. Sezgin, M. Tanoğlu, O. Ö. Eğilmez, and C. Dönmez, "Mechanical behavior of polypropylene-based honeycomb-core composite sandwich structures," *Journal of Reinforced Plastics and Composites*, vol. 29, no. 10, pp. 1569–1579, 2010.
- [75] S. A. H. Roslan, M. Z. Hassan, Z. A. Rasid et al., "Mechanical properties of bamboo reinforced epoxy sandwich structure composites," *International Journal of Automotive and Mechanical Engineering*, vol. 12, pp. 2882–2892, 2015.
- [76] A. Niknejad, M. M. Abedi, G. H. Liaghat, and M. Zamani Nejad, "Prediction of the mean folding force during the axial compression in foam-filled grooved tubes by theoretical analysis," *Materials and Design*, vol. 37, pp. 144–151, 2012.
- [77] J. Xiang and J. Du, "Energy absorption characteristics of bio-inspired honeycomb structure under axial impact loading," *Materials Science and Engineering A*, vol. 696, pp. 283–289, 2017.
- [78] M. Nouri Damghani and A. Mohammadzadeh Gonabadi, "Analytical and numerical study of foam-filled corrugated core sandwich panels under low velocity impact," *Mechanics, Materials Science & Engineering*, vol. 7, pp. 176–200, 2016.
- [79] S. Shi, Z. Sun, X. Hu, and H. Chen, "Flexural strength and energy absorption of carbon-fiber-aluminum-honeycomb composite sandwich reinforced by aluminum grid," *Thin-Walled Structures*, vol. 84, pp. 416–422, 2014.
- [80] L. Tian, H. Pan, R. Ma, L. Zhang, and Z. Liu, "Full-scale test and numerical failure analysis of a latticed steel tubular transmission tower," *Engineering Structures*, vol. 208, article 109919, 2020.
- [81] H. Yin, G. Wen, S. Hou, and K. Chen, "Crushing analysis and multiobjective crashworthiness optimization of honeycomb-filled single and bitubular polygonal tubes," *Materials and Design*, vol. 32, no. 8–9, pp. 4449–4460, 2011.
- [82] J. Simpson and Z. Kazanci, "Crushing investigation of crash boxes filled with honeycomb and re-entrant (auxetic) lattices," *Thin-Walled Structures*, vol. 150, article 106676, 2020.
- [83] Z. Wang and J. Liu, "Numerical and theoretical analysis of honeycomb structure filled with circular aluminum tubes subjected to axial compression," *Composites Part B: Engineering*, vol. 165, pp. 626–635, 2019.
- [84] Z. Wang, J. Liu, Z. Lu, and D. Hui, "Mechanical behavior of composited structure filled with tandem honeycombs," *Composites Part B: Engineering*, vol. 114, pp. 128–138, 2017.
- [85] D. Mohamad, A. Syamsir, Z. Itam et al., "Numerical simulation on the statics deformation study of composite cross arms of different materials and configurations," *IOP Conference Series: Materials Science and Engineering*, vol. 530, no. 1, 2019.
- [86] D. Mohamad, A. Syamsir, S. Beddu et al., "Numerical study of composite fiberglass cross arms under statics loading and improvement with sleeve installation," *IOP Conference Series: Materials Science and Engineering*, vol. 530, article 012027, 2019.
- [87] T. Jahangiri, Q. Wang, F. F. da Silva et al., "Fiber reinforced plastic (FRP) composite selection for the composite cross-arm core," in *Electrical Design of a 400 kV Composite Tower*, T. Jahangiri, Q. Wang, F. F. Silva, and C. L. Bak, Eds., pp. 15–65, Springer, Cham, Switzerland, 2020.
- [88] V. Peesapati, C. Zachariades, Q. Li et al., "3D electric field computation of a composite cross-arm," in *2012 IEEE International Symposium on Electrical Insulation*, pp. 464–468, San Juan, PR, USA, June 2012.
- [89] I. M. Rawi and M. Z. A. Ab Kadir, "Investigation on the 132kV overhead lines lightning-related flashovers in Malaysia," in *2015 International Symposium on Lightning Protection (XIII SIPDA)*, pp. 239–243, Balneario Camboriu, Brazil, September 2015.
- [90] R. Burgueño, M. J. Quagliata, A. K. Mohanty, G. Mehta, L. T. Drzal, and M. Misra, "Hybrid biofiber-based composites for structural cellular plates," *Composites Part A: Applied Science and Manufacturing*, vol. 36, no. 5, pp. 581–593, 2005.
- [91] P. Wambua, J. Ivens, and I. Verpoest, "Natural fibres: can they replace glass in fibre reinforced plastics?," *Composites Science and Technology*, vol. 63, no. 9, pp. 1259–1264, 2003.
- [92] S. Beddu, A. Syamsir, Z. A. M. Ishak, Z. M. Yusof, N. S. Hudi, and S. Nabihah, "Creep behavior of glass fibre reinforced polymer structures in crossarms transmission line towers," *AIP Conference Proceedings*, vol. 2031, article 020039, 2018.
- [93] H. K. Sharaf, M. R. Ishak, S. M. Sapuan, N. Yidris, and A. Fattahi, "Experimental and numerical investigation of the mechanical behavior of full-scale wooden cross arm in the transmission towers in terms of load-deflection test," *Journal of Materials Research and Technology*, vol. 9, no. 4, pp. 7937–7946, 2020.
- [94] M. R. M. Asyraf, M. R. Ishak, S. M. Sapuan, and N. Yidris, "Conceptual design of creep testing rig for full-scale cross arm using TRIZ-morphological chart-analytic network process technique," *Journal of Materials Research and Technology*, vol. 8, no. 6, pp. 5647–5658, 2019.
- [95] M. R. M. Asyraf, M. R. Ishak, S. M. Sapuan, and N. Yidris, "Conceptual design of multi-operation outdoor flexural creep test rig using hybrid concurrent engineering approach," *Journal of Materials Research and Technology*, vol. 9, no. 2, pp. 2357–2368, 2020.
- [96] M. R. M. Asyraf, M. R. Ishak, S. M. Sapuan et al., "Evaluation of design and simulation of creep test rig for full-scale crossarm structure," *Advances in Civil Engineering*, vol. 2020, Article ID 6980918, 10 pages, 2020.

- [97] H. K. Sharaf, M. R. Ishak, S. M. Sapuan, and N. Yidris, "Conceptual design of the cross-arm for the application in the transmission towers by using TRIZ-morphological chart-ANP methods," *Journal of Materials Research and Technology*, vol. 9, no. 4, pp. 9182-9188, 2020.
- [98] S. Zainuddin, A. Mascunra Amir, Y. R. Kibi, M. Khairil, S. Zarina Syed Zakaria, and M. Rizal Razman, "Social engineering model of natural resources management of Palu City," *Journal of Engineering and Applied Sciences*, vol. 14, no. 1, pp. 275-279, 2019.
- [99] S. S. S. Ali, M. R. Razman, and A. Awang, "The nexus of population, GDP growth, electricity generation, electricity consumption and carbon emissions output in Malaysia," *International Journal of Energy Economics and Policy*, vol. 10, no. 3, pp. 84-89, 2020.
- [100] S. M. Sapuan, K. R. Purushothman, M. L. Sanyang, and M. R. Mansor, "Design and fabrication of kenaf fibre reinforced polymer composites for portable laptop table," in *Lignocellulosic Composite Materials*, S. Kalia, Ed., pp. 323-356, Springer Nature, Gewerbestrasse, Switzerland, 2018.
- [101] M. R. Mansor, S. M. Sapuan, A. Hambali, E. S. Zainudin, and A. A. Nuraini, "Conceptual design of kenaf polymer composites automotive spoiler using TRIZ and Morphology chart methods," *Applied Mechanics and Materials*, vol. 761, pp. 63-67, 2015.
- [102] N. Mazani, S. M. Sapuan, M. L. Sanyang, A. Atiqah, and R. A. Ilyas, "Design and fabrication of a shoe shelf from kenaf fiber reinforced unsaturated polyester composites," in *Lignocellulose for Future Bioeconomy*, H. Ariffin, S. M. Sapuan, and M. A. Hassan, Eds., pp. 315-332, Elsevier Inc., Amsterdam, Netherland, 2019.
- [103] S. M. Sapuan, *Tropical Natural Fibre Composites: Properties, Manufacture and Applications*. Springer Science+Business Media Singapore, Singapore, 2014.
- [104] S. M. Sapuan, "A conceptual design of the concurrent engineering design system for polymeric-based composite automotive pedals," *American Journal of Applied Sciences*, vol. 2, no. 2, pp. 514-525, 2005.
- [105] N. M. Ishak, D. Sivakumar, and M. R. Mansor, "The application of TRIZ on natural fiber metal laminate to reduce the weight of the car front hood," *Journal of the Brazilian Society of Mechanical Sciences and Engineering*, vol. 40, no. 2, pp. 1-12, 2018.
- [106] M. A. Shaharuzaman, S. M. Sapuan, M. R. Mansor, and M. Y. M. Zuhri, "Conceptual design of natural fiber composites as a side-door impact beam using hybrid approach," *Journal of Renewable Materials*, vol. 8, no. 5, pp. 549-563, 2020.
- [107] A. M. N. Azammi, S. M. Sapuan, M. R. Ishak, and M. T. H. Sultan, "Conceptual design of automobile engine rubber mounting composite using TRIZ-Morphological chart-analytic network process technique," *Defence Technology*, vol. 14, no. 4, pp. 268-277, 2018.
- [108] R. A. Ilyas, S. M. Sapuan, R. Ibrahim et al., "Thermal, biodegradability and water barrier properties of bio-nanocomposites based on plasticised sugar palm starch and nanofibrillated celluloses from sugar palm fibres," *Journal of Biobased Materials and Bioenergy*, vol. 14, no. 2, pp. 234-248, 2020.
- [109] T. Khan, M. T. B. Hameed Sultan, and A. H. Ariffin, "The challenges of natural fiber in manufacturing, material selection, and technology application: a review," *Journal of Reinforced Plastics and Composites*, vol. 37, no. 11, pp. 770-779, 2018.
- [110] S. S. Bhagawan, D. K. Tripathy, and S. K. De, "Stress relaxation in short jute fiber-reinforced nitrile rubber composites," *Journal of Applied Polymer Science*, vol. 33, no. 5, pp. 1623-1639, 1987.
- [111] K. N. Law, W. R. W. Daud, and A. Ghazali, "Morphological and chemical nature of fiber strands of oil palm empty-fruit-bunch (OPEFB)," *BioResources*, vol. 2, no. 3, pp. 351-362, 2007.
- [112] N. Amir, K. A. Z. Abidin, and F. B. M. Shiri, "Effects of fibre configuration on mechanical properties of banana fibre/PP/MAPP natural fibre reinforced polymer composite," *Procedia Engineering*, vol. 184, pp. 573-580, 2017.
- [113] I. S. M. A. Tawakkal, R. A. Talib, K. Abdan, and C. N. Ling, "Mechanical and physical properties of kenaf-derived cellulose (KDC)-filled polylactic acid (PLA) composites," *BioResources*, vol. 7, no. 2, pp. 1643-1655, 2012.
- [114] D. Bachtiar, M. S. Salit, E. Zainudin, K. Abdan, and K. Z. H. M. Dahlan, "Effects of alkaline treatment and a compatibilizing agent on tensile properties of sugar palm fiber reinforced high impact polystyrene composites," *BioResources*, vol. 6, no. 4, pp. 4815-4823, 2011.
- [115] M. H. Mustafa and B. Dauda, "Unsaturated Polyester Resin Reinforced With Chemically Modified Natural Fibre," *IOSR Journal of Polymer and Textile Engineering (IOSR-JPTE)*, vol. 1, no. 4, pp. 31-38, 2014.
- [116] M. Hosur, H. Maroju, and S. Jeelani, "Comparison of effects of alkali treatment on flax fibre reinforced polyester and polyester-biopolymer blend resins," *Polymers and Polymer Composites*, vol. 23, no. 4, pp. 229-242, 2018.
- [117] C. Y. Lai, S. M. Sapuan, M. Ahmad, N. Yahya, and K. Z. H. M. Dahlan, "Mechanical and electrical properties of coconut coir fiber-reinforced polypropylene composites," *Polymer-Plastics Technology and Engineering*, vol. 44, no. 4, pp. 619-632, 2005.
- [118] M. S. Huda, L. T. Drzal, A. K. Mohanty, and M. Misra, "Effect of chemical modifications of the pineapple leaf fiber surfaces on the interfacial and mechanical properties of laminated biocomposites," *Composite Interfaces*, vol. 15, no. 2-3, pp. 169-191, 2008.
- [119] K. Ryder, M. A. Ali, A. Carne, and J. Billakanti, "The potential use of dairy by-products for the production of nonfood biomaterials," *Critical Reviews in Environmental Science and Technology*, vol. 47, no. 8, pp. 621-642, 2017.
- [120] A. K. Mohanty, M. Misra, and G. Hinrichsen, "Biofibres, biodegradable polymers and biocomposites: an overview," *Macromolecular Materials and Engineering*, vol. 276-277, no. 1, pp. 1-24, 2000.
- [121] A. Al Mahmood, "Characterization of glass fibre reinforced polymer composite prepared by hand layup method," *American Journal of Bioscience and Bioengineering*, vol. 5, no. 1, p. 8, 2017.
- [122] A. Gregorova, R. Wimmer, M. Hrabalova, M. Koller, T. Ters, and N. Mundigler, "Effect of surface modification of beech wood flour on mechanical and thermal properties of poly (3-hydroxybutyrate)/wood flour composites," *Holzforschung*, vol. 63, no. 5, pp. 565-570, 2009.